

Authors:

Uwe Deichmann
Daniele Ehrlich
Christopher Small
Gunter Zeug

Using high resolution satellite data for the identification of urban natural disaster risk



GFDRR MISSION

The mission of the Global Facility for Disaster Reduction and Recovery (GFDRR) is to mainstream disaster reduction and climate adaptation in country development strategies to reduce natural hazards, at the national and local levels and to foster and strengthen global and regional cooperation among various stakeholders under the ISDR system to leverage country systems and programs in disaster reduction and recovery.

JRC MISSION

The mission of the Joint Research Centre is to provide customer-driven scientific and technical support for the conception, development, implementation and monitoring of European Union policies. As a service of the European Commission, the Joint Research Centre functions as a reference centre of science and technology for the Union. Close to the policy-making process, it serves the common interest of the Member States, while being independent of special interests, whether private or national.

IPSC MISSION

The mission of the JRC-IPSC is to provide research results and to support EU policy-makers in their effort towards global security and towards protection of European citizens from accidents, deliberate attacks, fraud and illegal actions against EU policies.

Table of Contents

Using high resolution satellite data for the identification of urban natural disaster risk < 1 >

Geoinformation in disaster risk identification < 5 >

Legazpi case study < 25 >

Implications and institutional issues < 39 >

References < 42 >

Technical Appendix < 45 >

Glossary of Terminology < 79 >

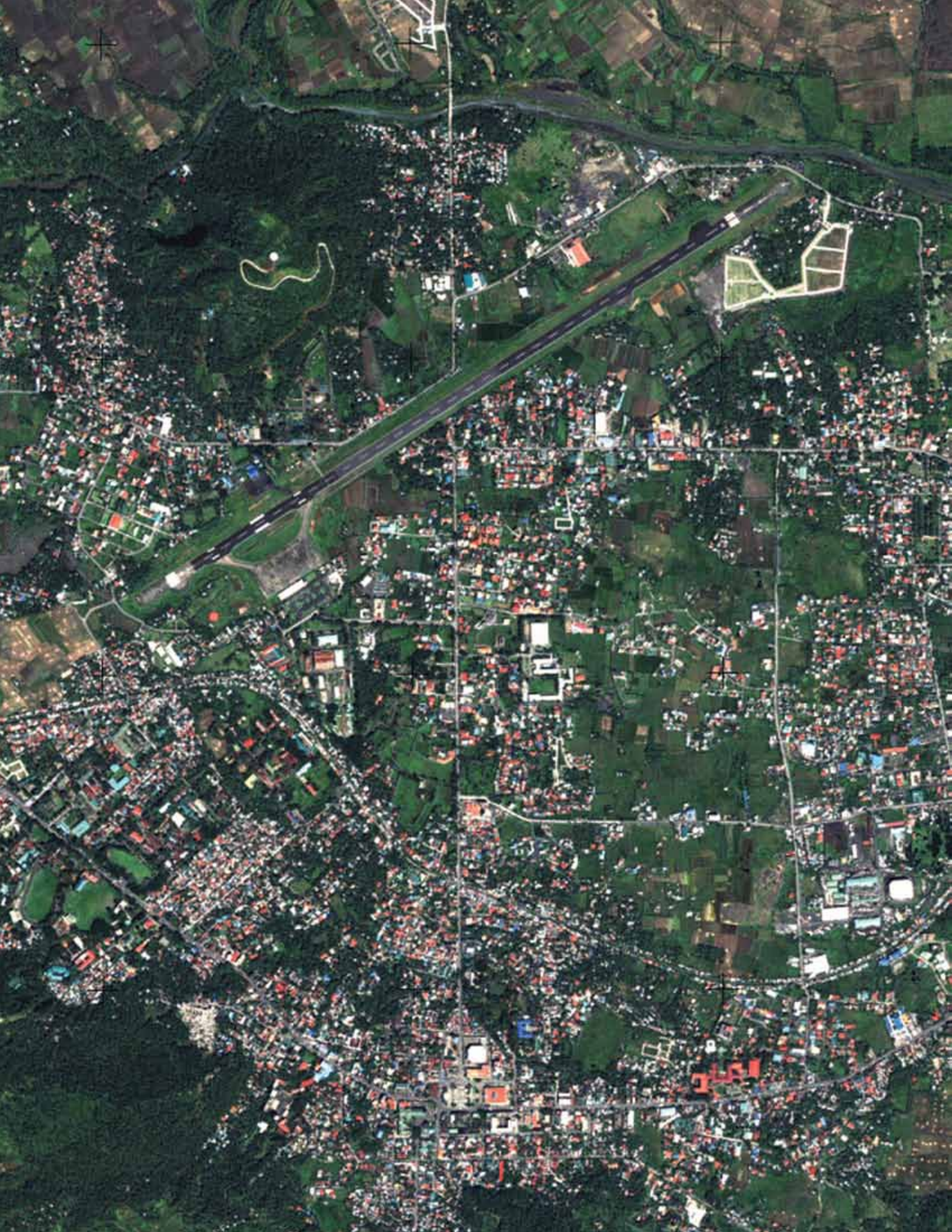
Endnotes < 80 >

©European Union and World Bank, 2011

The text in this publication may be reproduced in whole or part and in any form for educational or non profit uses, without special permission, provided acknowledgement of the source is made.

GFDRR Secretariat would appreciate receiving a copy of any publication that uses this report for its source. Copies may be sent to GFDRR Secretariat at the above address.

No use of this publication may be made for resale or other commercial purpose without prior written consent of GFDRR Secretariat. All images remain the sole property of the source and may not be used for any purpose without written permission from the source.



Using high resolution satellite data for the identification of urban natural disaster risk¹

Urban disaster risk

Natural disasters impose a significant cost on developing countries. A recent global risk assessment estimates average annual economic losses due to cyclones to be almost 40 billion USD and from earthquakes 22 billion USD (ISDR 2009).² Mortality due to these disasters is also significant. Almost 250,000 people were killed in earthquakes in the ten years between 1999 and 2008, more than 90% in just five events. A single event since then, the 2010 earthquake in Haiti caused more than 200,000 deaths. Annually, almost 70,000 people are killed by natural disasters annually—the vast majority in low and middle income countries and most in a small number of mega-disasters.³

The proportion of damages that occur in urban areas is not known but very likely significant. Many cities are located in hazard prone areas that also provide some other natural advantage—accessibility near rivers and shorelines or fertile soils near volcanic areas. Fast growing cities are densely packed, so if a hazard event occurs, more people will be affected and indirect impacts, such as epidemics following disruption of water supply, spread faster. This density also causes land to be scarce and therefore expensive. This causes poor migrants to locate in under-serviced informal settlements on the least desirable urban land—often areas subject to flooding or landslides. Dwelling units in urban areas are also larger and constructed with more solid materials than in rural areas. They can often withstand greater force, but when they fail because of substandard building practices, loss of life and damages are larger. A large share of the loss of life in recent earthquakes in Sichuan (2008) and Kashmir (2005) has been in the collapse of multi-floor buildings.

Rapid urbanization in many parts of the world also means that the number of cities and the urban population in areas where natural hazards occur will be growing for some time to come. Recent estimates suggest that the population in large cities exposed to tropical cyclones increases from 310 to 680 million between 2000 and 2050, and exposure to severe earthquakes from 370 million to 870 million (World Bank 2010, Lall and Deichmann 2009). Reducing disaster risk in urban areas is therefore a pressing challenge for city, state and national governments.

The general distribution of potential hazard risk is well known. Global data collection of storm tracks, seismic fault lines, landslide risk and flood areas allows an initial classification of natural disaster hotspots (World Bank 2005, UNDP 2005, ISDR 2009). Many hazards are also recurrent and so there will be general awareness of risk in cities exposed to them. But what is often lacking is operationally relevant and publicly available risk information upon which public policy and private sector response can be based. The value of such information is large—it helps save lives and reduce economic losses (Box 1).

Box 1: Benefits of improved hazard risk information at the local level

For the public sector:

- It increases transparency in decision making, both in terms of direct interventions such as structural mitigation or protective infrastructure, and for institutional or regulatory approaches such as zoning exclusions of hazard prone land.
- It facilitates monitoring areas of fastest urban growth which may be in areas previously avoided because of hazard risk.
- Information collected for ex-ante risk assessment also supports post-disaster emergency response and provides a baseline for damage assessment and reconstruction planning.

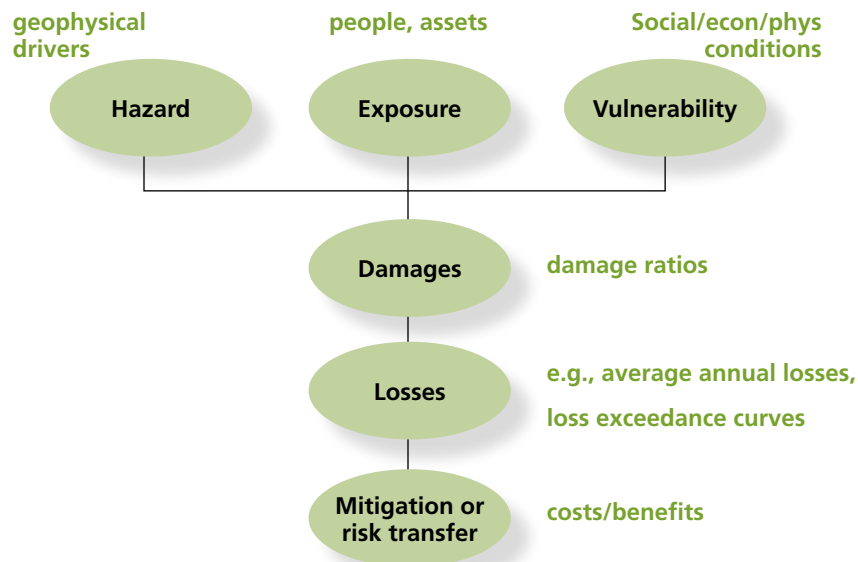
For the private sector

- Transparency facilitated through publicly available information encourages private sector risk mitigation and risk transfer through insurance.
- By making hazard risk explicit, the value of the structural integrity of a building will be reflected in its price, helping owners make better choices about retrofitting and allowing tenants to pay a rent that reflects risk.

The value of detailed risk information has been recognized in high income countries, where earthquake or flood risk maps are routinely prepared for populated areas. Urban risk assessments have also been conducted in some megacities in low and middle income countries that face frequent hazard events.⁴ Larger cities such as Istanbul or Bogota

have the resources to collect detailed geophysical and socioeconomic information that is required for detailed risk analysis (e.g., Ghesquiere et al. 2006). Smaller and medium sized cities usually don't have the capacity and resources to do so. But these smaller cities are both numerous and are home to a large population. For example, in 1970 the Philippines had

Figure 1: The hazard risk assessment task



about 15 cities with a population between 100,000 and 500,000 in areas of severe cyclone risk. By 2020, there will be more than 80 such cities with a combined population of more than 20 million.

The objective of this report is to demonstrate the use of geo-spatial tools and data sets that provide a cost-effective way to support disaster risk assessment in smaller and medium sized urban areas. The main portion of this report is meant as an introduction to professionals involved in hazard risk management who are unfamiliar with remote sensing techniques. The report focuses on applications that can be implemented at the municipal level by staff with relatively little specialized training. More advanced applications that are not covered in this report will more often be implemented by central government or state level analysts, academics or consulting firms. However, a more technical treatment of remote sensing techniques for risk management is provided in the Annex for the interested reader.

Figure 1 shows the main steps involved in risk assessment. Geophysical hazard events, such as cyclones or earthquakes, turn into natural disasters when they affect human or economic systems that cannot withstand their impact. Natural disaster risk, therefore, is determined by *hazard characteristics* (e.g., the probability of an event of a given magnitude), *exposure* and *vulnerability*. Vulnerability summarizes the characteristics of exposed people or physical assets that make them more or less likely to be affected by a hazard event. Risk assessment is the process in which the three components of disaster risk in a particular place are identified and quantified. Combined with information on likely damages to exposed assets, the risk assessment yields estimates of likely losses over time. These in turn inform cost-benefit analysis of possible mitigation investments or risk transfer.

Since all hazard risk components vary across space, risk identification must rely on geographic information. Traditionally, such information has been collected using field observation—geo-physical and socioeconomic surveys—in an expensive and time consuming process. New technologies that support the development of a data base for risk identification include tools for data capture and for infor-

mation management. Data capture using satellite remote sensing tools has made the largest strides in the last few years. Remotely sensed images collected from space based satellites now provide a level of detail that is beginning to rival aerial photographs that are taken from low flying planes—a more expensive and cumbersome process especially in remote or poor regions. Satellite images and air photos provide a wealth of information, but many factors relevant to hazard risk still need to be surveyed on the ground. Global positioning systems (GPS), by collecting precise geographic referencing (e.g., a latitude/longitude coordinate of a house or physical feature), greatly facilitate integration of field observation with image and other geographically referenced data layers.

On the data management side, geographic information systems (GIS) provide the platform for information integration, analysis and dissemination. Data *integration* is the process of linking information from many different sources by essentially using geographic location as an indexing system. Data are organized as layers which then allow creation of new data sets such as a map of flood plains derived from elevation, river bank and rainfall data. And it enables complex queries such as identifying all dwelling units occupied by poor households on land with steep slopes and unstable soil types. Geographic data *analysis* ranges from simple queries to complex modeling exercises. In the hazard risk analysis context this includes scenario analysis that can generate estimates of recurrence periods from a limited time series of actual hazard event data. Finally, spatial data *dissemination* includes traditional paper map production, but also online mapping over the Internet, for example, to disseminate cadastral information linked to flood risk estimates.

GIS based hazard risk analysis and information disclosure provide highly effective tools to support risk reduction. But the main bottleneck tends to be the availability of credible baseline information of a high enough resolution to be useful for policy analysis and decision making. The purpose of this report is to evaluate how newly available, very high resolution (VHR) satellite images can provide a cost-effec-

tive source of such information. Such data are now routinely used for post-disaster damage assessment. To reduce damages and losses in the first place, they need to be harnessed much more effectively for ex-ante risk assessment.

The remainder of this report consists of two main sections and a technical annex. Section 2 provides an overview of geographic technologies to support urban hazard risk assessment with an emphasis on VHR imagery. The discussion is aimed mostly at planning professionals and policy makers. A more technical

survey of many of these issues is provided in the Appendix. Section 3 illustrates the concepts and techniques with a case study for Legazpi municipality in the Philippines. This city is exposed to several hazard types—including cyclones, earthquakes, floods and volcanic eruptions—and has experienced several natural disasters in the past. Section 4 of the report concludes with a summary of the main implications of this review and a brief discussion of institutional issues in operationalizing a satellite data based risk assessment methodology.

Geoinformation in disaster risk identification

Technologies to support disaster risk identification

A number of novel technologies help address and quantify disaster risk. The most relevant are (1) space and airborne earth observation systems that provide pictures of the surface of the Earth, (2) field data collection tools recording precise geographical location thanks to GPS technology, (3) tools for spatial data handling such as geographical information systems (GIS) and image processing (IP) systems that are far more accessible than they used to be, and (4) web based dissemination of geospatial data for the visualization of the tools. These technologies are briefly described in the section below.

Earth Observation

Earth Observation (EO)—or remote sensing—essentially involves taking pictures of the Earth surface from above. The platforms used are airplanes or space crafts carrying cameras or imaging systems. Airplanes usually carry analogue or digital cameras that store all the images on board and return them at landing. The collected images are processed using photogrammetric equipment or image processing systems to correct for oblique (i.e., off-center) viewing angles or other distortions. The resulting, usually digital, air photos are then typically used in geographic information systems (GIS) to extract and analyze relevant information. Image acquisition from space-based systems works somewhat similarly. Space crafts are equipped with optical scanners—similar to those used in digital cameras—that are equipped to downlink the recorded information as a radio signal to a ground based receiving station where the signal is reconstructed into satellite images for further processing.

Plane-based and space-based systems are complementary. Each has advantages for specific applications. Aerial photography is probably still the most common way to collect information for crisis management, risk assessment and related activities. It is often cost effective when a large area needs to be covered. The high fixed cost of chartering and flying an airplane is balanced by the cheaper cost of collecting a large number of images. When the area of interest is relatively small, as is usually the case for cities, satellite imagery can be cheaper. Aerial photography allows for high flexibility. Flight campaigns can be planned to collect imagery at the resolution and the area extent required, often simply by changing the flight elevation and the acquisition path. Satellite sensors—that collect from fixed satellite orbits—return imagery with consistent detail and geometric characteristics. This consistency is an advantage for image processing specialists who develop procedures and algorithms for the standardized extraction of information from the imagery. Finally, even though satellite sensors have improved greatly in recent years, air photos typically have higher resolution, which makes them useful for high precision mapping applications.

Two types of imaging systems are borne on earth observation satellites: optical and radar sensors. Optical sensors record the light reflected similar to hand held digital cameras.

The actual technology differs somewhat as satellite sensors use optical scanners rather than the charge-coupled devices. Also, satellite based scanners are equipped to detect radiation at wavelengths outside the visible parts of the electromagnetic spectrum, such as infrared light. This is helpful in detecting certain types of land cover such as vegetation which is clearly visible at that wavelength.

Radar (or more precisely synthetic aperture radar, SAR) technology works differently. SAR systems emit radio waves and detect the signal that is scattered back from objects on the ground. The advantages of these compared to optical systems are that they can collect information through dense cloud cover, and they can directly provide precise information on ground elevation. Measurement of elevation is useful for terrain modeling, an important task for many hazard applications, and for monitoring changes in land surface, for example, from subsidence or landslides.

The supply of satellite images is constantly increasing. National space programs, including an increasing number in developing countries, and commercial satellite image providers advertise earth observation products with different characteristics satisfying many application areas including disaster management (GEOS, 2007). Meteorological EO systems typically cover large areas with a resolution that is adequate to describe the environmental process under investigation. For example, Meteosat monitors weather patterns at 5 km resolution every 30 minutes. The information is used to locate cloud cover and water vapor. Finer resolution meteorological satellites provide imagery at 1 km and at intervals of 6 hours. In addition to cloud cover they also measure temperature. This information is routinely used to describe weather patterns and to track tropical cyclones. Environmental satellites, such as Modis or Meris have moderate resolution, typically 250 and 500 meters and daily coverage. Others, like Landsat, with 15 m resolution orbit around the earth, less frequently, for instance 16 days. Environmental satellites have been used to monitor environmental disasters that include forest fires, floods, landslides, lava flows and volcanic eruptions.

A major breakthrough for the application of remote sensing for operational applications has been the latest generation of very high resolution (VHR) optical satellites with a pixel size of 1 meter or less. VHR images can resolve individual elements at risk such as buildings, transport infrastructure or pipelines. They also more closely resemble standard air photos. In contrast to more traditional satellite data, VHR images can be interpreted visually even with minimal training. Automatic processing on the other hand requires sophisticated procedure and software due to the complexity of the VHR imagery. Table 1 summarizes the technical characteristics of the available VHR satellite imagery that are the focus of this report.⁵

Optical VHR satellites acquire images in two different ways. One generates a so-called panchromatic image, which captures the entire visible spectrum and therefore resembles a standard black-and-white photograph. A second set of images—the multi-spectral bands—capture visible light in specific wavelengths, typically red, green, blue, that together make up a color image; plus sometimes one or more bands outside the visible spectrum such as infrared. The panchromatic images tend to have finer geometric resolution than the color bands (Figure 1) and there are image processing techniques that combine the high spatial resolution of the panchromatic band with the color information from the multi-spectral bands. Satellite images can also be displayed with non natural colors, which can sometimes be a source of confusion (Figure 2 d). Typically the near Infrared (IR) band is displayed with red color (Figure 2 d) to highlight the presence of vegetation. The information contained in color and IR bands is extremely effective in computer based information extraction algorithms.

Table 1. Optical satellite imagery useful for disaster risk and damage assessment (modified from Ehrlich et al. 2009)

	Detail	Color	Size of image (length of one side)	How often on the same place on Earth	Special characteristics
Satellite	Spatial resolution [m] (at nadir)	Spectral resolution	Swath Width [km]	Orbit repeat cycle (max. revisit time) [days]*	Notes
GeoEye	0.41	Panchromatic	15.2	3	
	1.65	Red, Green, Blue Near Infrared			
WorldView-1	0.5	Panchromatic	17.6	(1.7)	Stereo capability
Quickbird	0.6	Panchromatic	16.5	1-3.5	Stereo capability
	2.4	Red, Green, Blue Near Infrared			
EROS-B	0.7	500-900 (pan)	7	3 (?)	Stereo capability
Ikonos	0.8	Panchromatic	11	14 (1-3)	Stereo capability
	4	Red, Green, Blue Near Infrared			
OrbView-3	1	Panchromatic	8	16 (3)	
	4	Red, Green, Blue Near Infrared			
KOMPSAT-2	1	Panchromatic	15	(5)	
	4	Red, Green, Blue Near Infrared			
Formosat-2	2	Panchromatic	24	(1)	
	8	Red, Green, Blue Near Infrared			
Cartosat-1	2.5	Panchromatic	30	116 (5)	Stereo capability
SPOT-5	2.5	Panchromatic	60	(2-3)	Stereo capability
	10	Red, Green Near Infrared Mid Infrared			

*) maximum site revisit times at varying viewing angles

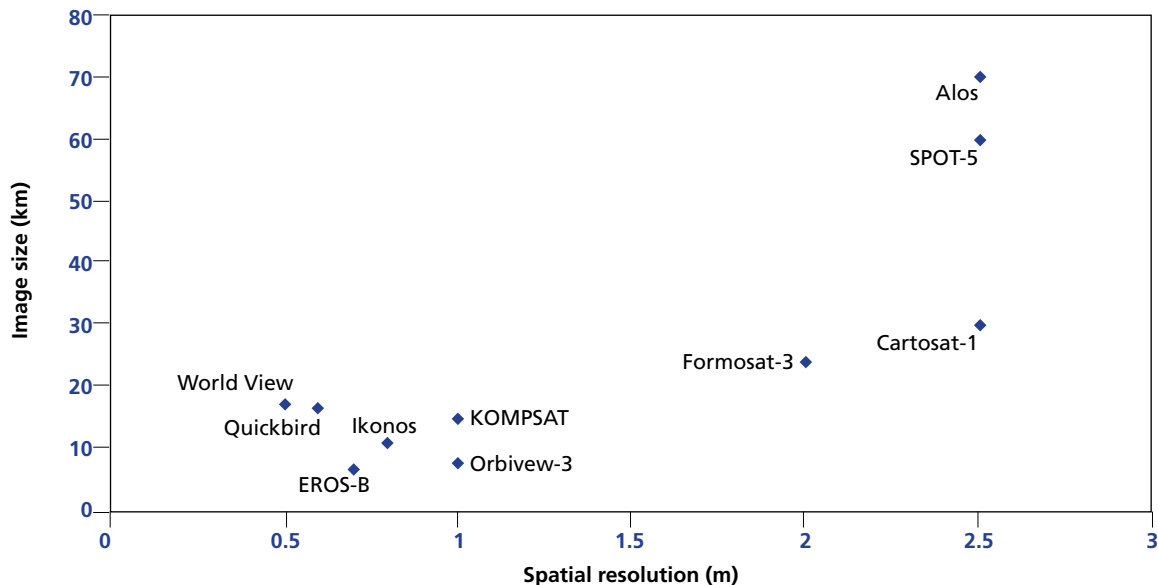
Figure 2. Example of detail and color available from VHR imagery over a 250 x 250 wide area collected over Legazpi Philippines. (a) Panchromatic Channel , (b) combination of panchromatic at 0.6 m and color channel at 2.5 m, (c) natural color at 2.5 m resolution; (d) false color composite at 2.5 m resolution.



The detail of the imagery is related to the size or footprint of the imagery (the swath width Table 1). The larger the detail, the smaller is usually the area that can be captured in a single image. The relative variation of the size of image and detail for a num-

ber of available optical imagery is depicted in Figure 3. The extent of the image and the detail are reflected in the cost of the imagery that can be obtained directly by the image providers.

Figure 3. The relation of spatial detail or resolution of the panchromatic band with the area covered by the image as indicated by the image size (or swath width). Very detailed images can cover small areas while less detailed images can cover larger areas.



The *orbit repeat cycle* determines the frequency with which the satellite passes over a given site on earth to acquire a new image. The orbit repeat cycle is fixed but often sensors have pointing capability that allows more frequent image acquisition. The orbit repeat cycle is critical in emergency response when post disaster imagery needs to be procured quickly. For risk assessment, recently archived imagery—images already collected and available from satellite data providers—are equally useful. Some sensors also allow for stereo image acquisition. This is the simultaneous acquisition of two images of a place from slightly different angles at virtually the same time. With these two images, commonly referred as a stereo pair, image processing techniques can measure the height of an object and thus provide three dimensional representations of buildings and landscapes.

Collecting auxiliary information on the ground

Even with the new generation of VHR images, interpretation of the satellite data greatly benefits from information collected on the ground. Hand held equipment is used to collect field pictures, field notes as well as the geographical coordinates of the location they were taken. The digital picture, notes and the geographical location are then combined and incorporated in geographical information systems. Pictures can include additional information such as the distance of the object photographed and direction of viewing.

GPS receivers. Global Positioning System (GPS) receivers are now widely used in consumer applications such as car navigation systems and cell phones. Using triangulation of signals from several satellites, GPS receivers calculate the precise geographical coordinates of the location. In risk assessment the

GPS receivers connected to digital cameras or video-cameras help collect information on the stock of buildings or other elements at risk. The geographic coordinates link the field information to the corresponding area on the satellite image, which supports classification and interpretation.

Several types of GPS receivers are available today. The main difference is their varying ability to improve the accuracy of the standard GPS signal, which is usually below 10 meters but can reach as high as 30 meters in unfavorable conditions. (1) Professional differential GPS are providing precision geographic information with centimeter precision. These devices are typically used for land surveying as well as for recording Ground Control Points (GCP) used for properly geo-referencing satellite images, most importantly to remove distortions in the satellite image due to atmospheric disturbance or viewing angle. Differential GPS receivers are bulky in size and usually mounted on a tripod during data capture. (2) High end handheld devices can also provide sub-meter precision when the GPS coordinates are corrected with measurements from GPS base stations. These correction signals can update the GPS measurement on the fly when it is available, using correction information broadcast from ground stations in some regions (e.g., EGNOS in Europe or WAAS in the USA). Post-processing can also be carried out using correction files available from regional GPS base stations whose location is known with great accuracy. Those base stations are available in most countries of the world and continuously log GPS signals. (3) Mass-market GPS receivers. They are intended for routing and navigation and are often used for outdoor sports. They provide a precision with an accuracy of approximately five meters. In addition to the US GPS system, the Russian GLONASS and a future European system—Galileo—are also designed to provide location information.

Digital cameras. Pictures from digital cameras provide valuable context for image interpretation and risk assessment more generally. Collecting the location of each image taken facilitates their integration with other spatially referenced information. The process of attaching location (e.g., latitude/

longitude) information to pictures is also referred to as geo-tagging. Some digital cameras are already equipped with GPS receivers that generate geo-tagged digital pictures. The models most suitable for fieldwork have a GPS receiver integrated in the camera body and get a positional accuracy of 1-5 meters. As soon as the camera is switched on the GPS receiver is searching for GPS signals. When at least three satellites are found the exact position is shown in the camera display. When the picture is taken, the GPS coordinates are saved within the image's Exchangeable Image File Format (Exif) file. Together with further metadata like date, time, focal length, shutter speed, and so on, the latitude and longitude (sometimes also altitude) coordinates are saved and can be later accessed using image processing or GIS tools.

GPS coordinates can also be linked to photographs using post-processing if pictures and location information are collected independently. Location information needs to be collected with an external GPS device. By synchronizing the timestamps of coordinates and digital photos, every picture can be linked to a geographic position. When location information cannot be captured with the digital picture automatically, photos can still be geo-tagged by identifying the location of pictures from digital maps. For this method several software tools are available (e.g. Geosetter which integrates Google Maps).

Palm tops. Personal Digital Assistant (PDA) or Pocket PCs – are also often equipped with GPS receivers. In field work, a PDA is useful for data entry using forms that store information digitally that can be readily linked to a GIS.

Portable laptops. Laptops are usually not directly used for field data capture, except when a car can provide the power supply. But they have multiple uses. First, lap tops can store digital maps, reports, presentations and other ancillary information that are of use during field missions. Second, the laptop is used to download, post-process and integrate the data assessed during the day in the field. This work is mainly done in the evening where the collected data can be controlled and revised for errors and directly transferred via internet connection to the headquarter.

Web mapping systems allow a user to interactively select geographical features from a list of options for visualization and printing. Setting up a web mapping system requires some specialized skills and delivering the information over the web requires a suitable hardware and software. A typical scenario for a disaster risk application could therefore be that specialized data centers process locally compiled data and make them available to local authorities through web-based systems.

An innovative system that is available to anyone with a suitable internet connection is Google Earth. It displays a complete global coverage of satellite imagery. For a large part of the world the images have one meter or better resolution and sometimes aerial photography is also available. The system allows for basic annotation and uploading of field pictures and, to some extent, GIS data. The most promising characteristic is that it can be used as a geographical reference on which data products generated by organizations working remotely can be overlaid on the Google Earth satellite coverage and published to a wider community. Zeug et al. (2009) present an example. They use Google Earth together with freely available third party tools for data analysis to create a flexible platform for supporting disaster management. Their example shows how frequent constraints for using GIS in developing countries—such as cost and training needs—can be overcome using a low-tech approach.⁶

The following sections discuss how VHR data and other geo-information techniques support the risk assessment process from determining hazard probabilities to quantifying exposure to capturing vulnerability factors. Since proper geophysical hazard assessment tends to be the domain of highly trained specialists, we cover this aspect with somewhat less detail. More information is provided in the Appendix.

Earth observation in hazard identification

Natural processes such as earthquakes, floods, volcano eruptions become natural hazard events when they affect people and assets. If damages are severe and overwhelm a community's coping capacity, a

natural hazard event turns into a natural disaster. This document discusses fast-onset disasters, those caused by hazards that release sudden destructive energy that physically impacts the built-up infrastructure and threatens life directly (Table 2). Slow-onset disasters such as land degradation or droughts that threaten living conditions through their effect on the environment or food production (Alexander, 2006) are outside the scope of this document.

One element that defines natural hazard risk is the likelihood of a significant natural hazard event to occur. It is expressed as the probability of occurrence at a certain level of magnitude within a given time period. Table 2 lists the ten most common natural hazards that cause mass emergencies. The table lists the event parameters describing the location and magnitude of the event, the site parameters that relate to the destructive energy released by the hazard at a precise geographical location. The table also identifies some selected parameters that can be derived from EO and used to model spatially the hazard event's destructive energy, the use of EO derived information to derive hazard related parameters and remarks on the use of EO for assessing hazard potential.

It is the energy released by the hazard that causes damages. Energy released by one hazard may also trigger other hazards through a domino effect. For instance, an earthquake or intensive rainfall during a cyclone may trigger a landslide. Disaster risk assessments need to take these induced effects into consideration.

Earthquakes

Earthquakes originate from sudden displacement of earth masses that release devastating energy through ground shaking. Seismological institutes are equipped to locate the epicenter and the magnitude commonly expressed in Richter scale. The earthquake probability of occurrence has been relatively well studied at global and regional scale. Seismic studies identify tectonic plates (fault lines), volcanoes and geological formations related to earthquakes. Equally important is to identify the likelihood of severe ground shaking caused by an earthquake which

Table 2: Natural hazards (1), their type of destructive energy when impacting exposed assets (2), parameters used to derive hazard risk maps (3), the potential use of EO in deriving such parameters (4) an the best suited EO datasets for the task if available (5).

	1) Event parameters Natural event	2) Site parameters Energy released trough	3) Variables used to quantify site parameters	4) EO data used to derive site hazards variables	5) Remarks on EO and information extraction
1	Earthquakes (E.g., Magnitude expressed on Richter scale)	Ground shaking (Typically measured based on damages i.e. Modified Mercalli)	Microscale zonation uses soil and geological information to quantify liquefaction potential	EO can be used to derive information for producing geological, seismic or soil maps.	Medium resolution imagery to spatialise point information from soil and geological maps. If land is exposed geology map.
2	Flooding	1. Inundation 2. Horizontal pressure from water column	Topography and drainage network	DEM	When in flat terrain it needs fine scale DEM
3	Storm/ cyclone (Wind speed)	Local wind	Topography	DEM	NA
4	Sea level surge (storm, tsunamis) Wave height	Horizontal pressure from water column	Topography of coastal area line and bathymetry	DEM for coastal area	Fine scale coastal DEM
5	Volcano eruption	Pyroclastic and ash fall	Explosiveness of volcano	Proximity to assets	NA
6	Lava flow	Horizontal pressure of lava flow	Topography in relation to source of lava flow	Landscape Map locating lava sources, DEM	Medium resolution DEM (SRTM sufficient)
7	Mud flows and lahars	Horizontal pressure of mud flows	Topography related to hydrography	DEM	Medium resolution DEM (SRTM sufficient)
8	Landslides	Failure of slopes with mass movements	Geologically instable slopes	DEM, Geology map, and land cover	For landslide potential SRTM sufficient For landslide measurement VHR DEM as well as SAR interferometry. Medium resolution land cover (e.g., Landsat satellites)
9	Rock and rubble fall, Surface landslides	Vertical or side impact of rock debris	Steep slopes of friable material in proximity to exposed assets	DEM, Geology map, soil map and land cover	Potential rock and rubble fall – SRTM sufficient Medium resolution land cover (e.g., Landsat satellites)
10	Wildfire	High temperature and combustion	Dry biomass map Topography and prevailing winds	Topography and land cover	Medium resolution DEM, and land cover (Landsat or equivalent)

Note: DEM: Digital Elevation Model; SRTM: Shuttle Radar Topography Mission—a global DEM at 90 meters resolution.

is related to soil characteristics. A global earthquake shake probability datasets GSHAP (Giardini, 1999) provides local ground shaking probability at coarse resolution and is often used for earthquake risk assessment. The Global Earthquake Model initiative is currently revising and updating this information.

At the local level, more macro-level information on earthquake probabilities needs to be combined with local information on shaking and liquefaction potential. The liquefaction potential is the process by which saturated material can temporarily lose strength because of strong shaking. These factors are determined by local geological and soil conditions which usually require field studies and cannot be determined from satellite data. However, satellite information can be useful to model potential earthquake effects once geological survey information has been translated into so-called shake maps that show the likely earth movement (e.g., peak ground acceleration) at a given place for an earthquake of specific magnitude.

A strong earthquake causes the collapse or structural damage of buildings and other man made objects such as transport infrastructure. Casualties result mostly from collapse of the buildings. After the event, collapsed buildings are readily observable from VHR satellite imagery. In fact, post-earthquake satellite images are often used to provide a snapshot of the intensity and the areal extent of the disaster in the immediate aftermath through the analysis of the collapsed buildings (Figure 5). Lower intensity shaking can cause structural damage to the building stock and collateral damage. Earthquakes for example can trigger landslides that may interrupt communication networks in mountainous areas (Figure 6, top). Landslides may also interrupt the natural river flow and create unstable natural dams that can flood upstream villages and create a new hazard to downstream settlements should the dam give way (Figure 6, bottom).

Figure 5: Example of damages to infrastructure Pakistan (2005)



Figure 6: Domino effect caused by the Sichuan earthquakes; inundation due to natural dam (top) (from Ehrlich et al. 2009), and interruption of road network (SPOT 5 imagery)



on buildings and infrastructure. Fast flowing water increases pressure and damages. Inundation also weakens buildings and other structures, especially those constructed with natural material (e.g., wood). This reduces the structural integrity of buildings and makes costly repairs or replacement necessary. Inundation has a number of indirect effects that may be as devastating. This includes shutting down the power system and compromising the sewage system.

Assessing the probability and magnitude of floods requires detailed landscape topography information usually in the form of a digital elevation model (DEM). Combined with hydrological models, DEM derived drainage networks are used to delineate likely inundation areas and flood height. A DEM can be derived from topographic maps. Where those are not available, elevation can be derived from satellite data. For regional scale flood modeling, existing global DEM data will often be sufficient for initial risk analysis. Generating specific flood scenarios in urban areas requires much finer detail that can be made available from DEMs derived from stereo VHR satellite data or stereo aerial photography.

Cyclones and Tornadoes

The main characteristic of cyclones—also referred to as hurricanes or typhoons—and tornadoes is the catastrophic energy released by high wind speeds. Strong rainfall and storm surges in coastal areas add to the destructive potential of tropical storms. Cyclones and the weaker tropical storms originate in tropical waters. Tornadoes originate on land with localized, but possibly catastrophic outcomes when they impact settlements and cities. Storms and cyclones can be tracked using meteorological satellites which facilitates predicting the location of landfall and potential impact on land. The effect can be mitigated by landscape features such as topography or impervious surfaces such as forested areas. As with floods, VHR supported terrain modeling can help identify areas most at risk during strong storm events.

Storm surges and tsunamis

Sea level surges can occur due to at least two reasons. The most frequent is the pressure exerted by

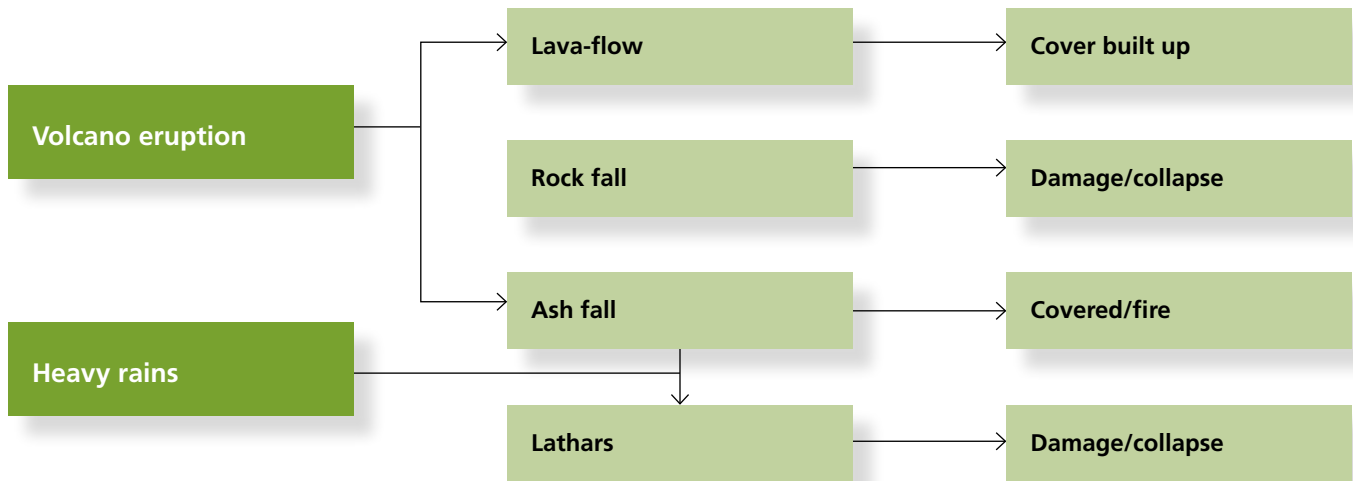
tropical storms and cyclone winds on the sea surface. This pressure can generate waves several meters high. Strong coastal surges can also occur due to sudden movements of earth masses under large water bodies caused by undersea earthquakes or large underwater landslides that generate tsunamis. The tsunami wave propagates through water bodies and can impact coastlines hundreds of kilometers away from the origin of the displacement.

The wave generated by a sea level surge or a tsunami becomes devastating when it hits built-up areas. Damage to assets occurs due to inundation or the lateral pressure exerted by the water. Modeling the lateral pressure needs to account for the draining characteristics of the inundated area. In fact, it is the channeling of the water mixed with debris that usually creates the most destructive impacts. Again, precise information on terrain characteristics derived from satellite imagery—low elevation zones, drainage networks and landscape friction—guide the risk assessment. Earth observation also yields information on natural mitigation factors such as coastal mangroves.

Volcano eruptions

Volcanic activity generates a number of hazards (Blong, 1984). Laval flow trajectories are typically modeled using the lava eruption point and drainage network based on a DEM that can be derived from earth observation (Kervyn, 2008; Bonne et al 2008). Lava flows are unforgiving. Built up structures and road infrastructure on the path of a lava flow will be completely destroyed or compromised. Explosive eruptions also eject ash and rocks that create damages within a radius of the volcano. That radius can be estimated and the corresponding risk zone calculated within a GIS. The harmful effect of rock falls is the gravity related energy accumulated during flight that impacts buildings and infrastructure. Ash flow may also be devastating especially when combined with rain generating mud flows, also called lahars. Lahars and other mud flows are best modeled with a combination of a DEM that identifies the drainage network and geological or soil information derived from maps or field surveys.

Figure 7: Hazard generated by volcano activity and main effects on built up.



Landslides

Landslides are rapid movements of volume surface material under gravitational influences, often triggered by earthquakes or heavy rainfall. Mass movement of material can be catalogued as soil slips, debris flow, rock-falls, rockslides, complex landslides, compound failures, and rock avalanches (NRC 2004). Causes for landslides include rainfall, seismic shaking, landscape alteration and natural processes of erosion that undermine slopes (Keefer and Larsen, 2007). Landslides typically occur where the landscape steepens, and small differences in topography can produce large differences in the likelihood of ground failure (NRC, 2004). The impact of landslides is twofold. Earth movement destabilizes buildings or infrastructure built on top of the slope. Damages can also occur due to lateral pressure of land masses or rubble that can bury houses or other structures.

Landslide probability assessment can be done at the individual slope, regional and global scale. At local scale perhaps the most important innovation of remote sensing is the use of airborne mounted lasers (called LIDAR: light detection and ranging) to produce fine scale topographic maps (NRC, 2004). The gravitational forces that can be assessed from elevation models can be combined with local geological maps, geomorphology and land cover maps to determine landslide potential.

Regional scale landslide assessments employ satellite data describing morphology, vegetation, as well as drainage conditions of the slope. Earth observation techniques also facilitate mapping of landslide events using before and after imagery. At the global level, remote sensing derived terrain and vegetation data sets provide the basis for broad assessments of landslide risk (Hong, et al 2007, Nadim et al 2006).

Wildfires

Wildfires pose a risk to settled areas and other assets when there is a significant combustible fuel build-up consisting of dry vegetation. Wildfires regularly cause property damage, especially in North America, Southern Europe and Australia. While wildfires play an important ecological role, their effects can be severe if fires had been suppressed for extended periods. Various earth observation products support wildfire risk modeling. Medium spatial resolution imagery, such as Landsat or Modis, provide information on land cover and biomass accumulation as an indicator of fire potential. Terrain and geographically detailed climate data further support risk assessment and sophisticated GIS models facilitate simulation of the spread of fires under various weather scenarios. Finally, remote sensing is used to map burned areas. Burned areas and burned properties are easily recognizable on satellite imagery.

Exposure / Elements at risk

In the standard natural hazard risk model, exposure refers to the people or assets that are in harm's way when a hazard event occurs. Once areas of significant probability of hazard events are delineated, the next risk assessment step is to identify exposure. Since people are mobile, their exact location cannot easily be modeled—although sophisticated emergency models predict, for instance, daytime and nighttime population distribution. More typically, risk assessment focuses on delineating the location and characteristics of buildings and other structures that may be damaged.

The built (or constructed) environment consists of housing, engineered structures and transportation systems that reflect a city's cumulative investments in physical capital (Mileti, 1999). Impacts of natural hazards can lead to direct economic damage—the reconstruction or replacement value of the damaged structures—as well as indirect damage such as lost income while productive assets are unusable. The location of physical structure also provides information on human exposure. Occupied structures in hazard zones such as homes or office buildings imply that people are likely exposed to injury or death directly by the force of the hazard or indirectly, for example, when a building collapses.

The main task, and the focus of this section, is to delineate urban areas, their main features and even individual structures. This information, in GIS format, can then be related to hazard probability profiles. The problem in many developing country cities is that available information on built-up areas is either non-existing or out-of-date. Topographic maps have traditionally been the most important data sources. Usually derived from aerial surveys, topographic maps conform to a high and consistent standard of mapping. At large cartographic scales (i.e., covering small areas), topographic maps delineate individual building footprints and details of other physical infrastructure. But such mapping is expensive, in some countries available topographic maps date back to the 1960s and have often been produced only at coarser scale (e.g., 1:50,000 or 1:100,000). For cities where current maps are unavailable and that are growing fast and

often without much administrative monitoring or oversight, satellite data provide an invaluable source of up-to-date information on the extent and nature of buildings, infrastructure and other features that may be threatened by natural hazard events. Needless to say, such information is useful for many other routine city management functions as well.

Satellite imagery have been used to develop land cover maps and land use maps, at 1:50 000 scale and coarser. Such maps tend to focus on agriculture and natural systems, and settlements and cities are typically lumped together as “artificial surfaces.” The type of satellite data mostly used is the medium resolution satellite imagery available from Landsat for which Andersen (1971) initially introduced a classification scheme. A classification based on later Landsat Thematic Mapper data has been conducted for the USA (Vogelman et al. 1998) as well as for Europe (CORINE, 1994) and Africa (FAO, 2008). Coarse resolution land cover maps generated for environmental and global change studies also include the built up class (for instance, in the International Geosphere-Biosphere Program). These layers are also used to derive improved global population density datasets.

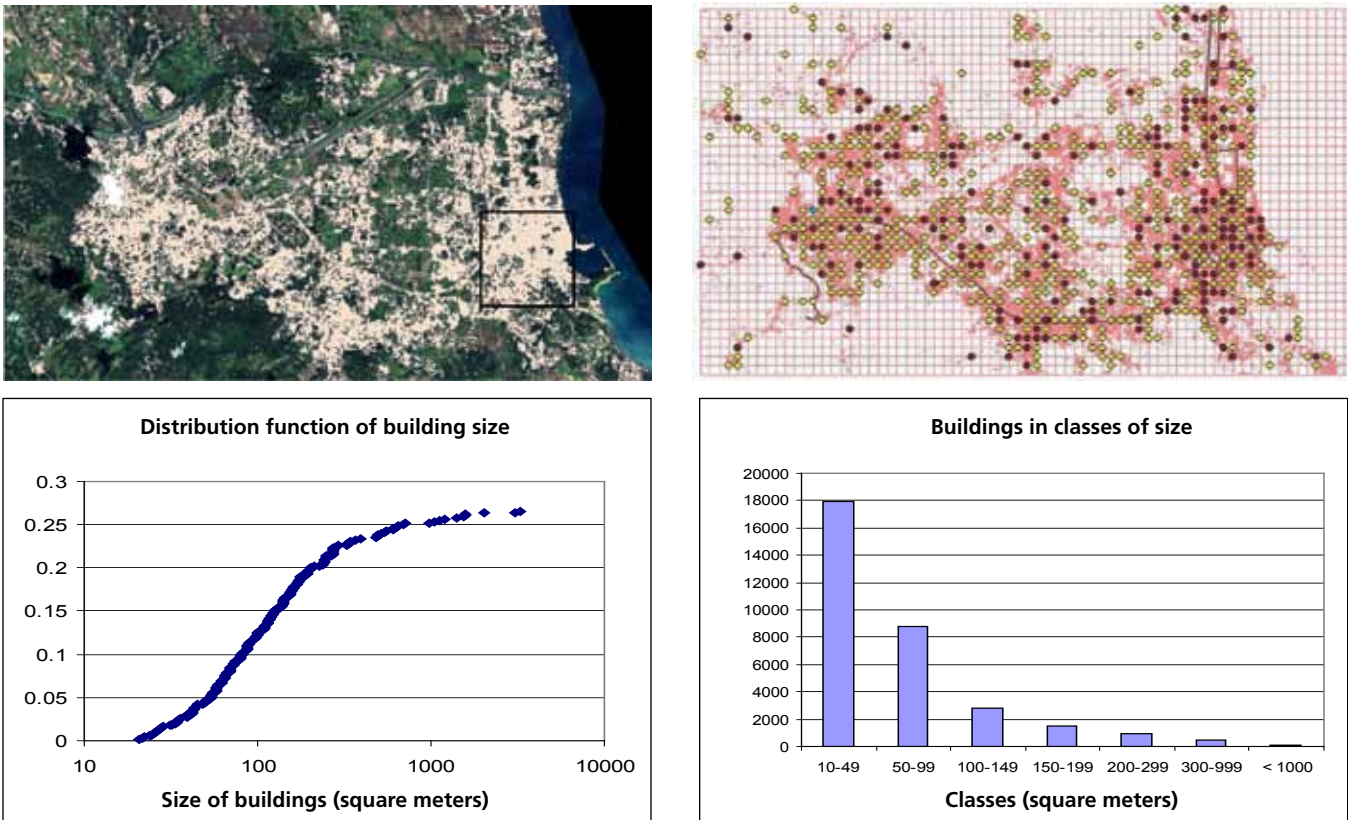
The urban/artificial surface classes in land use or land cover maps provide an approximate measure of the built-up area. Several built-up sub classes might be used in the more sophisticated classification schemes. But for urban risk assessment, these classifications derived from medium resolution satellite data are usually insufficient when the goal is to differentiate risk to people and assets, or if expected damages are to be quantified. Assessment at the individual city levels therefore requires the use of VHR imagery that provides detailed information on objects contained in built up areas and thus can be extracted as quantitative information more suitable for disaster risk analysis. New 1 m resolution or better VHR imagery shows every single building, as well as road infrastructure and other structures that make up a settlement and a city. The accuracy and precision of the resulting information depends on the extraction techniques which are in turn related to the cost of processing. The discussion in the following sections provides an overview.

Operational methods

Using VHR data operationally to produce what is essentially an up-to-date digital representation of a city involves a set of choices. The first choice is whether to use some form of sampling or to proceed with complete enumeration. The advantage of sampling is that by processing a limited number of well-chosen subsets of an image, fairly reliable summary statistics can be derived for the entire city. Stratification of sample areas can be based on a simpler map of urbanized areas, perhaps classified into broad sub-sections such as residential, commercial,

and industrial areas. The sample areas are then processed in detail and the resulting information is extrapolated, for instance in proportion to the area of each built-up class. Ehrlich et al. (2010), for example, used systematic sampling and an estimator that also provides the distribution function of building size (Figure 8). The disadvantage of sampling is that it fails to produce a data set with information for every single building. If hazard probabilities vary significantly across the urban area, risk assessments will be difficult to obtain unless a detailed risk zonation guides the stratification.

Figure 8: Built up area, systematic sampling, distribution function of building size and number of building per building class for city of Legazpi in Philippines (From Ehrlich et al. 2010)

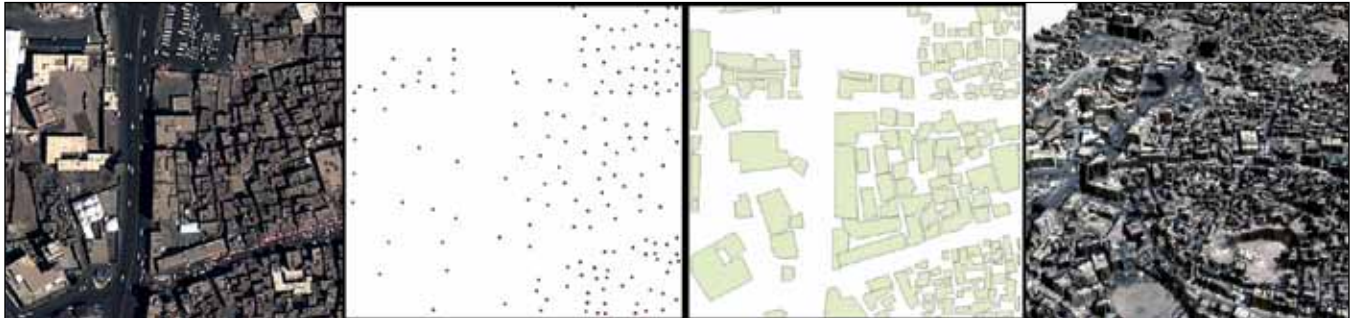


Full enumeration is more costly, time consuming and tedious, but will often be justified. Complete information provides a more reliable quantification of exposure, it will be useful for many other purposes, and it greatly facilitates ex-post impact assessment. Enumeration involves the detection and labeling of every single building from VHR imagery. The infor-

mation is typically encoded as GIS layer as a digital building stock map. The building stock map is then used in combination with other maps to generate disaster risk scenarios.

The second major choice is how the structures and assets are represented in the database. In order of complexity, this can be a simple map of built-up

Figure 9: The figure shows a 250 x 250 m large area collected over Sana'a, the counting based on simple enumeration, the encoding of foot-print of buildings, and the extraction through stereo imagery of area and height information to derive volume. Volume is the preferable information to have and provides information on floor space used for loss estimations and for population assessments.



areas perhaps stratified by land use, the detection and labeling of buildings represented as points, the creation of building footprints encoding a building area assessment, and incorporating building height to derive three dimensional building representations (Figure 9).

Built-up area map. The simplest way of representing an urbanized area is by delineating the overall extent that is covered by man-made structures. One efficient and rapid method to generate a digital map of urban extent from VHR imagery is by means of a built-up area index which can be derived using automated computer techniques. It uses an algorithm that evaluates the textural characteristics of different areas in a satellite image (Pesaresi et al., 2008). For instance, the computer program can detect regularities such as 90 degree corners which are typical of manmade rather than natural features. The built up area index is typically computed over larger regions such as an entire metropolitan area. It is not designed to discriminate within the built-up areas. But when applied in relatively sparsely settled urban areas with VHR imagery, the approach can capture single buildings or clusters of buildings similar to information that is typically found on maps at 1:10 000 scale. It is thus an improvement over land cover maps that usually provide information at coarser than 1:25,000 scale. A simple built-up area map is also useful as the basis for sampling to derive statistically based enumeration of the building stock.

Point representation. A second option that provides more detail is to represent individual structures in a database as points. In the simplest form, the detection is carried out by visual inspection of a satellite image displayed on a computer screen. An analyst places a point on each feature and labels it appropriately. Since the satellite image is properly referenced in a known geographic coordinate system, the real-world location of the feature is also captured. The point data can subsequently be analyzed in a GIS, for example to extract the number of buildings of a certain type within a flood zone. This basic approach to creating an inventory of structures is typically accurate and fairly rapid. Research in the image processing community is well underway to develop means for automatic detection of individual buildings.

Point assessment does not provide information on size of buildings, which is important, for instance, to estimate their value. Any building density estimation based on point data could be severely biased. Simple detection and labeling is still often used for providing rapid assessment of the housing stock especially in a post disaster scenario when the number of damaged buildings needs to be measured against the total number of buildings.

Building area assessment. Delineating each individual building or structure is more time consuming than point representation but supports a broader range of applications. Machine assisted procedures to create building footprints do not yet provide sufficiently ac-

curate output for operational purposes. So, manual encoding—essentially tracing each building on a satellite image displayed on a computer screen—tends to be the most robust technique for now. Building footprint maps yield useful measures for risk assessment such as density, space between buildings, size of buildings, or proximity of buildings to potential hazards.

Building volume assessment. The most precise building assessment is obtained by measuring the volume of single buildings. For risk assessments, the number of floors in combination with the footprint area provides information on floor space from which cost and loss functions can be calculated. Floor space is also useful to more precisely estimate population densities and exposure. Estimating building volume requires height and area. Area can be derived from the footprint. There are two options for estimating height of structures. One is to derive height by evaluating the shadows on the image. In combination with information about the specific orbit parameters of the satellite image, shadow length can be related to height. A more precise estimate of height can be obtained from processing of stereo imagery. This requires two images, slightly offset, of the same area. It is thus more costly—requiring acquisition of two images—and processing stereo imagery for assessment of height information requires specialized software and expertise. The added information that can be extracted, not just building height, but also terrain features, will often justify the expense for risk assessment and other urban applications.

Vulnerability

The third major factor that determines natural hazard risk is vulnerability. It refers to the characteristics of people or assets that make them more likely to be affected by a natural hazard event. Injury or mortality are often caused indirectly, for instance by collapsing buildings. So the vulnerability of people and physical assets is closely linked. Physical vulnerability relates the intensity of the hazard to the degree of damage of an exposed element. Based on empirical observation or engineering assessments, it expresses the degree of damage—typically expressed on a scale from zero to one—when the element at risk is exposed to a hazard event of a given strength. Physical vulnerability is hazard specific. In construction science structural damages are related to the intensity of the hazard through vulnerability or fragility curves.

Physical vulnerability is related to the quality of construction—that is material and construction practices—encoded in engineering guidelines or building codes which define the solidity of the physical infrastructure (Figure 10). Poorly built buildings will be more likely to collapse and thus have high vulnerability to impacts from earthquakes (Spence, 2009) or floods, for instance. Vulnerability is hazard specific. Inexpensive structures such as huts may be less vulnerable to earthquakes than masonry buildings. Yet, huts may not cope with the wind pressure of tropical storms and therefore are more vulnerable than masonry buildings.

Figure 10: Example of different type of building typologies. (a) Informal dwellings made up from assembled material, and (b) formal well engineered buildings. The structural vulnerability is strictly related to the typology of buildings.



Vulnerability can thus be characterized based on building types. Several classification systems of building types exist. The one presented below uses information from civil engineering summarized in the World Wide Typology of Buildings (WWTB) and includes non-engineered buildings that are the result of empirical observation from various studies. Non-engineered structures are informal or temporary dwellings that represent a large share of dwellings in many cities of the developing world. In the classification scheme below, three classes—class 1 to 3—include formal buildings that were derived by aggregating the typology available from the World Wide Typology of Buildings (WWTB) and three classes are also reported in Lang (2002). Class 4 and 5 include

buildings that are found in informal settlements and in rural areas, and class 6 includes temporary shelters for displaced people (Table 3).

Structural characteristics of buildings from which vulnerabilities are derived are typically assessed from ground surveys using the data collection tools discussed earlier. However, VHR imagery can provide partial information based on a number of parameters directly measurable from the image including height, size, those that can be inferred based on setting and context (Muller et al 2007), as well as socio-economic information that is often country or region specific. The image analysis that uses such an approach typically proceeds from the more general to the more specific in a top down approach (Estes et al., 1983).

Table 3: Simplified building typology classification systems that combines formal and informal buildings. Class 1 to 3 are based on description of World Housing available from <http://www.world-housing.net/>

B Type	Definitions	Brief description of structural characteristics of building type.	Where	On Damage
1	Advanced technologies Reinforced concrete and Steel structures	Structures constructed with highest standards. Typically employed for large and tall buildings. Disaster affected areas in developed countries will all comply with these standards. Includes WWBT class 9	Cities and large metropolitan areas	Sustain pressure and vibration
2	Reinforced Concrete Frame Buildings	Building constructed according to engineering standards. Typically on cement pillars with roof/pavements also in cement. By and large WWBT class 6, 7, 8	Settlements, Mostly in high income countries	Sustain pressures, shakes
3	Traditional building with rubble stone, field stone, adobe masonry or wood	Traditional building standards using local expertise and material (mortar, adobe, bricks, wood). It largely varies from geographical areas. The dwellings follow traditional building practices but are not constructed with scientific/engineer criteria. Typically not constructed to absorb shocks to natural disasters. WWBT class 1-4 and 10	Large part of dwellings of the worlds are constructed with these standards	These buildings are typically damaged during catastrophic events
4	Assembled material in informal settlements	Dwelling constructed with assembled material for a lack of resources, typically found in poor neighborhoods of urban centres and settlements.	Dwelling type in many low income communities	Typically very instable and vulnerable to damage
5	Perishable material	Dwellings from natural material that include wood that needs to be constantly fixed and repaired.	Rural settlements in tropical countries	Typical dwellings in farming communities
6	Temporary, Removable	Those made of material that requires constant maintenance and those that are regularly moved.	Temporary settlements	Vulnerability very dependent on hazard type

Source: Authors compilation from various sources.

Learning from past disasters

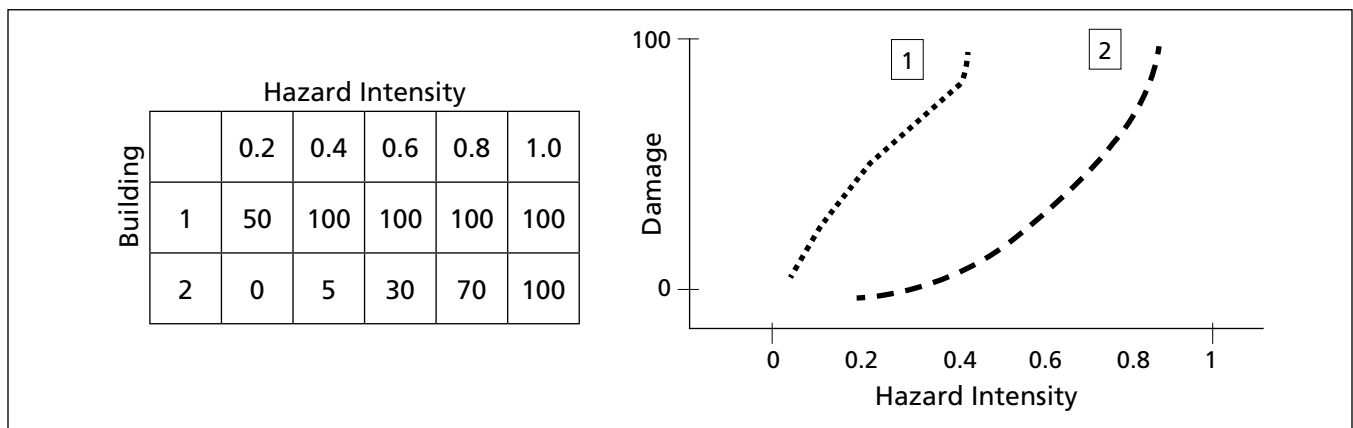
An important source of information for determining the physical vulnerability of buildings is damage assessment from previous hazard events. Hazard specialists develop models that relate the intensity of the hazard with the damages that ensued. Two parameters are required to calculate the vulnerability curve: damages and hazard intensity. The damages are reported on y-axes and expressed on a scale of 1 to 100 (or percentage of it) with 100 % expressing total destruction. The x-axis shows the intensity of the energy released by the hazard and is scaled to capture the minimum damage to the weakest structure to the highest damage to the strongest structure (Figure 11).

When the damage is widespread and buildings have collapsed, the damages can be assessed using post disaster VHR imagery. The damage can be detected more accurately when pre-disaster imagery is available, allowing for comparison with pre-disaster situations. The collapsed buildings display unique patterns on very high resolution imagery identifiable on panchromatic and multi-spectral imagery. The overview provided by post disaster satellite imagery is unique and damages can be assessed even in the most inaccessible places. However, satellite im-

ages can not be used to assess structural damages on buildings that are still standing. For that purpose, field surveys are required. Field surveys are carried out using hand held equipment described in a previous chapter that can be quickly incorporated in a GIS database.

Vulnerability functions are hazard dependent and are constructed for only those hazards that modulate their intensity including earthquake, hurricanes and floods. For other hazards that include landslides or lava-flows, the destruction is often so severe that re-settlement or complete reconstruction is required. Earthquake vulnerability functions have been developed for many regions mostly in high income countries (Kirchner et al, 1997, 2006, Scawthorn 2006, Lang , 2003, Douglas, 2007, Vickery et al., 2006). Vulnerability to tephra fall, pyroclastic flow, and earthquakes are available for selected regions of high volcanic activity including Caribbean, Azores, Tenerife (Spence et al. 2005). However, vulnerability is understudied. In fact, the unavailability of vulnerability or fragility curves for the different housing typologies and hazard profiles in many countries is probably the biggest shortcoming in disaster risk assessments (Hollenstein, 2005). Even high income countries like Italy that routinely experience disasters caused

Figure 11: Example of empirically derived vulnerability matrix that shows damage percentages at different hazard intensity levels (in columns) for two building types (rows). These matrices are typically derived by field visits that record building stock and relative damages in disaster affected areas. Large numbers of damage observation can be used to construct physical vulnerability curves (right) that related hazard intensity and damage level for single hazardous events. Vulnerability matrices and curves provide the critical parameter without which disaster risk assessment can not be calculated.



by earthquakes lack the data collection methodology for generating databases that can be used to empirically build vulnerability curves (Colombi et al. 2008). This shortcoming is particularly severe for developing countries whose building stock is largely informally built and damages are not recorded in a systematic manner.

Building characteristics relevant for vulnerability assessment

Building size. The relation between building size and vulnerability is somewhat ambiguous and therefore highly context specific. On the one hand, larger or taller buildings are more likely to have been engineered to standards that should consider hazard risk. On the other hand, where building practices and standards are lax or not enforced, larger buildings may be more vulnerable than smaller, informal structures built using lightweight materials. The contribution of building size in reducing or increasing vulnerability therefore needs to be evaluated on a case by case basis.

Building height. As described in the section on exposure, building size and height can be obtained from VHR images using various manual and image analysis techniques. Using stereo images, building height can be determined systematically for every building. Photogrammetric equipment allows for precise extraction of height information. Automatic methods can provide less accurate estimates but much more quickly.

Color. Color can provide additional information on the typology of building. Color is also referred in remote sensing terminology as spectral resolution (Table 1). The more spectral bands available, the more the opportunities to discriminate materials based on their reflectance signal. The VHR satellite imagery listed in Table 1 is collected, by and large, at nadir (i.e., from directly above) or with small viewing angles. So it captures mostly roofs and the color of roofs can be related to the characteristics and typology of the building. For example, roofs made of perishable material are associated with informal buildings constructed with less resilient materials.

Age. Age of buildings can provide insight in building construction, which is based on technological development and history. Construction sciences have evolved and continue to evolve based on improvements in technologies. New norms, materials and standards are typically adopted. Newer buildings may be of improved quality with respect to older ones in the same city. Although the reverse is sometimes true where new building techniques have been introduced without regard for local conditions, while supposedly outdated, but time tested construction may be more suitable.

Settlement historical growth. Earth observation and geospatial information providing historical information on settlements can be used to determine the age of buildings. The standard technique is to map the current extent of a city based on recent VHR satellite imagery. In fact, current EO may provide the most updated plan of a given settlement given that topographic maps or city plans are not updated frequently. This updated situation map of the city can be compared with satellite imagery available for past dates and information from historic maps. Differences in settlement extent provide insight in the new developments and therefore the likely age, and therefore possibly construction quality, of buildings.

Geographical setting. In many fast growing cities in the developing world, the poorest housing is erected in marginal land that is often the least suitable for construction. Communities settle along the right of way of railway lines or major roads, on steep terrain, in flood prone areas, or in proximity to hazardous material storage. Small dwellings, densely spaced with little room for mobility and no obvious presence of public facilities is typical of poor communities. The geographical setting of the building stock, which can be assessed by means of VHR images, often provides a clear relationship between communities and their well-being. Similarly, the use of buildings, which can often be determined from satellite data, also provides information about the likely quality of construction. Building use can be classified in a number of ways and Table 4 provides first and second order classification types.

Table 4. Use of buildings simplified from description available from http://en.wikipedia.org/wiki/List_of_building_types

1. Dwellings	Condominium, Apartment bloc, Single house
2. Government	Parliament, Capitol, Consulate, City Hall, Fire station, Post office
3. Commercial	Office building, Bank, Shopping mall, Supermarket
4. Health	Hospitals, Clinics, Emergency aid
5. Industry	Power plant, Factory, Refinery
6. Transit	Airport terminal, Train station, bus station
7. Educational	University, Schools, Concert Hall, Museum, Movie Theatre,
8. Military	Fort, Castle, Fortification, Tower
9. Parking	Aircraft Hangar, Boathouse, Garage, Warehouse
10. Religious	Temple, Church, Mosque, Monastery, Chapel, Cathedral
11. Recreational	Stadium, Arena, Amphitheater
12. Agricultural	Farm house, Stable, Barn, Greenhouse

Context. Communities everywhere strive to improve their welfare by improving the quality of their building stock. Within a given region the dwellings are a reflection of the technological know-how and wealth of communities. Often socio economic indicators can provide insights on dwelling quality and material. Information on size and geographic setting derived from EO, for instance, can be combined with socioeconomic information from a census or survey. Such information is increasingly available for small geographic units such as enumeration areas or city wards.

Summary

This chapter has reviewed geographic technologies that can be used to improve the understanding of hazard risk. (1) Earth observation, in particular VHR satellite imagery, is the most relevant as it contributes information about all elements of the hazard risk equation—hazard probabilities, exposure and vulnerability. (2) GIS supports integration of disparate information sources to visualize and analyze

hazard relevant data, including scenario analysis. (3) Field data gathering equipment based on GPS technology that facilitates collection of auxiliary and contextual information that can be linked to other geographically referenced data.

VHR images are perhaps most useful in assessing exposure, which can be derived from enumeration of buildings or other structures that are clearly visible in the satellite images. This process requires relatively little specialized expertise or equipment, but—until automated technologies improve—is quite labor intensive. VHR also supports the estimation of hazard event probabilities. But this process is more complex, typically requiring integration of additional information such as climate data as well as specialized training in earth sciences or engineering. Vulnerability of exposed assets may be the most difficult to derive from VHR alone. But in combination with field collected information—which can be done cheaply by staff with minimal training—satellite images provide a comprehensive reference frame for organizing and analyzing vulnerability related information.



Aerial photo of Mount Mayon (Volcano), Legaspi, Bicol, Philippines

Legazpi case study

This section illustrates the concepts and techniques described in the previous parts of the report in the context of a case study in a medium sized city located in a region prone to several types of hazard events. The main focus is a simplified disaster risk model to be used to estimate potential losses based on physical damage to the building stock. Very High Resolution satellite imagery and field data generate information on hazard, exposure (mostly the building stock) and vulnerability. The information is structured within a Geographical Information System that provides the platform for integration, standardization and modeling. The methodology is tested on the city of Legazpi in the Philippines, as a case study, but its applicability aims to be global. This case study involves modeling two disaster scenarios: one for earthquakes and one for tsunamis. The scenarios provide quantification of physical damages to building stock, financial losses and population affected. The case study shows that with relatively little investment, a core disaster modeling system can be set up to provide a quantification of urban disaster risk. The outcome in an operational setting is an urban and spatial information system for hazard management. Such simple systems could be implemented in disaster hotspot cities of any size to raise awareness on disaster risk and to aid in planning and implementing mitigation measures.

Study area

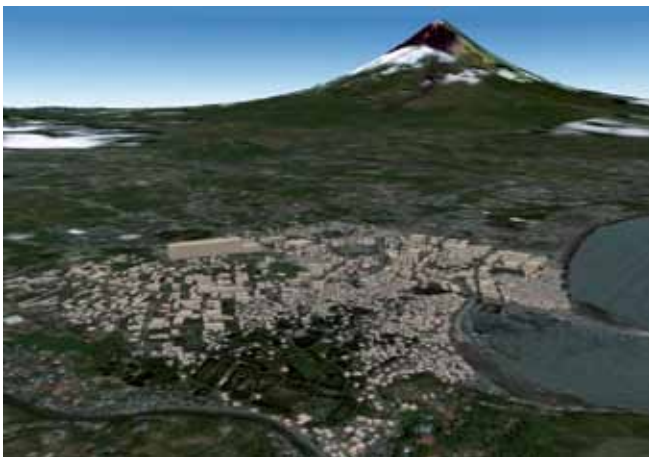
The Philippines are a hazard hotspot. According to EM-DAT (2009) during the last 30 years the Philippines experienced around eight natural disasters per year. The top ten disasters in the last decade (2000-2009) are all due to storms and caused \$ 1336.6 million in losses and killed 6654 people. The most devastating hazards are tropical cyclones (locally called typhoons), followed by floods and earthquakes.

Tropical cyclones have a damaging effect due to strong winds and torrential rains that can, in turn, trigger other hazards. For example, on November 30, 2006, super-typhoon Durian (locally known as Reming) made its landfall in eastern Luzon causing physical damage and human losses. Houses were destroyed due to strong winds, heavy rainfall and flooding. Volcanic activity of Mount Mayon earlier in the year left the volcano slopes covered with loose volcanic ashes. The combination of torrential rains from Durian and ash deposits led to massive mudslides that buried several villages in the region. According to EM-DAT (2009) 1,399 people lost their lives. The economic damage in the affected area was estimated at US \$ 66.4 million.

The case study focuses on Legazpi City, the capital of Albay province in the Bicol region of Luzon island that is part of the Northern Philippine archipelago. The city is located on the shores of Albay Bay on the foot of Mount Mayon and is exposed to several natural hazards (Figure 12). Mount Mayon is one of the most active volcanoes in the Philippines with 48 eruptions since recordings began in 1616 (PHIVOLCS 2009). Its last major eruption dates back to 1993 during which 77 people from the surrounding areas lost their lives. Legazpi, as the entire Philippine archipelago, is exposed to frequent earthquakes. As a consequence, the risk of an earthquake-triggered tsunami is high. The possible collapse

of part of Mount Mayon could induce a massive landslide that could also lead to a tsunami like wave. Apart from direct damage from wind and rainfall-induced flooding during typhoons, sea surges have potentially devastating effects on coastlines and infrastructure.

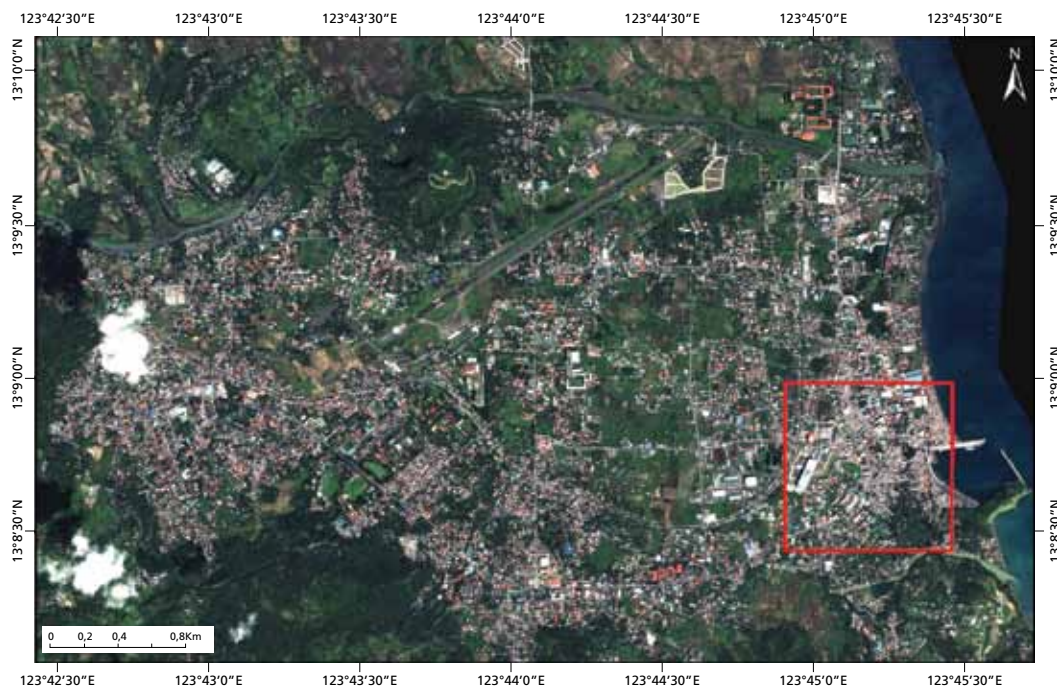
Figure 12: Landscape view of the city of Legazpi, the Albay Bay to the right, and the active volcano Mount Mayon in the background. Part of the building stock is shown in 3D,



The topography for Legazpi is relatively flat and swampy, crossed by rivers and creeks. Flooding is a frequent consequence of heavy rainfall caused by tropical cyclones and sea level surges. The settlements of Legazpi follow the coastline of the bay. Informal settlements are built directly on a gently sloping beach followed by flat land. A small harbor is protected by a pier. In the second row behind the harbor lies another district of poorly constructed huts and houses including a school. A small business and warehouse district extends towards the North followed again by residential areas with houses of different size, age and quality. The flat and swampy area in the interior is crossed by roads, along which many residential houses were built in the recent past.

A second business district is located two kilometers inland from the shore, surrounded by residential areas. The city of Daraga extends from this second business district west. Around ten kilometers to the north the slopes of the Mayon volcano ascend up to its peak at 2,460 m above mean sea level. Following a risk zonation from the authorities the closest villages are located around eight kilometers from the peak of the volcano on its fertile slopes.

Figure 13: Satellite image over Legazpi. The red box identifies the 1 km x 1 km sample area for which the loss model was applied (taken from Ehrlich et al. 2010)



Methodology

The analysis for Legazpi that illustrates the use of high resolution satellite data for risk assessment is guided by the standard disaster risk equation (UNDRO 1979). Here, it is applied to building damages and therefore combines information on hazard intensity, the exposed building stock and the structural vulnerability of buildings (Eq 1):

$$1. \text{ Damage Risk} = \text{Building stock} * \text{structural vulnerability} * \text{hazard}$$

The building stock is the sum of the buildings in a given area. The physical damage refers to the structural damage to the buildings not taking into account the content of the building (the non-structural damage) such as furniture or other valuable assets. The physical damage to buildings is measured as a fraction of the repair cost over the cost of re-building. A slightly damaged building may be reported as 10 percent damaged when it would require one-tenth of its replacement cost to repair. A collapsed building would be assessed as 100 percent damaged since the entirety of the building needs to be reconstructed. The total damage to the building stock is the sum of the damages from every single building.

Two other estimates can be derived: the financial losses and the affected population. The financial losses—losses in short—are directly related to the physical damages to the building stock (Eq 2). The value of the total stock is calculated based on the cost of construction and thus varies with construction material and construction type. The cost is assessed based on local prices for material and wages. The total value of the building stock is the product of the cost of construction multiplied by the number of buildings. The losses are the product of the physical damages expressed as a share of the total building stock times the value of the building stock.

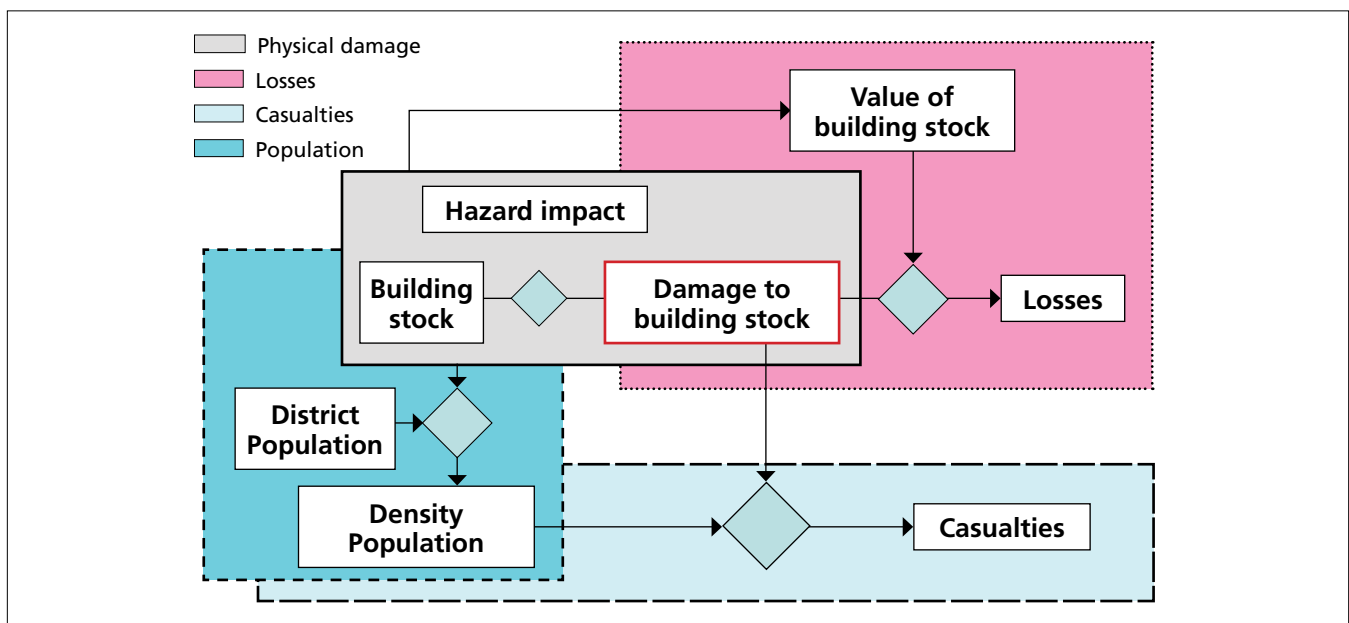
$$2. \text{ Losses} = \text{damaged building stock} / \text{building stock} * \text{value of building stock}$$

The affected population is assumed to be proportional to building damages (Eq 3).

$$3. \text{ Population} = \text{damaged building stock} / \text{building stock} * \text{total population}$$

Figure 14 shows the individual assessment modules that make up the risk modeling system: the physical damage, losses and casualty modules. The figure also shows the population module that is used to downscale population data when these are available in an aggregated form.

Figure 14: Workflow broken up in 4 modules, the physical damage module (gray), the loss module (pink) and the casualties modules (light blue), and the resident population model downscaled from district population statistics.



The foundation for the analysis is the assessment of the **building stock** that is used in every other module shown in Figure 14. In the **physical damage** module the building stock represents the exposed asset that is subject to the impact of the hazard. That impact is modulated by the intensity of the hazard. The loss module computes the value of the building stock based on local construction costs and then the losses based on fragility curves. In the population module the building stock is used as a proxy for human presence to downscale population figures. The four modules are described in turn below, first quantifying the exposed assets, namely the building stock and the population at risk, then modeling the damages based on hazard intensity.

Exposed assets

The exposed assets are the building stock and the population at risk. The building stock needs to be quantified and qualified based on the typology of buildings.

Quantifying the building stock

In disaster risk analysis the building stock is typically obtained by conducting ground surveys (e.g., Miura et al. 2008). The availability of very high resolution satellite imagery (VHR) allows generating building

stock inventories that also contain the spatial information on the buildings. This means that VHR imagery allows identifying and outlining every single building. With the building outline it is then possible to compute the building footprint area. In addition height of buildings can be derived from stereo imagery.

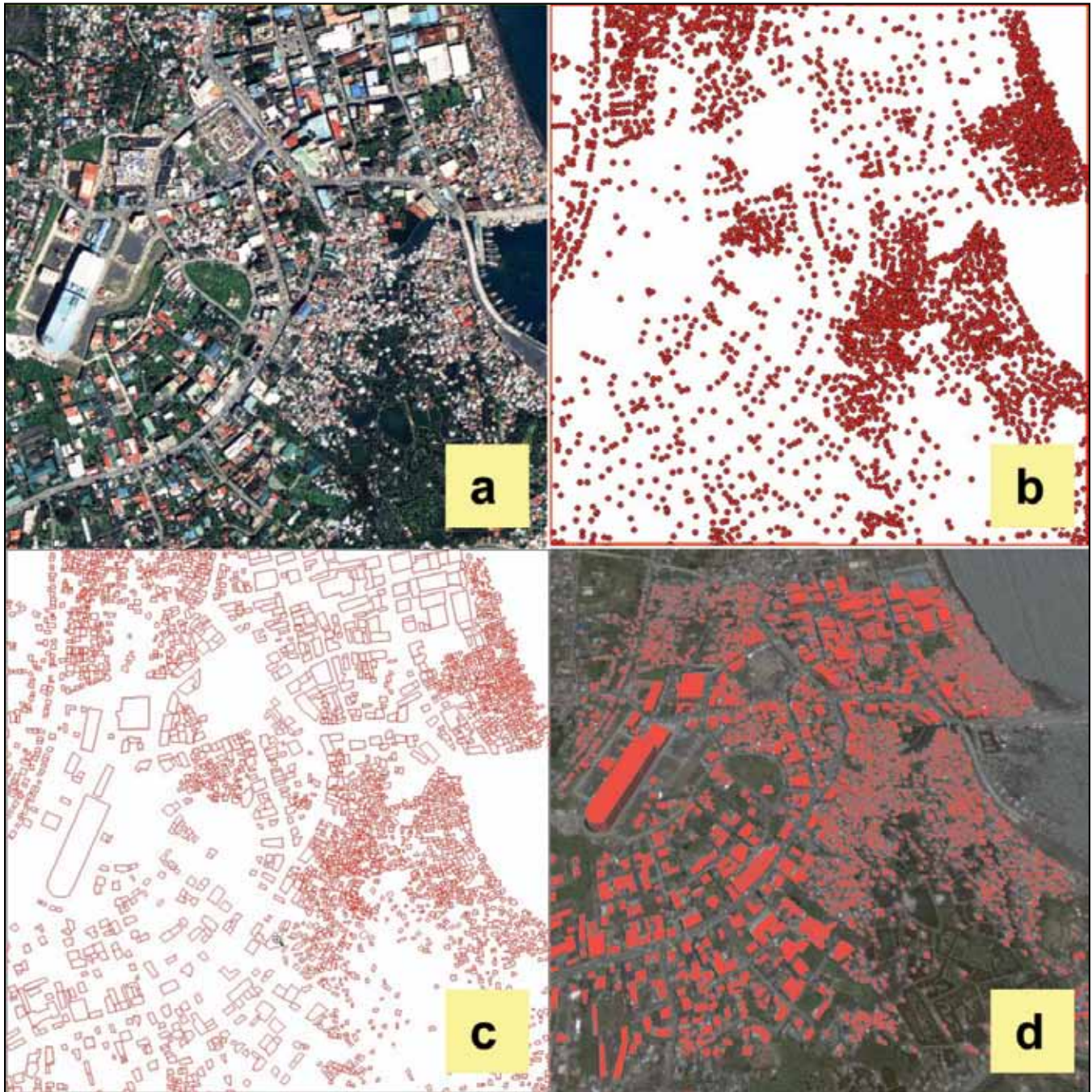
For the quantification of building stock three types of digital information products with increasing information content are shown in Figure 15. Figure 15a shows a pan-sharpened image from the Quickbird satellite from 2005 with a spatial resolution of 0.6 m. The high resolution allows the identification and location of buildings to generate a building presence data layer which is encoded as a dot layer and shown in Figure 15b. Building footprints can be outlined generating the building footprint areas which are encoded as polygons (Figure 15c). Finally, the building footprints may have the building height as an attribute thus providing building volumes (Figure 15d).

The information derived from these layers is shown in Table 5. In the present study the building footprint was used to measure the building stock and moreover to assess potential damages and losses. The building volume which is more costly and demanding to generate is a more precise measure that should be used when more precise modeling is carried out.

Table 5: Building stock for settlement sample area shown in Figure 13.

	Building location (no. of buildings)	Building footprint (area measure)	Estimated building volume
Building stock:	2990	254,916 m ²	1,584,067 m ³

Figure 15: Pan-sharpened Quickbird imagery (a). Building locations (b), building footprints (c) and building volumes (d).



Box 2. Information content of building stock derived from VHR imagery.

The scale and precision of the information derived from satellite images are a function of data input and data processing. Figure 15 above shows the results of processing QuickBird and Ikonos satellite images. Three information products—defined as information layers—with different information content can be derived:

- **Building locations (BL)** – with buildings located as dots.
- **Building footprints (BF)** – with building roofs or building bases outlined. This allows measuring the area occupied by buildings and thus provides basic information on building sizes and shapes.
- **Building volumes (B3D)** - buildings are outlined and a height measure is also available. This information layer provides also information on volumes of buildings.

The building location can be generated from all three information products. The area occupied by buildings can be estimated based on the average building footprints from BL and can be precisely derived from BF and B3D. The building volume can be estimated from BL based on an average building area, from BF based on an estimated average building height. And precisely from B3D by summing the volume of every single building.

Box Table: Deriving building stock statistics from information layers.

Building stock	Building location (Figure 15b)	Building footprint (Figure 15c)	Building 3D (Figure 15d)	To be used in the calculation of
Measures (from low to high precision)				
Number of buildings	Yes	Yes	Yes	Value, population presence and vulnerability
Area occupied by buildings	Estimated based on average building footprint area	Yes (see figure)	Yes	Value, population presence and vulnerability
Volume of buildings	Estimated based on average building footprint area and average building height	Estimated based on building footprint area and estimated average building height	Yes	To compute vulnerability, and likelihood to be exposed to hazard (e.g.tsunami)
Indirect measures				
Density building stock	<u>Point/area</u> density Yes (low precision)	Area/area density	Volume/area density	e.g. to compute vulnerability measure
Floor space	Estimated based on average building floor space	Assessed based on building footprint area	Assessed (based on number of floors and floor building space)	To compute value of building and potential population presence

Quality of the building stock

The quality of the building stock of a settlement, city, or country varies based on materials used, construction practices and enforcement of building standards. The quality of buildings determines the resilience to hazardous events referred to as structural vulnerability. Structural vulnerability is summarized by fragility or vulnerability curves. To calculate

and measure these curves, the building stock is typically subdivided in categories of building types. The classification below (Table 6) provides five categories of building types to be used in Legazpi. The list was adapted from the global inventory of building types available from the World Housing Encyclopedia (WHT 2009), from disaster risk work conducted in Manila (Miura et al. 2008), and from the authors' experience in the field.

Table 6: Categories of building type used in Legazpi to qualify the building stock.

Building type	Definitions	Brief description of structural characteristics of building type.	On Damage
1	Reinforced concrete frame with brick in fill walls	Structures constructed with highest standards. Typically employed for large and tall buildings. Will include hazard related building codes	Sustain pressure and vibration
2	Brick traditional with reinforced concrete columns	Buildings constructed according to engineering standards. Typically on cement pillars with roof/pavements also in cement.	Sustain pressures, shakes
3	Brick traditional	Traditional building standards using local expertise and material (mortar, adobe, bricks, wood). It largely varies from geographical areas.	These buildings are typically damaged during catastrophic events
4	Assembled material (brick and corrugated iron)	Dwellings constructed with assembled material for a lack of resources, typically found in poor neighbourhoods of urban centres and settlements.	Typically very instable and vulnerable to damage
5	Timber and bamboo or assembled material	Dwellings from material that needs to be constantly fixed and repaired.	May be resilient to earthquakes but very vulnerable to floods

Figure 16: Examples of the typology of buildings in Legazpi.



The enumerated building stock was classified in the five building type categories of Table 6 (see also Figure 16). Information gathered during the field visits informed further building classification within the area of interest. The main criteria used for labeling every single building was the building size (footprints), and the spacing of the buildings. Additional information related to the buildings' geographical location, their distance from the coast, and patterns

of building agglomerations. For example, very small buildings, spaced very closely with little footprint area are deemed to be of low quality in poor neighbourhoods (building type 4). Large buildings are classified as well constructed and likely to provide good resilience (building type 1 and building type 2), although in practice this would need to be confirmed on a case by case basis.

Figure 17: The qualification of the building stock on the 1 km x 1 km area under investigation.



Estimating exposed population

Natural hazards may hit the building stock in a very selective manner and only fine scale population datasets can provide an accurate estimate of the population affected. When fine scale population data are

not available, downscaling of available statistics collected at district level can produce useful estimates. The built-up area or the building stock is often used as a proxy variable for population presence.

Figure 18: Estimating population based on coarse administrative population figures and building stock. The district population totals (a), the built-up area under consideration (b), and the building footprints for the area under study (c).

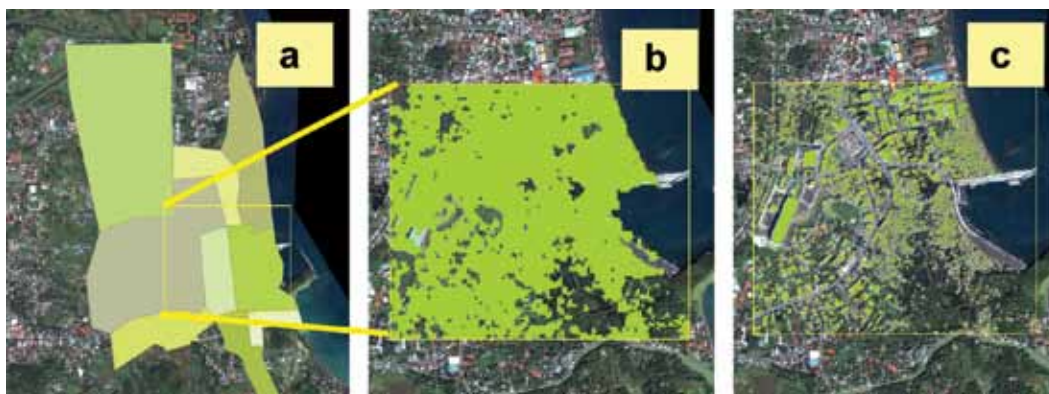


Figure 18a shows the districts for which population totals are available. Two district population figures were available: one provided by the World Health Organization (WHO) and based on the National Census of 2006 and an estimate from the Municipality of Legazpi for 2008 (Table 7). Both statistics used the same district boundaries. The two statistics are within the range of error of population estimates. For the estimation of affected people, the statistics from WHO are more suitable since they are closer in time to the satellite image from which the building stock was derived. The downscaling procedure proceeded as follows. The first step is to compute the total population of the districts that intersect the area under study (Figure 18a). Assuming that densities within these adjacent districts are homogeneous an area proportion between total population in districts and the area of interest yields the total population of the area of interest (Table 7).

Table 7: Downscaling of population statistics available at district level based on built-up area and building stock.

	Area (km ²)	WHO 2006	Municipality 2008
Districts intersecting the 1 km x 1 km study area	2.29	33,283	30,171
1 km x 1 km	1	14,534	13,175

The next step is to compute density measures. These can be derived for the built-up area as a whole (Figure 18b), or they can be related to the area taken up by buildings only (Figure 18c). Results are reported in Table 4, where the area unit of measurement is a 10 m x 10 m square. The figures suggest that over the entire built-up area (which includes roads, some open space between houses, etc.), there are slightly fewer than 2 people per 10 m grid square. If we only consider the buildings, there are approximately 6 people per 10 m square. This could be considered a measure of the average building space occupied by a household. Based on data collected from the field visits these estimates seem reasonable.

Table 8. The densities for the built-up area and the area of building footprints based on estimates of Table 3.

	Area (km ²)	Density over 10 x 10 m area
Built-up area in 1 km x 1 km	0.82	1.77
Building footprint area in 1 km x 1 km	0.25	5.81

Damage scenarios

Two scenarios have been implemented, one for tsunamis and one for earthquakes. They only include direct damages, not indirect effects such as landslides triggered by an earthquake. The two scenarios were selected in consultation with local experts as potential events with a high probability of occurring in the Legazpi region. The earthquake scenario assumes an event with an intensity of 8 on the Modified Mercalli Scale (MM). The tsunami event assumes a wave height of 4 m at the shoreline, impacting the coastline at right angles. In practice, probabilistic models would be developed by hazard specialists to assess the return period for a given intensity and to assess various scenarios with different intensities.

The impact scenarios are based on a building damage model structured within a geographical information system. The current models were developed using knowledge gathered from open sources, reviewed literature and field visits. Model parameters could be refined further based on consulting additional experts and professionals in the area.

Earthquake disaster risk

Earthquakes originate as a result of abrupt displacements of the earth crust. Each major displacement is usually followed by smaller adjustments referred to as aftershocks. The displacements generate seismic waves that are propagated through the earth crust and are abated as a function of distance and geology. The shaking varies in space and as a function of

the seismic waves through which the energy is propagated. The overall shaking at a given point—what is referred to as earthquake intensity—is measured as peak ground acceleration. The peak ground motion acceleration is computed based on earthquake magnitude, distance from epicenter and geological and soil characteristics that determine the soil liquefaction potential that may amplify or reduce the effect of the wave.

The city of Legazpi spans an area of over 30 km². It displays different geological and soil characteristics that include swamp areas, volcanic soils and more solid ground closer to the hills in the South of the city. Soil or geological map information for the area were unavailable for Legazpi. For this exercise we assume that, for the 1 km x 1 km area shown in Figure 13, the shaking intensity would remain constant.

Earthquake physical damage

The damage to the building stock for a given earthquake intensity is also determined by the structural vulnerability summarized by fragility curves. These curves express damage to a given category of buildings as a function of intensity. While widely available in high income countries, vulnerability curves are often not available in low income countries. In the Philippines for example, vulnerability curves for earthquakes are available for the building stock of Manila (Miura et al. 2008). That building stock however is different from Legazpi. Legazpi has a large proportion of informal, often wooden, housing that is not considered in the Miura et al. (2008) study.

For this exercise we have simulated an earthquake with intensity 8 of the Modified Mercalli (MM) scale.

MM is a standard scale used for measuring earthquake intensities that provides a qualitative relationship between shaking intensity, type of buildings and degree of damage. It ranks earthquake effects on a scale of 1 to 12, with 1 indicating that the tremor is not felt by persons, and 12 implying almost complete destruction. The intensity scale 8 is ranked destructive with an average ground peak acceleration of 0.25-0.30 g, where g is the speed of gravitational acceleration (9.8 meters per second squared; Smith, 2008). Its effects are described as:

“Damage slight in specially designed structures; considerable in ordinary substantial buildings with partial collapse. Damage great in poorly built structures. Fall of chimneys, factory stacks, columns, monuments, walls. Heavy furniture moved, Sand and mud ejected in small quantities, Changes in well water, Persons driving cars disturbed.”

Because of the lack of vulnerability curves for Legazpi city, the qualitative description of the MM was translated into damage percentages used in the simulation as shown in Table 9. This is an approximation with obvious limitations. First, hazard intensity-damage relations need to be measured systematically on probability functions of increasing damage states, as shown in Miura et al. (2008). Second, these relations need to be developed for the building stock under analysis that includes both the formal housing and informal housing stock. For this illustrative case study in Legazpi, the estimates in table 5 suffice. For an operational implementation, improved vulnerability estimates could be derived for instance using a Delphi method as proposed by Miura et al. (2008).

Table 9: Empirical fragility curves for earthquake intensity MM 8 adapted to the building typology of Legazpi.

Building Type	Description building type	Damage description	Damage
1	Reinforced concrete frame with brick in-fill walls	Slight	5%
2	Brick traditional with reinforced concrete columns	Slight	10%
3	Brick traditional	Considerable	30%
4	Assembled material (brick and corrugated iron)	Great	80%
5	Timber and bamboo or assembled material	Great	60%

Applying the damage proportions in Table 5 to the estimates of total building stock—measured as the total area covered by building footprints in each building type category—yields estimates of total damages by type of building. They are shown in Table 10.

Earthquake losses

The monetary losses can be estimated similarly to physical damage. Losses relate to the replacement value of the building that, in turn, is related to the quality of building material. The building stock value considered in this exercise is the cost of reconstruc-

tion. These estimates were made available by local construction engineers in Philippine Pesos (PHP). The values available were then converted into US Dollar (USD) per surface unit. The total value of the building stock of a given building type is the product of the footprint area times the cost per unit area. The losses are then the product of the expected damage expressed as percentage for a given building type. Table 10 shows the value for each building type together with the total value of the building stock. Damages and losses are given according to the values of the fragility curves.

Table 10: Earthquake losses to the building stock based on the typology of buildings.

Building type	Total building stock (m ²)	Value (USD/ m ²)	Total value of building stock (USD)	Damage (%)	Total damage (m ²)	Total losses (USD)
1	18328.3	435	7,972,810	5	916.4	398,640.5
2	73413.6	250	18,353,400	10	7,341.4	183,534.0
3	102151.1	110	11,236,621	30	30,645.3	3,370,986.3
4	60548.4	65	3,935,646	80	48,438.7	3,148,516.8
5	383.3	10	3,833	60	230.0	2299.8
Overall	254824.7		41,502,310		8,7571.8	8,755,783.4

Earthquake affected population

The entire population within the area under study would be affected by the earthquake (Table 10). The potential fatalities can be estimated from the collapse ratio. We hypothesize that the buildings would collapse when damage is higher than 60% for either brick or concrete buildings. In this simulation this occurs for categories 4 and 5 that account for over 60,000 square meters of buildings. That living space would account for up to 4,800 people. This is a crude and probably worst-case estimate, since the actual number of people possibly affected by collapsing buildings will be influenced, for instance, by the time of day of the event. During day time, many people will be outside, while losses may be highest during nighttime. Estimates from past events would help refine these numbers.

Tsunami disaster risk

The impact of storm surges or tsunamis on built-up and populated areas can be devastating. Sea level surges or tsunamis may originate from earthquakes, underwater landslides or due to the wind pressure exerted by cyclones. Due to the strong energy released a large volume of surges may travel long distances in the open ocean. The occurrence of tsunamis is highly dependent on their source and wave propagation. The city of Legazpi could be affected by a tsunami, either when triggered by an earthquake from a nearby tectonic structure or by a debris avalanche reaching Albay Bay if the peak of Mount Mayon collapsed.

The damaging effect of tsunamis depends on wave height and wave speed. The wave height is a function of local bathymetry, on land topography and shoaling—the increase in height due to bathymetric characteristics. The velocity and wave height deter-

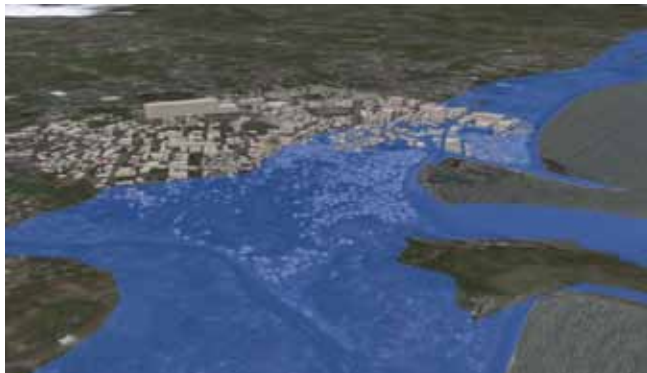
mines the pressure exerted on buildings and therefore their destructive behavior. The tsunami wave diminishes as a function of distance, topography, and surface characteristics often referred to as surface roughness. Modeling precise wave impacts on built-up infrastructure requires in-depth modeling which is beyond this case study.

An often applied method for calculating the effects of tsunami inundation is a simple ‘bathtub’ approach, assuming the water flows inland until it reaches a specified elevation equal to the expected wave height at the shore (White et al. 2003). This approach has been used, for example, to model inundation potential due to a tsunami wave in Alexandria, Egypt (Eckert and Zeug 2009).

Tsunami physical damage

The Legazpi case study employs an inundation model developed by the UK Tsunami Initiative (NERC 2009). For modeling the potentially inundated areas the following is assumed: on flat lying coastlines the extent of the inundated zone depends more on surface roughness than on topography. The applied model (see equation 4) calculates the inundation distance from the shoreline resulting from a certain tsunami wave height assuming also that the water flows inland with a distance that is proportional to the height of the wave at shore and to a friction factor that slows the water flow. The friction factor is measured based on “roughness coefficients” that are mainly determined by land use and land cover.

Figure 19: Simulation for a the inundation caused by a 4 m high tsunami wave over Legazpi.



Roughness coefficients for land use categories in the Legazpi region are listed in Table 11. As this exercise is limited to a study area in a central part of the town with mixed use (residential, commercial, business), the only land use considered is of the type “built-up”. For a full scenario covering the full city area, the corresponding land uses can be derived from satellite imagery.

Table 11: Roughness coefficient based on land use.

Landuse type	Roughness coefficient
Mud flats, ice, open fields without crops	0.015
Built-up areas	0.035
City centre	0.100
Forests, jungles	0.070
Rivers, lakes	0.007

The inundation distance from the shore and produced by a tsunami of height H_0 is calculated as follows:

$$(4) X_{max} = 0.06 H_0^{4/3} / n^2$$

where n is the surface roughness coefficient as derived from Table 7 and H_0 the wave height at the shore. The simulated tsunami is based on a historic tsunami event in Luzon and Mindoro islands with a wave height of 4 m at the shoreline (Imamura et al. 1995). This resulted in the inundation distances shown in Table 12. This distance from the shore up to which inundation may reach inland differs by land use types. In a 4 m scenario, the inundation of roads, for example, could extend up to 7 km distance from shore due to their low roughness.

Table 12: Inundation distance from shore based on roughness coefficients and eq. 1.

Land use type	Roughness coefficient	X_{max} [4 m scenario]
City centre	0.100	38 m
Trees and forest	0.070	78 m
Built-up areas	0.035	311 m
Open fields and roads	0.015	1.7 km
Rivers and lakes	0.007	7.8 km

The damage to the building stock is a function of the energy from wave impact and the vulnerability of the buildings expressed as fragility curves. As these fragility curves for a tsunami are not available for this part of the Philippines, fragility curves that have been reported for the July 2006 South Java tsunami (Reese et al. 2007) have been applied. This assumes that the building stock of Legazpi is similar. One factor influencing damages is the inundation height. The study distinguished three intensity levels: for an inundation height less than 1 meter, between 1 and 2 meters, and for over 2 meters (Figure 20). Apart from water depth, several other factors are influencing the degree of damage and could be incorporated based on empirical evidence from past events or suitable assumptions. These include flow velocity, the amount of debris and whether or not a house is shielded by other buildings.

The building types applied in this study were regrouped to fit with the building classes reported by Reese et al. (2007). The damage observations were translated into

percentage of damage for each of the three intensity zones. Assuming the 4 m wave scenario all buildings fall into one of the three inundation zones. Table 13 shows 5 different building types and corresponding fragility values for the three intensities.

Figure 20. Inundation height zones of a 4 m tsunami wave.



Table 13: Building types and corresponding damage values per building type.

Building types (Reese et al. 2007)	% damage (inundation < 1 m)	% damage (inundation 1-2 m)	% damage (inundation > 2 m)
1 Reinforced concrete-frame with brick infill walls	5 %	15 %	20 %
2 Brick traditional with RC-columns	10 %	25 %	60 %
3 Brick traditional	25 %	70 %	100 %
4 Assembled material	25 %	70 %	100 %
5 Timber/bamboo	25 %	70 %	100 %

Tsunami damages and losses

The three intensity zones provide damages and losses shown in Table 14 to Table 16. Each zone has a different amount of exposed assets (the total building stock) and percentage of damage for the different

building types. Table 14 identifies the building stock for the 1m inundation height and Table 15 and Table 16 for respectively the 1 m to 2 m and the 2 m and higher inundation heights.

Table 14: Damages for the intensity determined by 1 m inundation height.

Building type	Total building stock (m ²)	Value (USD/ m ²)	Total value (USD)	Damage (%)	Total damage (m ²)	Total losses (USD)
1	2126.9	435	925214.6	5	106.3	46260.7
2	9783.7	250	2445915.0	10	978.4	244591.5
3	6517.9	110	716964.6	25	1629.5	179241.2
4	6661.9	65	433024.2	25	1665.5	108256.0
5	46.1	10	460.7	25	11.5	115.2
Overall	25136.4		4521579.0		4391.2	578464.6

Table 15: Damages for the intensity determined by a 1 m to 2 m inundation height.

Building type	Total building stock (m ²)	Value (USD/ m ²)	Total value (USD)	Damage (%)	Total damage (m ²)	Total losses (USD)
1	2126.9	435	925214.6	15	319.0	138782.2
2	16816.6	250	4204142.5	25	4204.1	1051035.6
3	12765.7	110	1404221.5	70	8936.0	982955.1
4	15867.9	65	1031412.9	70	11107.5	721989.0
5	172.0	10	1720.3	70	120.4	1204.2
Overall	47749.1		7566711.7		24687.1	2895966.1

Table 16: Damages for the intensity determined by more than 2 m inundation height.

Building type	Total building stock (m ²)	Value (USD/ m ²)	Total value (USD)	Damage (%)	Total damage (m ²)	Total losses (USD)
1	0.0	435	0	20	0	0
2	9340.7	250	2335185.0	60	5604.4	1401111.0
3	12482.4	110	1373061.8	100	12482.4	1373061.8
4	33504.0	65	2177757.4	100	33504.0	2177757.4
5	106.8	10	1067.9	100	106.8	1067.9
Overall	55433.9		5887072.1		51697.6	4952998.1

Tsunami affected population

The population affected is that residing in the three intensity zones. It is estimated by intersecting the inundation zones with the distribution of the population before the hazard event. The estimate shows more than 4,200 people to be affected by a 4 m tsunami wave within the 1 km x 1 km test area alone. Fatalities for such an event are not estimated for two main reasons. First, there are no good estimates for mortality during similar events that might provide guidance. Second, fatalities are often due to the debris floating in the water that would require development of a hydrodynamic impact model.

This case study application for Legazpi illustrates how the data sources and tools discussed in Section 2 can be applied for urban risk assessment. The use of VHR satellite images makes it far easier to extract up-to-date indicators of interest—on hazard, exposure and vulnerability. The integration of all data in a GIS supports their joint analysis to generate policy relevant risk information. The following section discusses some of the institutional issues that need to be considered for these techniques to be more widely applied, especially in medium sized cities located in hazard prone areas.

Implications and institutional issues

The study presented in this report had two main objectives. The first has been to provide an overview of geo-information tools that are useful for relatively low-cost and relatively low-tech risk assessments that can be conducted even by smaller municipalities. Section 2 of this report introduces the main concepts, highlighting the great utility of the new generation of very high resolution satellite data for filling data gaps that continue to plague risk assessment in many countries. The Appendix provides a more technical review of remote sensing and analysis of earth observation products. The second objective was to provide a case study illustrating how these tools can be used. Section 3 describes an application that generates basic estimates of risk from earthquakes and tsunamis in Legazpi, Philippines. Both, the overview and the case study use the standard hazard risk model, where risk is a function of hazard probabilities, exposure, and vulnerability of the exposed elements.

The following paragraphs summarize some of the main lessons from this study. They also highlight some of the institutional issues that will emerge when individual cities or urban managers at the state or central government level want to strengthen hazard risk assessment capacity.

Start small. Many large cities with well-known hazard risk have conducted sophisticated risk assessments, often implemented by international consulting firms. Bogota and Istanbul are well documented examples. For most smaller and medium-sized cities the cost and complexity of a sophisticated geo-physical and economic risk assessment present barriers that are difficult to overcome. But, as shown in the examples in this report, even relatively simple analysis that does not require highly specialized skills can have high pay-offs. Even the initial step of getting up-to-date geographic data products such as printed satellite maps into the hands of urban managers can trigger greater awareness and better decisions. More sophisticated analysis can follow and well documented initial efforts help raise support from higher levels of government or international donors. In fact, a municipality showing its motivation to get serious about disaster risk reduction by implementing an initial, local assessment can overcome the hazard or disaster funding paradox: it is often far easier to mobilize resources from national or international sources for recovery and reconstruction after disaster strikes, than to obtain support for a *priori* risk assessment and mitigation.

Use those resources that are most abundant locally. Risk assessment requires a broad range of skills. Some of these are scarce in all but the largest cities. This includes geologists or remote sensing specialists. But some resources are abundant at the local level. One is knowledge and experience of local conditions. In most cities, many of the risk factors will be well-known as hazard events have occurred before. Action is often not taken, not because the risks are unfamiliar, but because they are not well documented which is a pre-requisite for making the case for mitigation.

The second abundant local resource in many developing country cities is relatively low-cost labor. A surprising fact about satellite data products is that as their level of resolution and sophistication increases, the best tools for interpreting them tend to be simple manual techniques rather than sophisticated automated procedures. While medium resolution vegetation mapping from Landsat images can be done using standard computer algorithms, for example, the best way to extract features from a VHR image of a city is to trace them manually on a computer screen. This can be done locally with relatively simple hardware and software. Furthermore, relevant information about the characteristics of these features—such as building materials, quality of construction or occupancy rates—needs to be collected in the field. Here again, locals have an advantage from reduced travel costs to knowledge of the terrain and conditions. Taken together, local resources can be mobilized to develop a comprehensive urban GIS database that includes information relevant for identifying exposure and vulnerability to hazards.

Think beyond hazards. Even when exploiting local resources, acquisition and initial processing of VHR satellite data, as well as hardware and software for database development and analysis, will represent a significant investment for a municipality. These costs become far more justifiable when one considers that most of the information collected for hazard risk assessment is identical to that required for many other urban management functions. Information on the housing stock, public buildings, transport right-of-ways, or public services infrastructure describes exposure, and information about their status and quality sheds light on vulnerability. But at the same time, this information is critical for good urban management, for instance as the basis of zoning decisions, prioritizing public investments, and scheduling operations and management tasks. Closely aligning information policies across municipal departments will save funds and increase effectiveness.

Beyond cost savings, there are additional reasons why disaster risk reduction and general city management need to be closely integrated (see Lall and

Deichmann 2009). Many risk mitigation activities are simply good urban management practices, such as organizing regular trash collection to avoid drainage channels filling up with garbage; ensuring that steep and unstable slopes or areas on floodplains are not made available for settlement or commercial activities; or promoting good building practices and enforcing minimum safety standards for new construction. So, hazard risk management should not be considered as separate from other urban management but seen as an integral part of it.

Get economies of scale for more sophisticated tasks.

While urban hazard management activities are best performed at the local level, some hazard assessment functions are required only periodically or are too specialized to be replicated in each municipality. For instance, assessing hazard probabilities requires geologists, seismic specialists, hydrologists or engineers. Most physical hazard characteristics, such as ground shaking probabilities or flood zones, do not change frequently, so an assessment will be valid for some time. Satellite data also do not need to be procured and pre-processed very often. Depending on the speed of urban change, annual or biennial images will be sufficient. Such specialized and periodic tasks are therefore best outsourced, either to the private sector, or to a government institution at the state or national level that specializes in remote sensing or hazard modeling.

Be transparent. Information gets more useful the more people have access to it. Credible information on natural hazard risk that is widely disseminated has many benefits. It makes zoning and other planning decisions more transparent, it allows land and housing prices to reflect risk, allows citizens to make informed decisions about the trade-off between cost and risk, and it encourages private sector mitigation or risk transfer through insurance. Cities should therefore promote an open data policy that maximizes use of publicly generated information by all stakeholders.

This report is about one set of tools—geospatial data collection and analysis—that supports better hazard

risk assessment in cities. High resolution satellite images can provide information that is not easily derived from other sources. But this information is only one piece of the puzzle. Satellite derived geospatial data needs to be embedded in a broader risk assessment approach that relies on administrative data,

ground surveys and expert assessments. By providing an up-to-date and easy-to-interpret snap shot of a city and its environs it can help answer policy relevant questions such as probable future losses, priority areas for retrofitting buildings, and safer land use management options.

References

- Alexander, D., 2006. Globalization of disaster: trends, problems and dilemmas. *Journal of International Affairs*, 59, 1- 22.
- Anderson, J. R. 1971. Land use classification schemes used in selected recent geographic applications of remote sensing: *Photogrammetric Engineering and Remote Sensing*, 37: 379-387
- Blong, J., 1984. *Volcanic hazards, a sourcebook on the effects of eruptions*. Academic Press, Sidney.
- Bommer, J., R. Spence, M. Erdik, S. Tabuchi, N. Aydinoglu, E. Booth, D. del Re and O. Peterken. (2002). Development of an earthquake loss model for Turkish catastrophe insurance. *Journal of Seismology*, 5: 431-446.
- Bonne, K., Kervyn, M., L. Cascone, S. Njome, E. Van Ranst, E. Suh, S. Ayonghe, P. Jacobs and G. Ernst. 2008. A new approach to assess long-term lava flow hazard and risk using GIS and low cost remote sensing: the case of Mount Cameroon, West Africa. *International Journal of Remote Sensing*. 29: 6539-6564.
- Colombi, M, B Borzi, H. Crowley, M. Onida, F. Meroni and Rui Pinho. 2008. Deriving vulnerability curves using Italian earthquake damage data. *Bulletin of Earthquake Engineering*, 6: 485-504.
- Congalton, R.G. and K. Green, 1998, *Assessing the accuracy of remotely sensed data: principles and practices*, CRC Press, Boca Raton, FL.
- CORINE (1984): Land Cover Technical Guide, publ. 1994 EU, ISBN 92-826-2578-8 Available at <http://reports.eea.europa.eu/COR0-landcover/en>
- Dilley, M., Chen R., Deichmann U., Lerner-Lam L., Arnold M., 2005. Natural Disaster Hotspots: A global Risk analysis. The International Bank for Reconstruction and Development, The World Bank and Columbia University, Washington. Pp 142.
- Douglas J., 2007. Physical vulnerability modelling in natural hazard risk assessment. *Natural Hazards and Earth System Science*, 7: 283-288.
- Eckert, S., Zeug. G. (2009): Assessing Tsunami Vulnerability in Alexandria, Egypt by using optical VHR satellite data. In: Proc. of the 33rd International Symposium on Remote Sensing of Environment. May 04-08, 2009. Stresa, Italy.
- Ehrlich, D., H. D. Guo, K. Molch, J. W. Ma, and M. Pesaresi, 2009. Identifying damage caused by the 2008 Wenchuan earthquake from VHR remote sensing data. *International Journal of Digital Earth*, 2m 4:1-18.
- Ehrlich D., G. Zeug J. Gallego, A. Gerhardinger, I Caravaggi, M Pesaresi, 2009. Quantifying the built-up stock from VHR optical satellite imagery for assessing disaster risk. Geocarto International, *In Press*.
- EM-DAT 2009: The OFDA/CRED International Disaster Database – www.emdat.be, Université Catholique de Louvain, Brussels (Belgium);
- Estes, J. E., J. Hajic and L. R. Tinney, 1983. Fundamentals of image analysis: analysis of visible and thermal infrared data. In Colwell, R.N., D.S. Simonett and F. T. Ulaby (eds), *Manual of Remote Sensing*, Vol 1. American Society of Photogrammetry, Falls Church Virginia, pp. 987-1124.
- FAO, 2008. Africover, <http://www.africover.org/>
- FEMA55. "Coastal Construction Manual", Third Edition, Federal Emergency Management Agency
- GEOS (Group on Earth Observation), 2007. The full picture. Tudor Rose, London. Pp 287.
- Ghesquiere, Francis, Luis Jamin and Olivier Mahul. 2006, Earthquake Vulnerability Reduction Program in Colombia - A Probabilistic Cost-benefit Analysis, Policy Research Working Paper #3939, World Bank, Washington, DC.
- Giardini, D., 1999. The global seismic hazard assessment program (GSHAP) – 1992/1999. *Annali di geofisica*, 42: 957-974.
- Hollenstein, K, 2005. Reconsidering the risk assessment concept: Standardizing the impact description as a building block for vulnerability assessment. *Natural Hazards and Earth System Sciences*, 5: 301-307.

- Hong, Y., Adler, R, and G. Huffman, 2007. Use of satellite remote sensing data in the mapping of global landslide susceptibility. *Natural Hazards*, 43:245-256.
- Imamura, F., Synolakis, C.I., Gica, E., Titov, V. Listanco, E., Jun Lee, H. (1995): Field survey of the 1994 Mindoro Island, Philippines, Tsunami. *PAGEOPH*, Vol. 144, No. 3/4.
- ISDR 2009 – GAR report
- Jensen, J. and D. Cowen, 1999. Remote sensing of urban/suburban infrastructure and socio-economic Attributes. *Photogrammetric Engineering and Remote Sensing*. 65:611-622.
- Kervyn, M., G. Ernst, R. Goosens. And P. Jacobs, 2008. Mapping volcano topography with remote sensing: ASTER vs. SRTM. *International Journal or Remote Sensing*. 29: 6515-6538.
- Kircher, C. A., Nassar, A. Al, Kutsu, O and Homes, W. T., 1997. Development of building damage functions for earthquake loss estimation, *Earthquake Spectra* 13(4), 663-682.
- Kircher, C., Whitman, R and W. Homes, 2006. HAZUS Earthquake loss estimation methods. *Natural hazards review*, 7: 45-59.
- Lall, S.V. and U. Deichmann (2009), Density and disaster: Economics of urban hazard risk, Policy Research Working Paper 5161, Development Research Group, World Bank, Washington, D.C.
- Lang, K (2002). Seismic vulnerability of existing buildings, Ph. D. Thesis. Institute of Structural Engineering, Swiss Federal Institute of Technology. Dissertation ETH No. 14446. pp. 190.
- Lu George, Chiu L. and Wong, D, 2007. Vulnerability assessment of rainfall-induced debris flows in Taiwan. *Nat. Hazards* 43:223-244.
- Mileti, D, 1999, Disasters by design, a reassessment of natural hazards in the United States. Josph H Press, Washington, D. C. 351.
- Miura, H., Midorikawa, S., Jujimoto, K., Pacheco, B., Yamanaka, H., 2008. Earthquake damage estimation in Metro Manila, Philippines based on seismic performance of building evaluated by local experts' judgements. *Soil Dynamics and Earthquake Engineering*, 28, 764-777.
- Muller, M., K. Segl, U. Heiden and H Kaurmann, 2006. Potential of high-resolutio satellite data in teh context of vulnerability of buildings. *Natural Hazards* 38: 247-258.
- Nadim, F. Kjekstad O., Domaas U., Rafat R., and P. Peduzzi. 2006. Global landslides risk case study. Chapter 2, Pp 21-77. in *Natural Disaster Hotspots Case studies*, Disaster management Series, No. 6. The World Bank.
- National Research Council, 2004. Partnerships for reducing landslide risk. Assessment of the National Landslide Hazards Mitigation Strategy. Committee on the Review of the National Landslide Hazards Mitigation Strategy, The National Academies Press, Washington, D.C., pp. 131.
- NERC, 2009: The Tsunami Initiative. Linking Insurance and Science. (www.nerc-bas.ac.uk/tsunami-risks)
- Office for the Coordination of Humanitarian Affairs (OCHA), 2008. Relief web. (www.reliefweb.int/rw/dbc.nsf/doc100?OpenForm)
- Peduzzi, P. (2006). The disaster risk index: overview of a quantitative approach. In: Birkmann, J. (ed.), *Measuring Vulnerability to Natural Hazards – Towards Disaster Resilient Societies*. UNU-Press Tokyo, New York, Paris.
- Pesaresi, M. , Gerhardinger A., Kayitakire F. (2008). A robust built-up area presence index by anisotropic rotation-invariant textural measure. *IEEE, Journal of Selected Topics in Applied Earth Observation and Remote Sensing*, 3, 180-192.
- PHIVOLCS (2009): Philippine Institute of Volcanology and Seismology, Volcano Monitoring and eruption prediction division. Chronology of historical eruptions of Mayon volcano. http://volcano.phivolcs.dost.gov.ph/update_VMEPD/Volcano/VolcanoList/mayon.htm
- Reese, S., Cousins, W. J., Power, W. L., Palmer, N. G., Tejakusuma, I. G., Nugrahadi, S. (2007): Tsunami vulnerability of buildings and people in South Java – field observations after the July 2006 Java

- tsunami. *Nat. Hazards Earth Syst. Sci.*, 7, 573–589, 2007
- Sakellariou, M. G., and M. D. Ferentinou, 2001. GIS-based estimation of slope stability, *Natural Hazards Review*, 2: 12 -21.
- Scawthorn, C., F. Asce, P. Flores, N. Blais, H. Seligson, E. Tate, S. Chang, E. Fiffilin, W. Thomas, J. Murphy, C. Jones, and M. Lawrence, 2006. HASUS-MH Flood loss estimation methodology. II. Damage and loss assessments. *Natural Hazard Review*, 7: 72-81.
- Spence, R., I Kelman, E. Calogero, G. Toyos, P. Baxter, and J-c. Komorowski, 2005. Modelling expected physical impacts and human casualties from explosive volcanic eruptions. *Natural Hazards and Earth System Sciences*, 5, 1003-1015.
- Spence R., 2009. Earthquake Risk Mitigation – The Global Challenge. In *Earthquakes and Tsunamis.*, Ed. Tugrul Tankut. Springer, The Netherlands. Pp. 35-52.
- Smith, K., 2008. *Environmental Hazards*, Fourth Edition. Routledge.
- UNDRO (United Nations Disaster Relief Coordinator), 1979. Natural disaster and vulnerability analysis. In: Report of Expert Group Meeting (9-12 July 1979). UNDRO, Geneva.
- UNDRO (United Nations Disaster Relief Coordinator), 1979. Natural Disaster and Vulnerability Analysis in Report of Expert Group Meeting (9-12 July 1979). UNDRO. Geneva.
- Vicerky, P., P. Skerlj, J. Lin, L. Twisdale, Jr., M. Young, F. Lavelle, 2006. HAZUS-MH Hurricane methodology. II: Damage and loss estimation. *Natural Hazards Review*, V. 7 pp. 94-103.
- Vogelman, J. E., T. Sohl, and S. M. Howard, 1998. Regional characterization of land cover using multiple sources of data. *Photogrammetric Engineering and Remote Sensing*. 64: 45-57.
- White, L. Vieux B., Armand, D and LeDimet F., 2002. Estimation of optimal parameters for a surface hydrology model. *Advances in Water Resources*, 3, 337-348.
- WHT (2009). *World Housing Encyclopedia*. An Encyclopedia of Housing Construction in Seismically Active Areas of the World. www.world-housing.net/
- Wikipedia (2009): The Mercalli intensity scale. <http://en.wikipedia.org/wiki/Mercalli>
- World Bank. 2004. *Natural Disaster Hotspots, Case Studies*. Disaster Risk Management Series No. 6. Washington pp. 184.
- World Bank, 2008. *Climate resilient cities*. The World Bank. Washington, pp. 150.
- World Bank-UN, 2010. *The Economics of Disaster Risk Reduction, Global Facility for Disaster Reduction and Recovery*, forthcoming.
- World Housing Types. <http://www.world-housing.net/>
- Small, C. , 2009. The Color of Cities: An Overview of Urban Spectral Diversity, in *Global Mapping of Human Settlements*, P. Gamba & M. Herold (eds), Taylor & Francis, In Press.
- Roberts, D.A., Dennison, P.E., Peterso, S., Sweeney, S., & Rechel, J. , 2006. Evaluation of airborne visible/Infrared imaging Spectrometer (AVIRIS) and Moderate Resolution Imaging Spectrometer (MODIS) measures of live fuel moisture an fuel condition in a shrubland ecosystem in southern California. *Journal of Geophysical Research*, 111, 1-16.
- Zeug, G., Brunner, D., Scavazzon, M. (2009): An efficient GIS concept for disaster management in developing countries based on virtual globes. *International Journal of Information Systems for Crisis Response and Management*. Vol. 4 (4).

Technical Appendix

A survey of the use of high spatial resolution optical satellite imagery for natural hazard risk identification and mapping⁷

Introduction

This survey provides a more technical overview of the use of high resolution satellite images for natural hazard and vulnerability identification and mapping in urban settings than the brief, more policy oriented overview in Section 2. Some of the information presented in Section 2 is covered here again so this technical appendix can be read on its own.

The survey is structured around a sequence of tasks commonly involved in the use of very high resolution (VHR) satellite images—also called high resolution optical (HRO) imagery. Extraction of information from imagery occurs in several distinct, but related, phases. The initial phase involves acquisition, display and enhancement of the imagery to facilitate reconnaissance. The reconnaissance phase involves visual interpretation to determine what information the imagery can provide. If the analyst determines that the imagery does contain useful information, in an extractable form, a quantitative analysis may be conducted to identify the features of interest and extract the information. The final phase is often referred to as mapping if the spatial geography is retained but it is also possible to extract non-spatial information. Mapping capabilities of VHR imagery are determined primarily by spatial and spectral resolution (explained below) and, to some extent, by temporal resolution.

In the context of this survey, VHR imagery is defined on the basis of spatial and spectral resolution. Spatial resolution determines the size of the smallest object the sensor can image coherently. It also determines the sharpness or detail with which larger objects can be imaged. Spectral resolution, along with dynamic range, determine how many and which colors a sensor can discriminate. This is important because many sensors can detect both visible and infrared light reflected and absorbed by different materials. In many cases, the infrared part of the spectrum provides information that makes it possible to discriminate between materials that may be indistinguishable in visible light alone. In this survey VHR imagery is defined as that having meter scale (1-10 m pixels) spatial resolution and multispectral (2-8 color bands) spectral resolution. This distinguishes VHR imagery from decameter (10-100 m) and kilometer (1000-10,000 m) resolution imagery often used for hazard mapping. It also distinguishes it from single band panchromatic imagery (analogous to black and white aerial photography) and hyperspectral imagery containing hundreds of spectral bands. These distinctions and their relevance are discussed in more detail below.

Reconnaissance, Identification and Mapping. It is also important to distinguish among the fundamental tasks of mapping, identification and reconnaissance. In the context

of this report, *Reconnaissance* is a preliminary survey to gain information to be used to define the Identification and Mapping tasks. *Identification* is the process of determining which of the objects turned up by the reconnaissance phase might be accurately mapped. *Mapping* is defined as the process of isolating the objects of interest, delineating their spatial location, extent and, in some cases, extraction of ancillary information about the objects. Taken in sequence these fundamental tasks can provide the basis of a strategy for systematic application of VHR imagery to hazard, exposure and vulnerability identification.

A Strategy for using VHR imagery. One possible approach to hazard assessment could involve a succession of processes intended to determine what relevant information can be extracted from the VHR imagery and to define an effective procedure for extracting the information, as well as some estimate of the accuracy of the result. The sequence of Reconnaissance, Identification and Mapping (R-I-M) described above mimics the process used by the human eye-brain system to extract information from visual stimulus. One benefit of the R-I-M strategy is that it outlines a procedure to determine whether the imagery contains useful information and, if so, to extract that information from the imagery. If the desired information cannot be identified in the imagery, or cannot be extracted unambiguously, there is no reason to invest time, effort and resources toward subsequent analysis.

Overview

Because VHR remote sensing relies on processes and technology not generally familiar to most people, it is necessary to define some basic concepts and terminology used to discuss the technology and processes. This section introduces these basic concepts and provides a brief summary of the main sections of the survey. A glossary is provided in the appendix for formal definition of the terminology used here.

In order to make a realistic assessment of what can and cannot be achieved with VHR imagery it is necessary to understand what the imagery can and cannot resolve. For this reason, decision makers and ana-

lysts should have some basic understanding of what VHR sensors actually measure and how they measure it. This comes down to a series of related trade-offs between spatial, spectral and temporal resolution. These trade-offs are common to all optical sensing systems and are unavoidable. The second part of this survey uses the concepts of resolution in the context of the decisions typically faced by decision makers and analysts when selecting and using the imagery. In addition to resolution issues, there are also some environmental factors (e.g. clouds) that determine what can and cannot be achieved with VHR imagery. These are also discussed in the context of what the users should specify when selecting or acquiring imagery for different purposes. Since imagery is basically a visual tool, the fundamentals of image display and enhancement are also discussed briefly.

Once the decision has been made to use VHR imagery, and the images have been selected or acquired, it is necessary to interpret the content of the imagery. Interpretation is a critical step in the process and one that is prone to potentially serious errors. The third and fourth sections discuss the types of features – both hazards and vulnerabilities – that can be recognized, identified and described with VHR imagery. A number of specific examples are provided to illustrate the types of features that can be resolved and their spatial setting. The interpretation of these features during the reconnaissance and identification phases of the analysis is central to the determination of what type of information can and cannot be extracted from the imagery. This provides a lead in to the mapping task.

Land cover mapping can take the form of either continuous physical quantities or discrete thematic classes. Each type of mapping has a wide variety of applications arising from its relative strengths but both basically depend on color. Monitoring can be thought of as multitemporal mapping. However, analysis of temporal changes in maps is more complex because it generally involves changes in both the target (land cover) and the imaging conditions (illumination) at the time each image is acquired. Distinguishing between these two types of change can be challenging.

Following the R-I-M strategy described above, the

survey is divided into sections that discuss the use of VHR imagery for each phase of the analysis.

Reconnaissance: Fundamentals of Image Selection, Display and Enhancement. The first phase of the analysis is generally the selection of appropriate imagery and its preparation for the reconnaissance task. This involves several decisions that influence the outcome of the analysis. Both decision maker and analyst should understand the capabilities and limitations of the imagery from the outset in order to determine what they should and should not expect from it. This section summarizes the key determinants of what VHR imagery can and cannot resolve and briefly discusses some of the ways the imagery can be presented during the reconnaissance phase.

Identification of Hazards. The second phase of the analysis involves identification of either hazards or vulnerabilities or both. This section discusses some of the ways that VHR imagery can supplement other sources of information about hazards in and near the urban environment. Several different classes of hazard are discussed in turn and examples of VHR imagery of each hazard are presented at multiple scales.

Identification of Vulnerability and Exposure. This section complements the previous section in its focus on VHR imagery's utility for identification of urban vulnerability and exposure. The discussion is presented in the context of spatial and spectral resolution and the importance of each in urban mapping.

Mapping Tools and Methods. The third phase of analysis involves semi-automated mapping of specific features in the urban environment and its surroundings. While the mapping is generally done by analysts, it is important for decision makers to understand the strengths and limitations of the tools used to do the mapping in order to understand the results being presented by the analysts. This section discusses several of the more commonly used tools and illustrates their strengths and limitations in a set of examples.

Multi-temporal Change Detection. This section discusses one of the areas where VHR imagery can

provide valuable information not generally available from other sources. Although still in its infancy, multi-temporal change detection is one of the most promising applications of VHR imagery. The brief discussion summarizes some of the fundamental capabilities and limitations of high spatial resolution change detection.

Synthesis. This section attempts to integrate the previous sections into a coherent synthesis of the underlying principles guiding the analysis of urban hazards and vulnerabilities. These are presented by contrasting strengths and weaknesses of the imagery and tools and summarizing some best practices for decision makers and analysts to consider when using VHR imagery.

Reconnaissance: Fundamentals of Image Selection, Display and Enhancement

Selection of imagery involves numerous tradeoffs. Understanding the nature of these tradeoffs is essential to making informed decisions about what imagery to use and what to expect from it. Key decisions made at the outset of the project determine what information can be extracted from the imagery. These decisions can be considered as a sequence of three distinct steps in the image analysis: Image selection (or acquisition), display and enhancement.

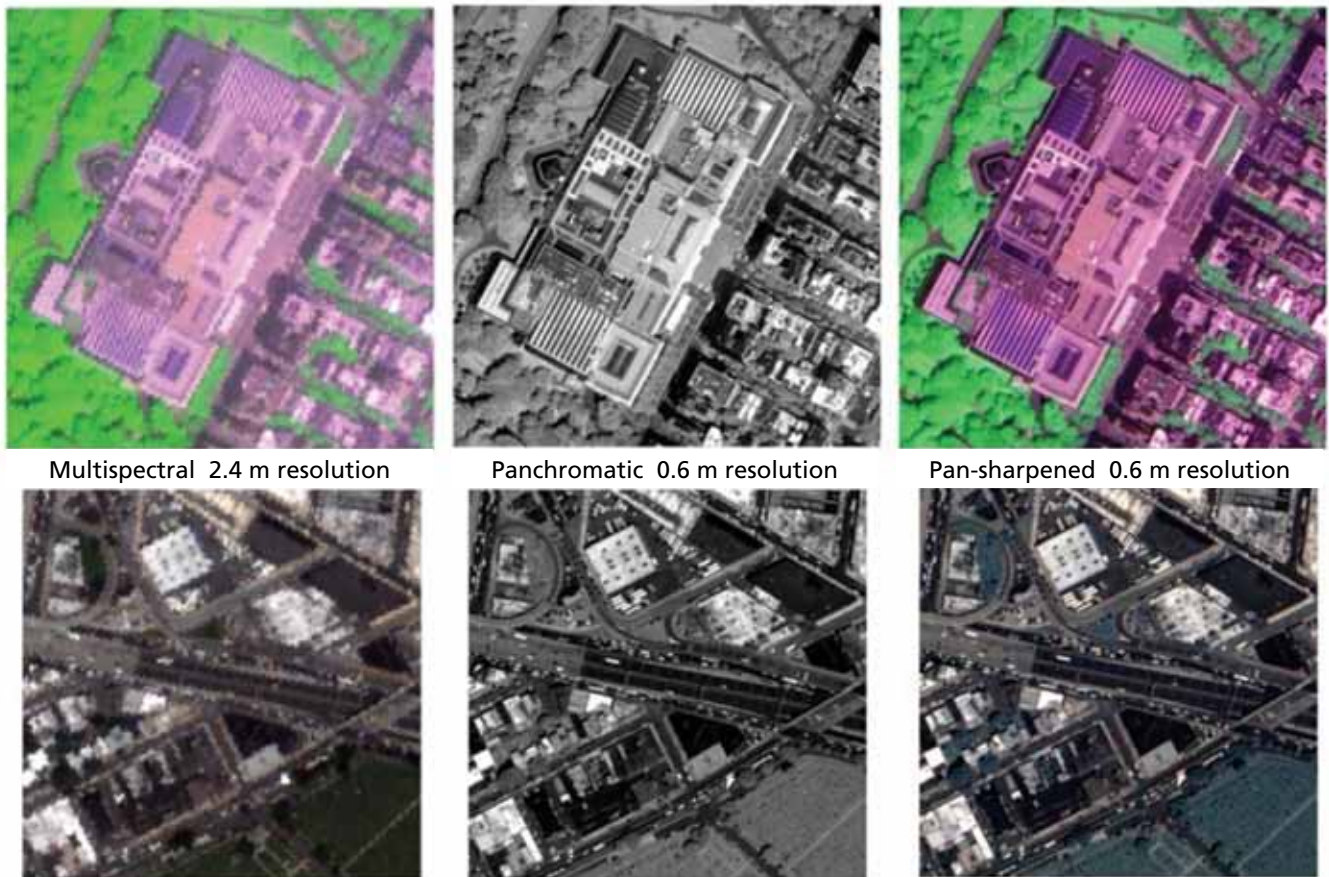
Image Selection – The first decision involves the choice of imagery used in the analysis. Factors to consider involve spatial and spectral resolution, acquisition date, viewing angle, illumination and atmospheric conditions as well as processing parameters to specify when ordering imagery. Most of these parameters are interrelated so selection of imagery generally involves unavoidable trade-offs between parameters. At present, limited coverage of most parts of the developing world means limited choices in terms of image collection dates and viewing conditions. However, this situation will change rapidly with the impending proliferation of VHR sensors and concomitant growth of imagery archives.

Spatial resolution (pixel size) determines the size of the smallest object that can be resolved. The gen-

eral rule of thumb is that the pixel size must be less than half the smallest dimension of the smallest feature of interest. In other words, at least two pixels are required to resolve a feature – generally more. At the time of writing, the choice of high spatial resolution sensors is rather limited (see appendix for listing of sensors and resolutions). For identification

of urban structures a resolution of one meter or finer is generally desirable. Comparative analysis of a diverse collection of 1 meter panchromatic imagery shows that most individual features in the urban mosaic (e.g. roofs, streets, trees, etc) have characteristic scales of 10 to 20 meters (Small, 2009). Examples of 0.6 and 2.4 meter imagery are shown in Figure A 1.

Figure A 1: Examples of multispectral, panchromatic and pan-sharpened Quickbird imagery.



The pan-sharpened images combine the color information from the 2.4 m multispectral imagery with the brightness information from the 0.6 m panchromatic imagery to produce a color image at 0.6 m spatial resolution. Although the pan-sharpened images do not contain as much information as true 0.6 m multispectral imagery, the brightness information from the panchromatic imagery provides valuable textural content to the multispectral imagery. The upper row of images shows a false color composite (R/G/B = 3/4/1) of the Metropolitan Museum of Art in New York. Note discrimination of individual trees on the cross streets made possible by using the near-infrared band 4 in the green channel. The lower row of images shows a natural color composite (R/G/B = 3/2/1) of the Long Island Expressway Cavalry Cemetery and warehouses in Queens, NY. Discrimination of vehicles on expressway and side streets depends on the spectral contrast between the vehicle and the underlying road surface.

Spectral resolution (number of color bands) determines the extent to which the sensor can resolve different colors. In the context of this discussion, color will refer to not only visible wavelengths of light to which the human eye is sensitive but also infrared wavelengths that are invisible to humans but detectable by other sensors. Panchromatic imagery is analogous to a black and white photograph in which overall visible brightness is represented by shades of gray. Multispectral imagery provides multiple spectral bands corresponding to brightness in specific wavelength bands (different colors). For example, the Quickbird sensor provides a single panchromatic band representing overall brightness in the visible and near infrared wavelengths as well as four multispectral bands representing blue, green, red and near infrared brightnesses. Multispectral bands can be combined into a composite image in which different spectral bands are loaded into the red, green and blue channels of the color image as in Figure A 1. Different band combinations can be used to emphasize different features in the image (explained further below). The fundamental decision regarding spectral resolution is whether or not it is necessary to resolve different colors or whether panchromatic imagery is sufficient. This is especially important if discrimination of vegetation is required because near infrared imagery is very effective for discriminating vegetation from other dark surfaces. While multispectral and panchromatic imagery can be purchased separately, they are generally available as a bundle at reduced pricing making it less expensive to purchase both together rather than separately.

There is a fundamental tradeoff between spatial and spectral resolution. Sensors are limited in their ability to collect photons of light energy. Reflected light from Earth's surface contains a limited number of photons distributed over visible and infrared wavelengths. The amount of incident light reflected at each wavelength determines the color of the reflector. Panchromatic sensors collect photons from a broad range of wavelengths so the number of photons per unit area is greater than it is for multispectral sensors which collect photons in narrower ranges of wavelengths. As a result, panchromatic

sensors can image smaller areas on the Earth surface than multispectral sensors can. The result is smaller pixels and finer spatial resolution for panchromatic sensors. Narrower spectral bands provide better color discrimination but this increased spectral information necessarily comes at the cost of spatial detail. However, higher spatial resolution panchromatic and higher spectral resolution multispectral are often collected simultaneously and can be combined into a pan-sharpened image (explained below) that offers both spatial detail and color discrimination as in Figure A 1. When choosing the appropriate sensor and imagery for a given task it is necessary to consider the type of information required and whether that information is best obtained from spatial or spectral observations.

A similar tradeoff exists between swath width limitations of all sensors. Smaller pixels necessarily mean narrower swaths. Narrower swaths mean that more swaths are required to cover a given area if it is larger than the sensor swath width. More swaths generally mean longer acquisition times with different viewing and illumination conditions for each swath. When choosing a sensor for a given task it is necessary to consider both swath width and spatial resolution in the context of the total area of coverage required. If multiple swaths are required, temporal resolution must be considered.

Temporal Resolution determines how frequently a sensor can image a specific location. Revisit times are determined by the satellite orbit but generally vary according to the viewing angle for pointable sensors. Most sensors are "nadir looking", meaning that they always point directly downward to image a swath on the ground directly beneath them. However, many high resolution sensors are pointable in that they can rotate (either the telescope or the entire satellite) to point at "off-nadir" targets that are not directly beneath them.

Typical revisit times for nadir-looking (directly downward) imagery are on the order of several days but off-nadir (oblique looking) revisit times can be considerably shorter. The trade-off is between temporal frequency and spatial distortion. Off-nadir looking imagery sees the target from an oblique angle which

introduces geometric distortion and considerably longer atmospheric path length. As a result, off-nadir images are subject to greater atmospheric effects and obscured views of high relief targets. The effect of longer atmospheric path length is generally reduction of image contrast. The effects of geometric distortion include layover (taller objects tilted away from the sensor), foreshortening (taller objects tilted toward the sensor) as well as parallax view distortion where taller objects obscure shorter objects behind them. In general, near nadir (satellite elevation angles greater than $\sim 75^\circ$) provides more information and is easier to interpret. All else equal, near-nadir imagery is strongly preferred. However, all else is rarely equal so viewing geometry must be considered in light of other factors influencing image quality.

There is yet another fundamental tradeoff between revisit time and viewing geometry. The more specific the viewing geometry requirements, the fewer acquisition opportunities exist. When tasking acquisition of new imagery it is possible to specify a range of acceptable view angles but more restrictive view angle requirements will generally increase the time required to acquire the image – particularly in areas where competition for satellite tasking is high. When ordering archive imagery the user is limited to what has already been acquired. While commercial providers generally try to obtain imagery as near nadir as possible, more imaging opportunities exist for off-nadir imagery so archives will often contain more off-nadir (elevation angles $> \sim 75^\circ$) than near-nadir imagery.

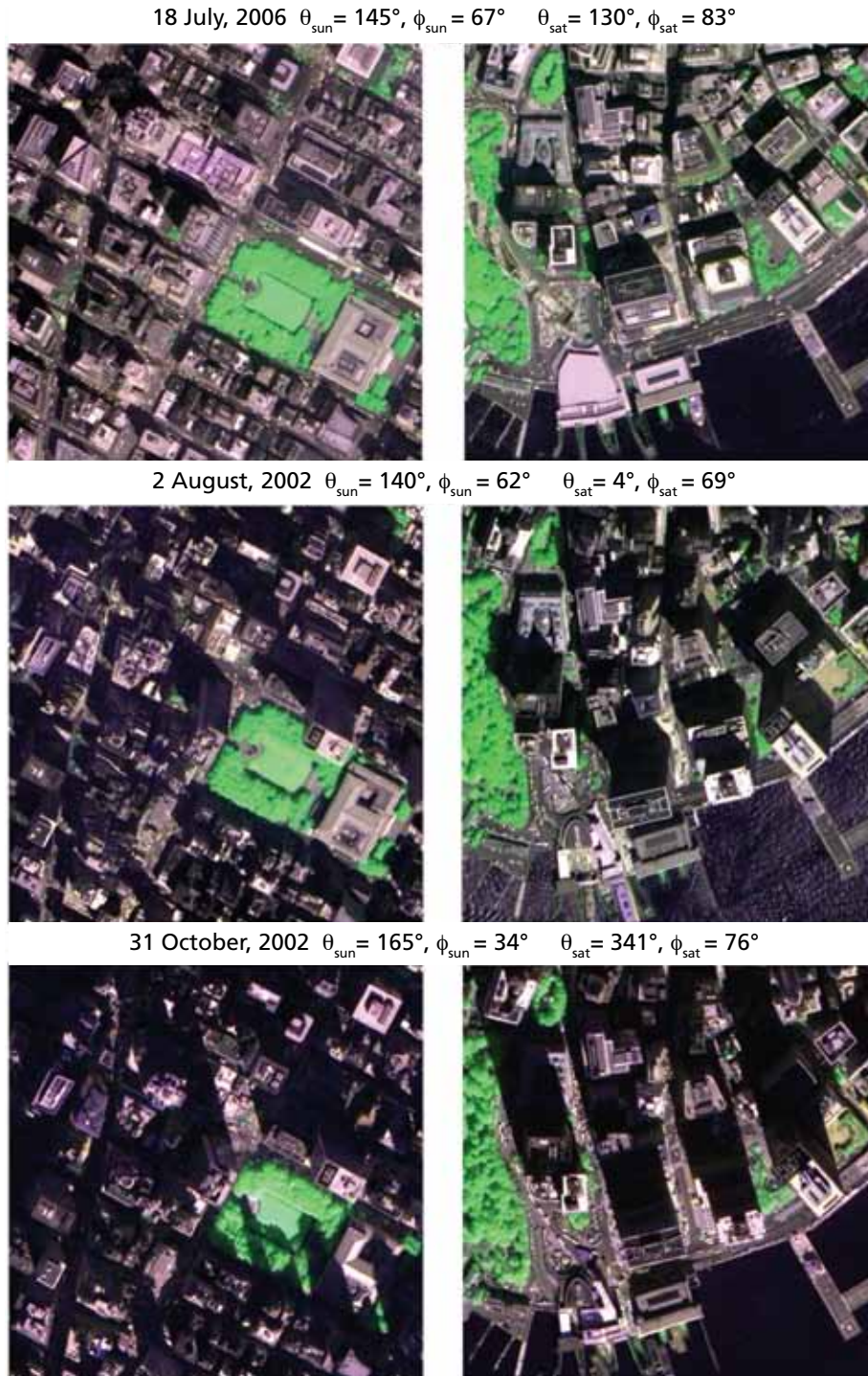
Viewing geometry is specified as azimuth and elevation angles. The *elevation angle* is the angle between the horizontal and the position of the satellite. Higher elevation angles (closer to 90°) correspond to near-nadir looking imagery and provide closer approximations of map views. The *azimuth angle* corresponds to the compass direction (0° =North, 180° =South) from which the sensor sees the target. The importance of the azimuth angle depends on the elevation angle. At high elevation angles geometric distortion and parallax effects are reduced so the azimuth angle is less important. At

lower elevation angles ($< \sim 75^\circ$) the azimuth angle becomes much more important because it determines which parts of the image is obscured by taller features. Examples of view angle effects are shown in Figure A 2.

Illumination geometry is also very important in urban environments because it determines the extent and location of shadows. Illumination angles are analogous to viewing angles but describe the position of the sun in terms of azimuth and elevation. As with viewing angles, the importance of solar azimuth depends on solar elevation. At higher solar elevations shadows are reduced. As solar elevation diminishes below $\sim 75^\circ$ shadows lengthen considerably. The solar azimuth determines the direction that shadows are cast – and therefore what they obscure. Solar azimuth and elevation are determined by the time of year, time of day and latitude. While less important in the tropics and equatorial regions, illumination conditions can have a pronounced effect on imagery collected at higher latitudes. Examples of illumination angle effects are shown in Figure A 2 and Figure A 3.

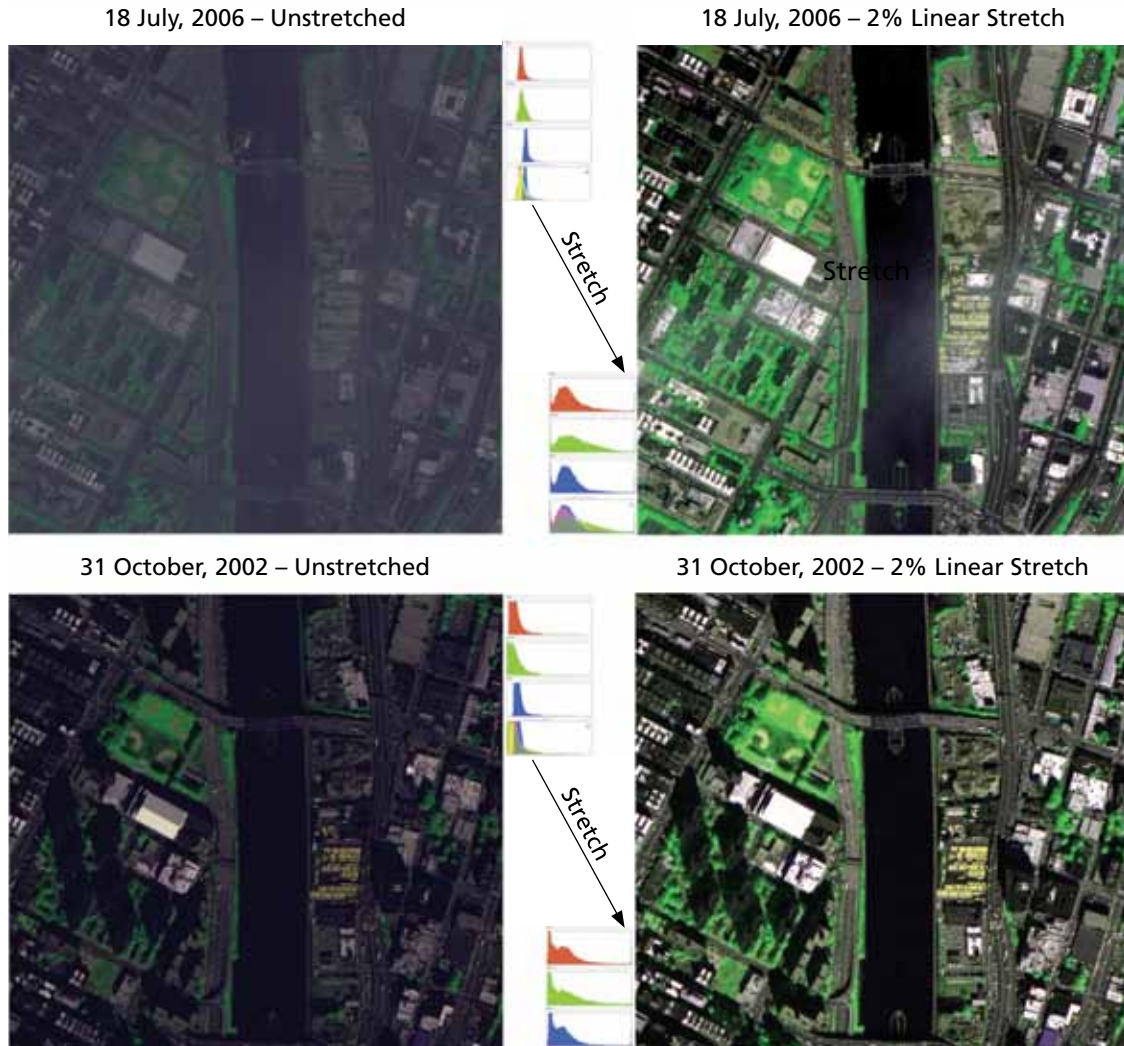
Clouds and atmospheric effects are the bane of optical imagery – particularly in the tropics. Clouds obscure ground targets both directly and indirectly with their shadows. While some information can often be extracted from shadow areas, it is generally limited to brightness of high contrast targets. Information about targets that are obscured by clouds is lost completely. Of all the atmospheric constituents, water is the most nefarious because it attenuates information in both obvious and subtle ways. Some clouds are obvious – others less so. Thick, convective clouds (e.g. cumulus) are generally obvious. Thin, diffuse clouds (e.g. cirrus) can be very difficult to detect visually – despite their effect on light transmitted through them. Haze and humidity are less problematic but can present serious challenges to interpretation and information extraction. Haze and humidity increase both scattering and absorption of sunlight thereby reducing the information available to optical sensors. The net effect of scattering and absorption is a loss of image contrast as dark objects appear brighter (from scattering of light by the intervening

Figure A 2: Effects of varying illumination and imaging geometry.



Varying illumination and imaging geometry for Times Square and Bryant Park in midtown Manhattan (left column) and the Financial District and Battery Park in lower Manhattan (right column). The August and July images were acquired under similar solar azimuth and elevation compared to the late October images but the July image was acquired from a more nearly vertical (nadir looking) satellite azimuth and elevation. As a result, the shadowed area is far greater in the October image while both the image geometry and illumination conditions are nearly ideal in July.

Figure A 3: Illustration of atmospheric scattering and suppression by linear stretching.



Upper row shows reduced contrast and blue cast resulting from haze scattering typical of New York in summer. The lower row shows higher contrast associated with clear sky conditions in October. The left column shows unstretched images in which the full range of brightnesses are displayed, while the right column shows stretched images in which the brightest and darkest 2% of pixels are saturated (white and black respectively). The result is enhanced contrast in midtones. The image histograms in the center column illustrate the effect of the stretch on the brightness of the image pixels. The long tailed brightness distributions result in most pixels having similar low display brightnesses thereby squandering most of the display dynamic range on a minority of bright pixels. The histograms show the brightness distribution of the red, green and blue channels as well as the overall brightness distribution that results from the compositing process. Although stretching increases the contrast of the July image considerably, it does not equal the higher contrast of the October image.

atmosphere) and bright objects appear darker (from absorption by the same atmosphere). Most imagery sources provide low resolution quicklook or browse images for the purpose of cloud screening prior to purchase. Large clouds are generally obvious; small clouds less so. Atmospheric conditions are more difficult to identify from browse images but can be offset somewhat with the contrast enhancement techniques discussed below. Examples of atmospheric effects are shown in Figure A 3.

Seasonal Effects and Vegetation Phenology – In addition to the solar illumination effects described above, the season in which an image is acquired can determine atmospheric conditions and the amount or state of vegetation cover. In monsoonal regions

clear sky imagery is most commonly available just prior to the onset of the monsoon. In temperate zones deciduous trees often obscure underlying urban infrastructure like streets and smaller buildings. In areas where deciduous trees are abundant leaf-off imagery is generally preferred for this reason. However, there is a tradeoff in that solar elevations are considerably lower in winter so the increased shadow area can offset the benefit of leaf-off visibility. In such cases, imagery collected either immediately prior to leaf-out, or immediately after leaf fall generally provides the best combination of high solar elevation and leaf-off visibility. A comparison of the same urban area in both leaf-on and leaf-off conditions is shown in Figure A 4.

Figure A 4: Example of the effect of vegetation phenology.



The left image of Queens NY was acquired 11 April 2005 before most deciduous trees had leaves. The right image was acquired 5 September 2003 when most trees were in full leaf. Note also the difference in wetland vegetation in the LL corner. The faint green in the April image results from partially leafed out trees while the bright green corresponds to herbaceous vegetation and maintained grassy areas like the highway medians and the racetrack in the UR corner. Both images are VNIR false color composites (R/G/B = 3/4/1) with a 2% linear stretch applied.

Image Display – The first decision facing the analyst is generally spectral band selection. At the time of writing, most VHR sensors offer either single band panchromatic imagery and/or four band Visible/Near Infrared (VNIR) imagery. In mid-2009 Digital Globe is

expected to launch the Worldview 2 satellite with an 8 band VNIR sensor. This will increase band selection options considerably. However, for the time being the most commonly used band combinations with four band VNIR imagery are the natural color

composite and two variations on the false color VNIR composite. In a *natural color composite* the red, green and blue bands are displayed in the red, green and blue channels of the display for color rendition similar to what the human eye would perceive. In *false color composites* the NIR band (4) is displayed in either the red or green channel. The result is much stronger contrast between vegetation and other dark surfaces as well as significant color shifts in more saturated (non-gray) targets. Loading the NIR band in the red channel produces a result comparable to film-based color infrared aerial photographs in which vegetation is red. Loading the NIR band in the green channel produces a more natural looking image in which vegetation is green – albeit generally much more saturated green than occurs in nature. Comparisons of natural and false color composites are shown in Figure A 5 and Figure A 1.

Pan sharpening is a processing technique that combines higher spatial resolution brightness information from the panchromatic band with lower spatial resolution color information from the multispectral bands to produce a color image combining the benefits of both higher spatial and spectral resolution. An example of pan sharpening is given in Figure A 1. Almost all the images used in this report have been pan-sharpened. In general, pan sharpening offers considerable benefit to the interpreter and should be included in the processing sequence whenever possible. One exception is in instances where accurate spectral information is needed for image classification or other analyses requiring the actual radiance values measured by different bands. Pan sharpening alters the radiance values of the multispectral bands thereby precluding Spectral Mixture Analysis (described below). However, for most analyses pan sharpening should be considered a standard processing step.

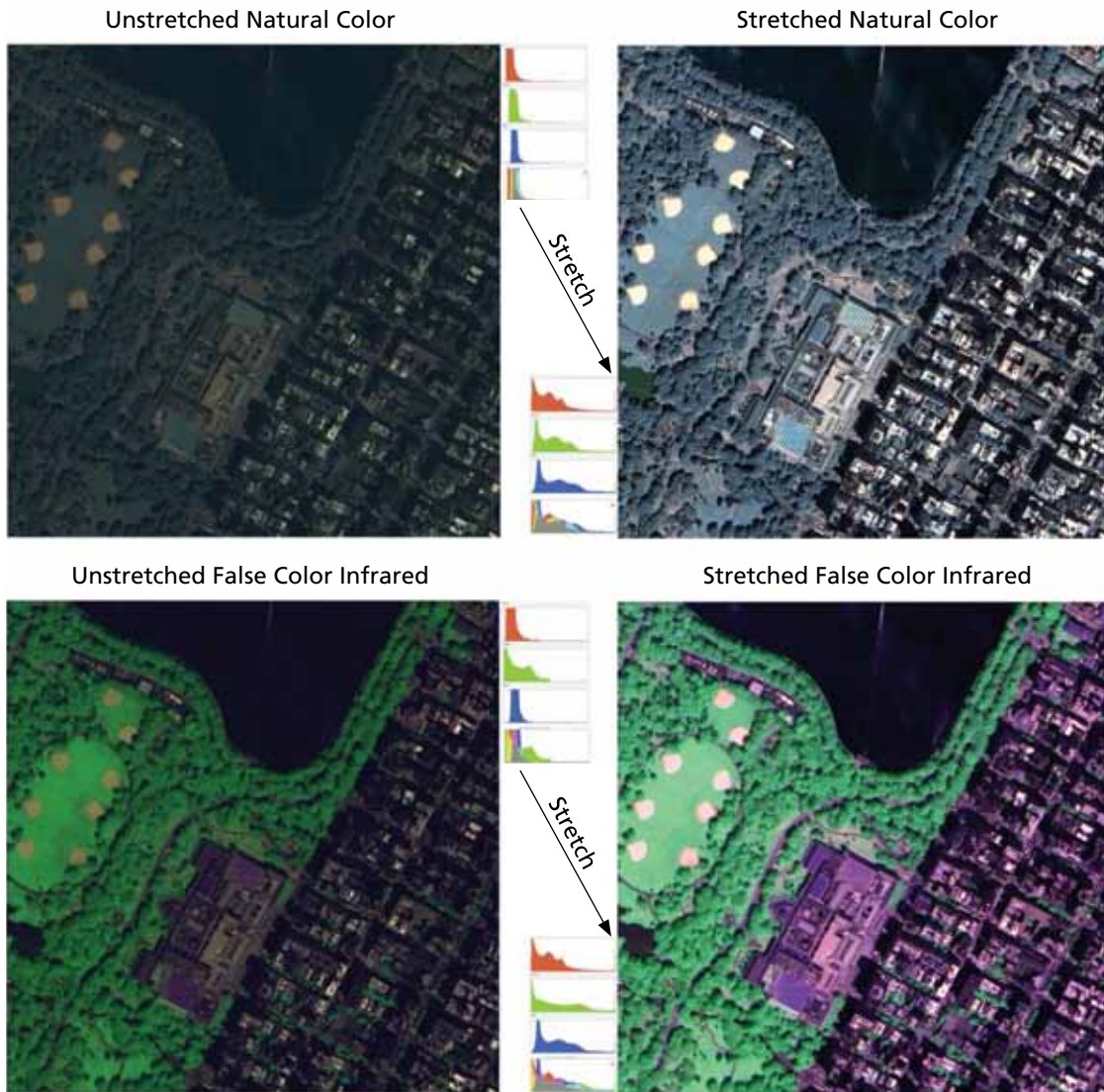
Image Enhancement – Image enhancement is distinct from display and analysis in that its purpose is to enhance visibility of the feature(s) of interest – relative to background and features of less interest. As such, it must follow display and should generally precede analysis. The two most important enhance-

ment tools for analysis and interpretation of urban VHR imagery are contrast enhancement and spatial filtering. Both can be applied to varying degrees, depending on what information is being extracted from the imagery.

Spatial filtering basically involves either blurring or sharpening the image. Low pass (smoothing) filters blur the image by averaging adjacent pixel brightnesses. Smoothing filters are generally used to reduce noise to ease interpretation. However, smoothing also attenuates information so should be used sparingly. Modern VHR imagery generally has superb signal/noise characteristics so smoothing is not generally required for interpretation. High pass (sharpening) filters do exactly the opposite of smoothing filters and enhance spatial contrast at different spatial scales. Similarly, edge enhancement filters emphasize contrast without amplifying noise to the extent that a simple sharpening filter can. The benefits (and costs) of spatial filtering depend on the imagery being analysed and the objectives of the analysis.

Contrast enhancement is generally achieved by applying a *stretch* to the bands being displayed. A stretch determines the display brightness of different pixel brightness values in the image. Technically, the stretch is a mathematical function that maps input pixel data values into output display brightness values. The simplest type of stretch is a linear stretch in which the display brightness of a pixel is directly proportional to its data value. A widely used linear stretch is the clipped 2% *linear stretch* in which the brightest and darkest 2% of image pixels are saturated to provide greater contrast of the intervening values. The result is loss of detail in the brightest and darkest 4% of objects in the image in exchange for greater contrast of the remaining 96% of pixels. Examples of linear stretches are given in Figure A 3 and Figure A 5. A variety of *non-linear stretches* also exist but the results are more difficult to interpret than those of linear stretches. Non-linear stretches are most useful as exploratory tools to display subtle features that may not be obvious in linear stretches.

Figure A 5: Illustration of image enhancement by linear stretching.



Upper row shows natural color composites (R/G/B = 3/2/1) while lower row shows false color composites (R/G/B = 3/4/1) with the near infrared band 4 in the green channel to enhance discrimination of vegetation. The left column shows unstretched images in which the full range of brightness is displayed while the right column shows stretched images in which the brightest and darkest 2% of pixels are saturated (white and black respectively). The result is enhanced contrast in midtones. The image histograms in the center column illustrate the effect of the stretch on the brightness of the image pixels. The long tailed brightness distributions result in most pixels having similar low display brightness thereby squandering most of the display dynamic range on a minority of bright pixels. The histograms show the brightness distributions of the red, green and blue channels as well as the overall brightness distribution that results from the compositing process. Note that the effect of the stretching operation is to distribute the pixel brightnesses more evenly over the available range of display brightness resulting in higher contrast throughout the image.

Identification of Hazards

While VHR imagery will generally be more useful for identification of assets and hazard vulnerability, in some cases, the physical features identifiable in VHR images can aid in identification of hazards. In many cases moderate resolution imagery and ancillary information like DEMs are sufficient to identify hazards. VHR imagery can contribute to their identification by providing fine scale details not apparent in the lower resolution reconnaissance imagery. In many less developed areas, VHR imagery will be the most detailed, and most current, source of geospatial information available.

Landslide – Two spatial aspects of landslide hazard that can be extracted from VHR imagery are soil exposure and slope distribution. While actual slopes cannot easily be measured from a single VHR image, it is possible to infer the presence of steep, potentially unstable slopes from a single image. In some cases, high resolution digital elevation models (DEMs) can be derived from multiple VHR images using stereography. The accuracy of these DEMs depends on a number of factors related to both the topographic roughness and viewing geometry. A detailed discussion of this technique is beyond the scope of this report but a compendium of relevant information is available at (<http://iris.usc.edu/Vision-Notes/bibliography/cartog946.html>). Most providers of VHR imagery offer DEM extraction as a service.

In many instances, VHR imagery can be used in conjunction with a lower resolution DEM in a manner consistent with the R-I-M strategy. The DEM can be used in conjunction with moderate resolution optical imagery as a reconnaissance tool to identify potentially unstable slopes posing a threat to assets. Even if the lower resolution DEM does not resolve the unstable slope itself, it can be used to identify the topographic gradients near the settlement that channel mass movements toward the settlement and highlight potential locations of upslope instability. Examples of a potentially unstable slopes and potentially vulnerable settlements are given in Figure A 6 and Figure A 7.

Flood – VHR imagery can provide ancillary information potentially relevant to flood hazard exposure. In this context, flood hazard includes water level increases associated with rivers and estuaries, coastal storm surge and tsunami as well as flash floods on smaller or intermittent watercourses. In the former cases the most relevant information provided by VHR imagery is related to surface roughness and land cover. Both roughness and land cover can influence the route and flow velocity of flood waters as well as the degree of downstream turbulence. In the case of flash floods VHR imagery can be used to map potential flow courses and channels that may direct flash floods toward settlements or infrastructure. As in the case of landslide hazards, the combination of a DEM and moderate resolution imagery can be used as a reconnaissance tool to identify potentially vulnerable settlements for which VHR may be acquired. Flood severity can be determined by height of inundation. Flood hazard maps, commonly used by the insurance industry, are often derived from a combination of high resolution imagery, flood simulation models and digital elevation models.

For settlements adjacent to coastlines and major rivers the reconnaissance images and DEMs can be used to identify the location of potentially vulnerable settlements and the VHR imagery can be used to identify geomorphic features that may influence the path or flow velocity of flood waters. Examples include berms, cliffs and sand bars that may serve as barriers to dissipate energy and reduce, or focus, impact of flood waters.

For settlements vulnerable to flash floods on smaller or intermittent flow courses the VHR imagery can actually be used to identify the drainage itself as well as geomorphic features such as cut banks and point bars that may be indicative of the nature of past floods. In many situations, VHR imagery can be used in conjunction with DEMs to identify the hydrographic apex – where upstream channel confinement gives way to an open, less constrained, flow course such as an alluvial fan or flood plain. These areas are often densely populated because they represent the upstream extent of fine sediment deposition where arable soils tend to occur. An example from the Huaycan valley in

Figure A 6: Successive enlargements of landslide vulnerability in Pisac, Peru.



The town is located on the Vilcanota river in the Sacred Valley of the Inkas. The Inka royal estate is located atop the steep slope 700+ meters above the town. The Inka estates and associated terraces were engineered to be earthquake resistant and have survived 500 years of seismic activity but the slopes on which they are built are subject to rockfalls. The modern town of Pisac is located at the base of a large steep, potentially unstable slope.

Figure A 7: Example of parallel identification of hazard and vulnerability in Huaycan Alto, Peru



Successive zooms in left column show potentially unstable slopes over a heavily developed stretch of arroyo. High resolution Quickbird imagery facilitates the identification of potentially unstable rock outcrops directly upslope from residential and agricultural assets. The imagery also reveals the diagonal downslope channel that could divert rockfalls from the outcrop westward toward the identified area rather than directly downslope.

Peru is given in Figure A 7. In many areas the VHR imagery can reveal flow courses that are not identified on topographic maps.

VHR imagery can also be very useful for identification of upslope land cover changes that are likely to influence runoff rate and flood risk within a watershed. Removal of vegetation exposes soil to rain and wind, thereby increasing its mobility. In addition, removal of vegetation can increase infiltration rate thereby accelerating saturation and reducing

the lag time between rainfall and runoff. The result can be increased risk of downslope mass movement and flash flooding. As such, VHR imagery can provide a valuable tool for preemptive identification of land cover changes that may increase risk of both these hazards. Examples of upslope land cover and downslope assets on the Caraballeda alluvial fan are given in Figure A 8. The city of Caraballeda Venezuela is built on an active alluvial fan and suffered extensive damage from upslope debris flows in December of 1999.

Figure A 8: Example of parallel identification of hazard and vulnerability for the area of Caraballeda, Venezuela.



The city of Caraballeda is built on an active alluvial fan. HRO can be used to identify potential source regions for upslope debris flows such as that which occurred on Dec. 2-3, 1999. Successive zooms in left column show most vulnerable areas at the hydrographic apex where the debris flow is no longer confined by the canyon. The impact of the 1999 flow is still visible in 2003. Right column shows the upslope source regions where vegetation removal by development causes increased runoff rate.

Fire – VHR imagery can be very useful for identification of fuels (any flammable material) that occur in proximity to human settlements or assets. In many cases the fuel source will be vegetation. The VNIR band on many multispectral VHR sensors provides a tool for identification of potentially flammable

vegetation because NIR reflectance is sensitive to vegetation health and chlorophyll content. Healthy green vegetation is generally far less flammable than dry, senescent vegetation. In pan sharpened imagery, texture information can highlight vegetation on the basis of canopy shadow while the color

can provide an indication of the health or greenness of the vegetation. VHR imagery can also be very useful for identification of fine scale topography that may influence airflow thereby stoking the fire. Steep slopes containing flammable material can ig-

nite and spread very quickly. An example of dense, potentially flammable vegetation on a steep slope in close proximity to residential, commercial and cultural assets in a rapidly developing area of Cuzco Peru is shown in Figure A 9.

Figure A 9: Example of dense, potentially flammable vegetation in close proximity to residential, commercial and cultural assets in Cuzco, Peru



Atop the eucalyptus covered slopes is the ancient Inka fortress of Sacsaywaman. Under drought conditions the eucalyptus groves could pose a fire hazard to both the modern city and ancient fortress.

While broadband imagery is potentially useful for distinguishing between green and senescent vegetation, hyperspectral imagery holds even greater promise for identification of potential fuel sources. Because hyperspectral imagery can resolve subtle differences in color associated with different types of vegetation and different states of water stress it can be used to map vegetation types with different potential for flammability. For example, different types of chapparal vegetation have different degrees of flammability under different leaf moisture conditions (Roberts refs). Fire prediction models can pre-

dict fire patterns and intensity but they require high spatial resolution inputs. This is an example where higher spectral resolution is equally important for its ability to distinguish more flammable water stressed vegetation from less flammable healthy vegetation.

Volcanic – Because of the importance of subsurface processes to volcanic activity, most applications of VHR imagery to volcanic hazard are primarily related to identification of active vents and landforms as well as geomorphic features that may channel downslope flows of lava, ash or mud. In the latter

case these features may be identified in much the same way as described above for floods. In the case of active vents VHR imagery can be used to supplement moderate resolution imagery and DEMs for identification of ejecta or condensing gas plumes that may reveal the presence of subsurface processes not distinguishable on moderate resolution imag-

ery. Examples of vent morphology and downslope flow courses on the flanks of Merapi volcano on the island of Java are given in Figure A 10 along with specific examples of vulnerable agriculture, dense rural settlements and urban infrastructure located in drainage courses likely to channel flows.

Figure A 10: Volcanic hazard and vulnerability on the flank of Merapi volcano.



Merapi is one of the more recently active volcanoes in Indonesia. Although the city of Yogyakarta is the most prominent focus of vulnerability analyses, dense rural populations are present on the flanks in closer proximity to the vent. The most vulnerable settlements and agricultural fields are those located in the valleys that could serve as conduits for downslope movement of ash and mud flows. Individual residences can be difficult to identify beneath the tree canopy, but the approximate extents can be determined at this scale.

Aeolian mass movement – In arid environments mobility of sand dunes can pose a serious threat to assets – particularly agriculture. While most dune fields can be monitored effectively with moderate resolution imagery, the close proximity of dunes to

fixed assets makes it possible to identify and map the asset as well as monitor changes in the spatial extent and morphology of the dune. An example is given in Figure A 11.

Figure A 11: Multiscale perspective of sand dune encroachment on agricultural and residential assets in Pisco, Peru.



Left image shows extensive intermingling of dunes and agriculture. Right image shows full resolution detail of sand encroachment on vulnerable settlement in upper part of left image. Stability of the dunes depends on prevailing wind speed and direction.

In many of these examples, risk identification could make use of multi-temporal image analysis to identify areas affected in the past and characterize the spatial distribution of occurrence. In instances of frequent recurrence this approach could be used to develop probabilistic models of recurrence. Such a strategy could use decameter (10-100 m) resolution imagery collected over the past 30 years to determine where and how often a particular event (say fire) happened and could use VHR imagery to resolve detailed features of the areas where the hazard recurred.

Identification of Vulnerability and Exposure

The primary application of VHR imagery to risk assessment is in the identification of vulnerability and exposure. Successful, robust application of VHR imagery to risk assessment depends on accurate identification of relevant features related to their physical properties. Because urban areas are composed of many different features, constructed from many different materials, identification of vulnerability

and exposure generally relies on visual interpretation of imagery rather than direct mapping of specific colors, as in the case of land cover mapping. Once specific features (e.g. housing, infrastructure) have been identified, various mapping methods can be employed to quantify their location and extent. However, the R-I-M strategy relies heavily on visual interpretation in the initial stages. As discussed previously, identification of hazards and exposure can often be done in parallel during the Identification phase of the analysis.

Infrastructure – One of the primary advantages of VHR imagery over moderate resolution imagery, like Landsat, is the ability to identify specific components of the built environment. The typical size of individual components in the built environment is generally between 10 and 20 meters (Small, 2009). Sensors with spatial resolutions of 10 meters begin to resolve individual features like buildings and smaller roads. Sensors with sub-meter resolution generally allow recognition, identification, and in some cases description, of these features. When sub-meter resolution panchromatic imagery is combined with lower resolution (1-5 m) multispectral imagery to produce

pan-sharpened imagery, both spectral and textural cues can be used in the Identification phase of the analysis. Four broad classes of infrastructure are resolvable with VHR imagery:

Transportation – The main categories of transportation infrastructure are roads, bridges, railways, ports and airports. Most of these features can be recognized by their linear, or curvilinear geometry. Spatial scales can vary considerably.

In many cases, *paved and unpaved roads* can be discriminated. In some cases the condition of a paved road can be inferred indirectly from the consistency of brightness along its length. Potholes and other damage resulting in removal of paved surface generally results in fine scale shadow and albedo (brightness) differences that result in color variations along the length of the road. Unpaved roads are often distinguishable on the basis of their variable width and by the fact that they are generally brighter and more consistent than the surrounding substrate. Discrimination of paved and unpaved roads also depends on age, exposure and composition of pavement. Fresh asphalt is very dark but weathering causes it to become brighter. Because of this and other factors, robust identification of roads is generally much more difficult than frequently assumed. Expectations of ease and accuracy of road extraction should be tempered accordingly.

Railways can be identified on the same basis as roads. However, even sub-meter resolution imagery can rarely distinguish roads from railways on the basis of the feature itself because the rails and ties are generally too small to be resolved individually. However, under certain illumination conditions (perpendicular, low angle) elevated track beds can be distinguished on the basis of shadow. In most cases, railways are distinguished by their lack of perpendicular turns and intersections and by trackyards and stations at their origination points.

Bridges can generally be identified indirectly as the intersection of a road or railway with a larger drainage feature such as a river channel or canyon. In the case of larger bridges crossing deeper drainages the actual structure of the bridge can be resolved an oblique viewing angle is available. Suspension

bridges can often be recognized by the shadows they cast. A comparison of nadir and oblique views of a suspension bridge is given in Figure A 3.

Residential and Commercial – In many parts of the world, perhaps most, commercial and residential infrastructure are indistinguishable because the same buildings are used for both purposes. The most common example being street-level commercial establishments with upper floors used as residences. The distinction is not always obvious from street level – rarely so from the aerial perspective. For this reason, the primary distinctions resolvable with buildings are related to their spatial scale, density and arrangement. Residential and commercial infrastructure generally requires less space than industrial infrastructure. Similarly, the spatial scale, density and organization of individual units can be useful for distinguishing formal from informal settlements (Figure A 12). While *formal settlements* are generally characterized by regular street grids (paved or unpaved) and some uniformity of scale (size of discrete units) and possibly structure (e.g. roof pitch), *informal settlements* are often distinguishable by their lack of uniformity and finer spatial scale. However, the diversity of dwelling types and the lack of a single accepted definition or criteria for informal settlements precludes simple categorization across settings. In more developed urban areas, high rise buildings are clearly associated with formal settlements – although residential and commercial uses are not necessarily obvious from the appearance of the building. In either case, however, the identification of high rise (> 10 floors) buildings is important for risk assessment because of the high population density occurring within the building as well as the inherent vulnerability of higher floors.

Informal Settlements – Rapid, unplanned urban growth in many developing countries results in a proliferation of informal settlements. The structure and evolution of these settlements is fundamentally different from planned settlements. While there is little consistency in informal settlements around the world, the structures are generally smaller, more heterogeneous in roofing material and less evenly spaced than planned settlements. Passages between buildings tend to be narrower and less uniform in spacing and layout.

Figure A 12: Example of informal settlement in close spatial proximity to potential hazard in Dhaka, Bangladesh.



The large, densely populated informal settlement is vulnerable to both flooding and water borne disease. The adjacent district of Gulshan is a high income business and residential area.



Industrial – Industrial infrastructure can often be distinguished on the basis of spatial scale. Individual buildings, as well as open spaces (storage and staging areas) and transportation thoroughfares are often larger than their commercial/residential counterparts in order to accommodate storage, manipulation and throughput of larger volumes of material. The presence of warehouses, tracks, shipping containers, cranes, storage tanks and factory buildings often provides visual cues. In addition, industrial infrastructure is often concentrated in specific areas distinct from commercial and residential activities.

It is important to recognize a fundamental limitation of remotely sensed imagery – perspective. Most sensors see cities from above so they mostly see rooftops and open spaces. A perspective unfamiliar to most people. Most familiar distinguishing features are at street-level on vertical faces of structures that are not well imaged by sensors. Spaces between buildings can only be seen from limited view angles so a significant caveat to identification of many of these features is the potential for occlusion - based on either viewing geometry or vegetation cover.

Population – Even current sub-meter resolution (> 0.5 m) sensors do not resolve individual people unambiguously. With current technology limited to 50 cm resolution, detection is questionable; Identification is out of the question. The reason for this is obvious when we consider that the horizontal dimensions of most individuals are less than 0.5 x 1.0 m. However, in many cases the presence of individual people can be inferred from the shadows they cast in direct sunlight. At low

sun angles an individual person can cast a horizontal shadow of at least two meters length thereby providing a high contrast target to nadir-looking sensors. In some cases the presence of population can be inferred from the spatial distribution of shadow-scale features in open spaces (Figure A 13). However, in most cases the presence of population must be inferred from the infrastructure associated with residential or high volume industrial or commercial activities.

Figure A 13: Example of non-residential informal structures in Ica Peru.



In pan-sharpened Quickbird imagery (top) the area left of the center diagonal thoroughfare contrasts sharply with the larger distinct buildings throughout the image - particularly the regularly spaced large buildings opposite the thoroughfare. The smaller roofs and lack of separation between units is typical of informal settlements. However, the area is an open air market and is not inhabited when the market is not open.



Agriculture – Of all the anthropogenic features detectable with remote sensing, agriculture is generally the most obvious. The combination of large spatial extent, geometric regularity and spectral homogeneity distinguishes most agriculture from other land cover types – including native vegetation. The presence of straight lines, polygons and circles are generally indicative of human activity. Agriculture occurs in all of these forms across a range of spatial scales. The other characteristic of agriculture most useful to remote detection is the spectral homogeneity associated with monocultures and fallow soil. Uniform arrangements of monocultural vegetation are often easily distinguished from native vegetation on the basis of the strong and spatially uniform near infrared reflectance. Because large areas are generally seeded with the same species at the same time the individual plants tend to grow at similar rates in a uniform arrangement within the area of an individual field. The resulting uniformity of height and arrangement tends to minimize canopy shadow between and within plants so the aggregate reflectance within the field tends to be considerably more uniform, and bright, than that associated with wild vegetation of varying size and canopy structure. However, these characteristics do not necessarily apply to fine scale agricultural land use. In many cases, fine scale agriculture is indistinguishable from wild vegetation – particularly when they occur together or interspersed. Examples of both are given in Figure A 6, Figure A 7, Figure A 10 and Figure A 11.

Environmental Assets – In addition to the more obvious vulnerable assets described above, high resolution imagery can also be used to identify, and sometimes map, other environmental assets vulnerable to natural hazards. Examples include forests and their biodiversity stock, biomass and carbon stocks, wetlands, fresh water sources and potentially arable land not under cultivation. The ability to which these assets can be effectively mapped depends on the extent to which they can be recognized and distinguished on the basis of their optical reflectance characteristics.

Cultural Assets – In many parts of the developing world, the most valuable fixed assets are part of the cultural landscape. Archaeological sites and indig-

enous ecosystems are common examples of cultural assets whose value is at least as great as the assets in the adjacent built environment – often far greater. Particularly when recognized as a non-expendable resource and conserved. In some cases, cultural assets may not even be completely mapped or yet excavated by inhabitants of the cultural landscape. In such cases, their identification and mapping may contribute directly to a region's economic development because identification and mapping are necessary prerequisites to preservation and development. The value of cultural patrimony to the development of a tourism industry suggests that these assets must be recognized and protected at least as actively as the more conventional assets described above. In many parts of the developing world the most serious threats to cultural assets are direct results of unplanned development and exploitation. An example of a cultural asset currently threatened by development is given in Figure A 9.

Visual Interpretation versus Mapping

Incorporating the concepts of spatial, spectral and temporal resolution into the R-I-M strategy requires an understanding of the distinctions between detection, recognition, identification and description. To *detect* an object in an image is merely to determine its presence given some prior expectation. To *recognize* an object is to perceive it clearly on the basis of some prior familiarity. To *identify* an object is to establish its identity sufficiently well to distinguish it from other similar objects. To *describe* an object is to provide a detailed account of its features. Together these tasks present a hierarchy of visual information extraction in which recognition requires the least amount of image detail (spatial and spectral) and description requires the most. In the reconnaissance phase the objectives are detection and perhaps recognition of specific hazards and vulnerabilities. In the identification phase the objectives are identification and possibly description. The mapping phase goes beyond the four tasks of visual interpretation with the objective of extracting quantitative information on the location, extent and, in some cases, the properties of specific objects or land covers.

Mapping Tools and Methods

The purpose of this section is to provide brief overviews of some analytical tools commonly used for mapping features with VHR imagery. This section is not intended to provide the theoretical basis of the analytical tool or a guide to its use. It is assumed that the reader will consult textbooks and software manuals before using the tool. This section is intended to provide a frank discussion of the utility of the most widely used types of tool for mapping tasks relevant to VHR imagery in urban environments. It is intended to help the reader determine which tool might be appropriate for a given task – either before or after the reader is familiar with the specifics of how the tool works. While these tasks are primarily the responsibility of the analyst, this guide may be useful for the decision maker who seeks a deeper understanding of the basis of the maps being provided by analysts. For reasons explained below, it is often important to question the validity of maps derived from remotely sensed imagery. In such cases, it can be very useful to have even a limited understanding of how the maps are derived.

Spectral Classifications – Spectral information is related to the color of an object – both in the visible and infrared parts of the spectrum. Spectral classifications categorize individual pixels on the basis of their color. These classifications methods fall into two categories: Continuous Field Maps and Discrete Thematic Classifications. Continuous field maps depict the land surface as continuous fields of a specific property (e.g. temperature) or material (e.g. vegetation) and can represent both continuous and discontinuous land cover characteristics. Continuous field maps are considered a form of “soft” classification because they represent each point on the land surface in terms of one or more continuously variable quantities - in contrast to “hard” or discrete classifications which represent each point on the land surface by membership in a specific thematic class. Thematic classifications therefore depict the land surface as discrete classes of land cover and assign each pixel membership in one, and only one, spectral class on the basis of the brightness values of the pixel in different spectral bands. In both continuous and discrete depictions the spatial context of the pixel is not considered; only the color.

Continuous Field Maps - The most versatile type of continuous field map is the endmember fraction map. Endmember fraction maps are derived from spectral mixture models which represent each pixel on the land surface as an areal mixture of different land cover types (e.g. vegetation, water, soil). For many applications endmember fraction maps provide a more useful analytical tool than thematic classifications. Particularly those that must accommodate continuous gradational transitions in land cover or physical properties that cannot be represented with discrete thematic classifications. A common example is vegetation abundance. Thematic classifications cannot represent continuous spatial variations in vegetation abundance and must impose arbitrary statistical boundaries that may have no counterpart in reality. By assigning spatial boundaries on maps where none exist in reality, discrete thematic classifications can misrepresent the land surface they purport to depict whereas a continuous field can represent the surface more accurately as robust, quantitative scaleable estimates of physical properties.

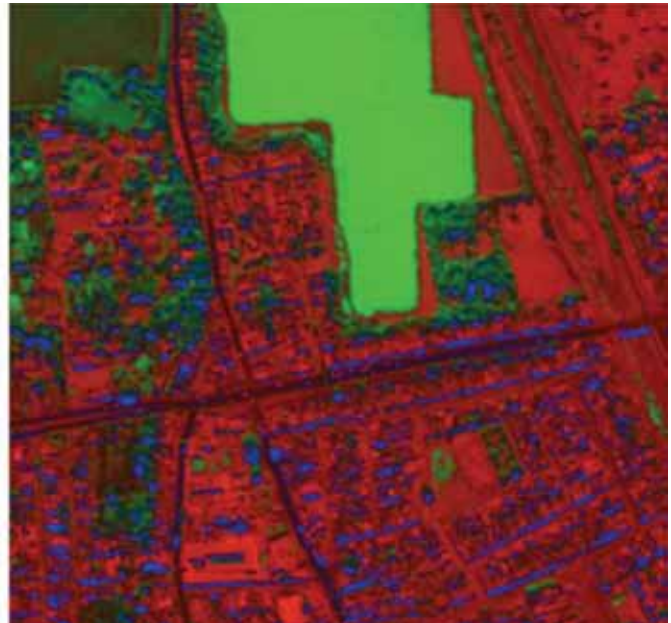
In many situations, endmember fraction maps provide a physically based representation of land cover components that can be easily and objectively validated as well as accurately upscaled. Neither thematic classifications nor empirical indices (e.g. NDVI) satisfy either of these conditions. Similar rationale apply to mapping spatial gradations in soil reflectance (possibly resulting from moisture content), substrate composition (possibly related to sand or gravel content) or volcanic ash cover. An endmember fraction composite derived from a simple three endmember mixture model is given in Figure A 14. The lack of spectral diversity in this image can be accommodated with a very simple three endmember model. Many urban areas have greater spectral diversity than this example and would require more endmembers to represent this diversity but the lack of diversity in this image is by no means unusual for developing urban areas. While not appropriate for every application, continuous field maps of Earth surface composition or properties can provide a valuable complement to discrete classifications while avoiding many of the difficulties of working with empirical indices like NDVI.

Figure A 14: Comparison of Quickbird false color composite and spectral endmember fraction image of Ica, Peru.

False Color Composite (r/g/b = 3/4/1)



Endmember Fraction Composite (r/g/b = S/V/D)



Inversion of a simple three endmember mixture model yields estimates of the spatial abundance of rock/soil Substrate, Vegetation and Dark surface (e.g. shadow, asphalt) for each pixel, resulting in the three continuous field maps combined in the endmember fraction composite on the right. Brighter, saturated areas are more spectrally pure (e.g. agriculture) while most of the urban mosaic is represented as spectral mixtures of substrate and shadow. Trees and the emergent crop in the upper left corner are mixtures of pure vegetation (illuminated photosynthetic foliage) and canopy shadow at the 2.4 meter scale of the Quickbird pixel. The fraction image compresses 4 bands of spectral information into a single 3 color composite.

Discrete Thematic Classifications – In contrast to soft classifications like mixture fraction mapping, discrete thematic classifications are considered “hard” classifications because each pixel is assigned membership in one, and only one, thematic class. All discrete spectral classification algorithms attempt to partition the spectral feature space with decision boundaries separating different classes of reflectance signature. The cardinal assumption in all spectral classification algorithms is that distinct classes have unique, or at least separable spectral signatures and therefore cluster in different parts of the spectral feature space defined by the spectral bands comprising a multispectral image. This assumption is warranted when the chosen classes have spectrally distinctive properties are homogeneous enough to form clusters in the spectral feature space. This condition generally requires that the spatial scale over which the land cover is spectrally

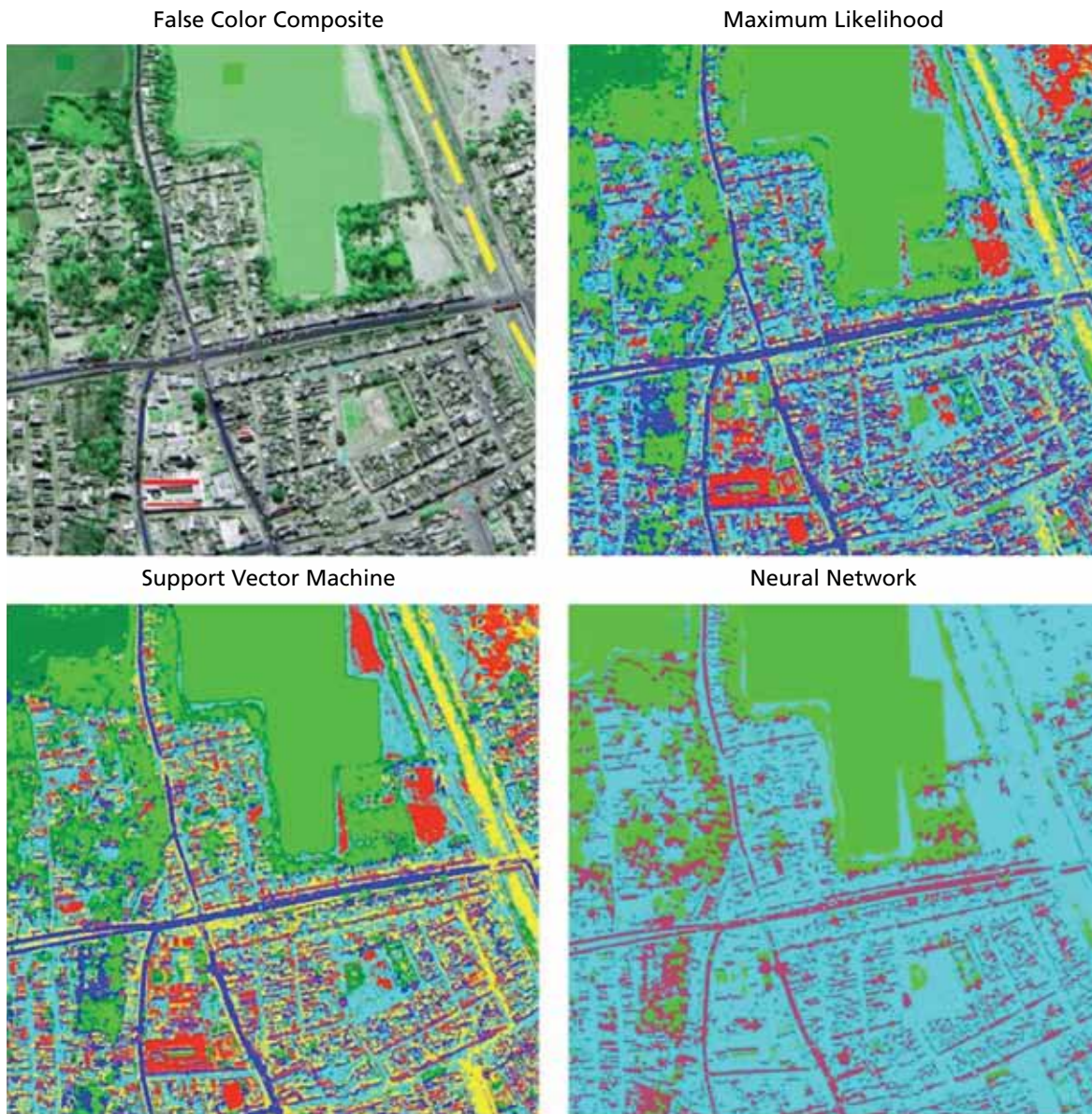
distinctive and homogeneous be significantly larger than the pixel dimension. This condition is occasionally satisfied in urban areas for pixel sizes smaller than 10 meters but rarely satisfied for pixel sizes larger than 20 meters (Small, 2009). This is one of the underlying reasons for 30 years of failed attempts to map urban areas using spectral classification algorithms on Landsat imagery.

The spectrally mixed pixels that characterize urban areas at moderate spatial resolutions violate the cardinal assumption on which discrete thematic classifications are based. With the advent of VHR imagery, the condition of spectral homogeneity is met more frequently but the number of spatially resolvable targets increases drastically with the increased spatial resolution. As a result, the number of thematically distinct classes frequently exceeds the number of spectrally

distinguishable reflectances with 4 band VNIR imagery typically available from VHR sensors. The implications of this are discussed in more detail below. The two main classes of thematic spectral classification algorithms are referred to as Supervised and Unsupervised. The difference is related to the presence or absence of ancillary training information from the analyst. Unsupervised classifications are purely statis-

tical, completely non-physical and do not consider the relationship of the image to the actual land surface it represents. Supervised classifications require ancillary information (training data) that relates each thematic class to a representative subset of pixels from the image. An example comparing different types of supervised classification applied to the same input image is given in Figure A 15.

Figure A 15: Comparison of supervised classification results.



Training samples for eight spectrally distinct thematic classes are shown as primary color patches on the false color composite image (UL). Each classification was run on the same image using the same training samples. The Maximum Likelihood algorithm (UR) distinguishes vegetation from other classes but does

not accurately distinguish trees from either crop. It also confuses bare soil with bright roofs and paved streets with shadow. The Support Vector Machine classification (LL) does considerably better on all classes but still confuses bare soil with some roofs and alluvium with some streets. The neural network classification (LR) detects only one class of vegetation, shadow and street classes and generally results in misclassification of all three with the remaining unassigned classes. Each of these algorithms can produce better, or worse, results depending on the accuracy-effort tradeoff.

Unsupervised Classification – Classification algorithms that use no training information from the analyst are referred to collectively as Unsupervised. The analyst specifies only the number of classes desired and some parameters on their separability. The most commonly implemented algorithms are K-means and ISODATA. Both algorithms attempt to partition the spectral feature space only on the basis of its topology and clustering. Both assume that distinct classes have unique, or at least separable spectral signatures. However, the algorithm decides what those classes are and assigns the decision boundaries according to the statistical properties of the feature space. The analyst sets a number of parameters influencing the number and separability of classes and the machine does the rest.

Supervised Classification – Classification algorithms that require ancillary training information from the analyst are referred to as Supervised. Supervised classification algorithms can be categorized into statistical and decision tree approaches. Decision tree classifications allow the analyst to prescribe decision boundaries as logical conditions or decisions. Statistical classifications use statistics derived from training samples to impose decision boundaries on the feature space.

Object-based Classification – Classification algorithms that incorporate the spatial context of a pixel into its classification render the image as a map of discrete features referred to as objects. The definition of objects in VHR imagery brings the R-I-M strat-

egy closer to the processes humans use to identify features of interest. In addition to tonal and textural characteristics of the image, object-based classifications introduce the concept of the spatially-contiguous object as a distinct entity. Dedicated systems have been developed for object-based analysis of VHR imagery. The complexity of the task is such that one of the more prominent systems divides the task into three distinct phases: definition and training of the algorithm, application of the particular algorithm to a specific dataset, and exploration of the solution space of results. A detailed discussion of object-based classification is beyond the scope of this report but the general approach is currently one of the most promising developments in image classification. It is expected to become more widespread in the near future but is currently not as widely used as spectral classifications.

Calibration and Validation

Calibration and validation are essential to most applications of remotely sensed imagery – although the implementations of each vary considerably depending on the task at hand. Calibration is the process of quantifying the response of the sensor system to a known input. Validation is the process of independent assessment of the accuracy of the product resulting from the analysis of the imagery. In many situations, calibration is conducted by the team that builds and/or operates the sensor system. Internal (within scene) calibration of most sensors is conducted within the instrument by imaging an internal radiance source of known output. Frequent internal calibrations allow instrument operators to compensate for instrument drift to assure inter-scene calibration through time. In some cases, additional calibrations are carried out by comparison of in situ reflectance measurements of a uniform, stable target on the earth surface with atmospherically corrected imagery of the target collected simultaneously (e.g. Pagnutti et al, 2003, Thome et al, 2003). An overview of calibration approaches is available at http://www.ccrs.nrcan.gc.ca/optic/calval/primer_e.php

Validation is fundamentally different for discrete and continuous classification products. Continuous classification products, like endmember fractions, generally correspond to a measurable physical quantity making validation straightforward in principle - although often logistically or physically difficult in practice. Validation of endmember fraction estimates is conceptually straightforward (in principle) because it only requires measurement of the areal abundance of that endmember in situ. How this is implemented in practice depends on the endmember and the difficulty of measuring its abundance in situ. Methodologies have been developed which allow VHR imagery to be used for vicarious validation of moderate resolution endmember fraction maps (Small 2009). Analogous vicarious validation methods could be applied to fraction maps obtained from VHR imagery if comparable imagery of significantly higher spatial resolution were available.

Discrete classification products, like thematic classes, rarely correspond to measurable physical quantities making their validation largely dependent on the user's assessment of a specific location's class membership. In some cases explicit criteria are defined to aid in determination of in situ class membership - in many cases membership is determined subjectively by the user in the field. A wide range of sampling theories and field validation methods have been developed for thematic classifications (See Congalton and Green (1998) for an overview). Even a brief summary of the diversity of approaches is beyond the scope of this report because the vast majority of validation and accuracy assessment methods have been developed for use with low to moderate resolution thematic land cover classifications and would not be appropriate (or even possible) with VHR imagery. In many of these approaches a fundamental ambiguity exists because thematic classes are often defined subjectively on the basis of criteria that are neither agreed upon nor measurable. It is generally assumed that the analyst or user has some independent criteria to determine which land cover class each validation site belongs to such that the validation exercise involves selecting a set of geographic locations, determining their appropriate class in situ and then cross checking the in situ class determi-

nation with the class assigned by the classification algorithm. The subsequent accuracy assessment involves statistical analysis of the binary errors associated with misclassified pixels.

In discrete thematic classifications a misclassified pixel incurs two errors simultaneously. An error of commission results when a pixel is assigned membership in a class to which it does not belong. A simultaneous error of omission occurs when the misclassified pixel is not accounted for in the class to which it does belong. Statistical analysis of classification accuracy generally involves extensive analysis of class-to-class misclassification to determine which classes the algorithm cannot distinguish accurately. The class-to-class misclassifications can then inform an iterative process where the analyst attempts to improve discrimination between spectrally similar classes. These discrete thematic validation methods are reasonable in situations where class membership is unambiguous, boundaries between land cover classes are discrete and land cover characteristics are uniquely distinctive and spectrally separable. However, even under the best of circumstances these methods are subject to multiple, unavoidable types of bias - both conservative and liberal (for an excellent summary see <http://nrm.salrm.uaf.edu/~dverbyla/online/error-matrix.html>). The underlying difficulties are largely a result of the discretization ambiguities discussed in the previous section.

Unlike land cover classification with moderate resolution imagery, most urban applications of VHR imagery involve identification and/or delineation of specific objects within the urban area. In these cases validation would involve in situ verification that the object actually is what the analyst or user expects. In some cases the objects classified are subject to similar caveats to those discussed above regarding the subjectivity of the user's in situ determination of the target's identity. In many cases, the user may be tempted to use the VHR imagery for vicarious validation of itself - essentially verifying that the classification agrees with visual interpretation. In these cases the potential for interpreter error enters the error budget. Interpreter error can be significant (<http://www.carnegieendowment.org/publications/index>.

[cfm?fa=view&id=150](#)) so this self-referential vicarious validation approach should only be used as an intermediary step to refine classification results prior to direct field validation.

Suggestions for Mapping and Classification

The previous section provides a brief summary and comparison of some commonly available mapping tools. How those tools are used depends on the task at hand and the resources available. The R-I-M strategy provides one possible framework for approaching the task of risk and vulnerability assessment. The actual implementation will obviously vary with the circumstance. However, a few basic principles apply to any situation where VHR imagery is being analysed.

Never use a tool you don't understand In light of the previous discussion on the non-uniqueness of most classification algorithms, the potential dangers of indiscriminate analysis should be apparent. In most urban environments it is difficult enough to obtain a robust result when the analyst understands the capabilities and limitations of the analytical tools. The potential for wasted time and nonsensical results is considerable when using one or more tools with multiple parameters if the analyst does not understand what the algorithm is doing and how the choice of algorithm and parameters can influence the result. Using a blind trial and error approach can waste considerable amounts of time, effort and resources. That time is always better invested in learning how the tools work before beginning the analysis.

Use each tool to its strength – As a corollary to the previous suggestion, it stands to reason that different algorithms have different capabilities and limitations that can vary with the dataset and problem they are applied to. Choose the tool on the basis of the task as well as its particular strength. For example, there is no need to use a Neural Network classifier to map vegetation abundance when a vegetation endmember fraction map will provide a more accurate result for far less effort. Conversely, it is not necessary to construct and invert a mixture model

when the objective is to obtain a thematic classification of spectrally distinctive agriculture classes that could be more easily distinguished by a supervised classification.

Do not trust the machine – The purpose of image analysis algorithms is help the analyst – not to replace the analyst. It is naïve to expect any machine to work flawlessly on a task as complex as image analysis. Results obviously need to be checked thoroughly and validated whenever feasible. However, it is also important to recognize the point of diminishing returns with any tool and know when the machine should stop and the analyst should take over. The purpose of analytical tools is to facilitate extraction of quantitative information from imagery. Every combination of tool and dataset together have limitations in terms of the information available for a given expenditure of time and effort. It is important to recognize these limitations.

Expectation management is the key to happiness – The purpose of this report is to provide analysts and decision makers with a deeper understanding of what can and cannot be accomplished with VHR imagery and currently available analytical tools. Understanding the utility and limitations of the imagery and tools is key to using them to advantage. Realistic expectations are a key to recognizing the point of diminishing returns and making most effective use of time and resources.

Multi-temporal Change Detection

Quantitative change detection is considerably more difficult with VHR imagery than with the moderate spatial resolution (10-30 m) imagery for which most current change detection methods were developed. The difficulty is related to viewing and illumination geometry. Most moderate resolution sensors are nadir-looking with swath widths of less than 10 degrees. As a result, they image their targets from the same very high angle on every overpass. In addition, the 10 to 30 meter spatial resolution is comparable to, or larger than, most individual objects in the urban mosaic but significantly smaller than the scale of the most prominent land cover classes (e.g. for-

est, agriculture, water bodies, etc). As a result, the spectral mixing that occurs at moderate spatial resolutions tends to homogenize reflectance variations within urban areas and other land cover classes. In cases where adjacent patches of different land cover types are sufficiently spectrally distinct this homogenization emphasizes abrupt transitional boundaries between them. The combination of intra-class spectral homogenization and consistent near-nadir viewing angle facilitates multitemporal change detection because it provides internally consistent spatial registration between multitemporal images while simultaneously enhancing inter-class spectral separability and reducing intra-class spectral variability.

With VHR imagery the situation is reversed. Pixel size is generally smaller than most of the objects in the urban mosaic so they tend to be oversampled and easily distinguishable. This would facilitate change detection – if multitemporal images were acquired under identical viewing and illumination geometries. For reasons explained in section 2, this is very rarely the case with VHR imagery. The three dimensional relief of most objects in the urban mosaic is comparable to, or greater than, the pixel size so even small differences in viewing geometry result in considerable differences in the planar projection of the 3D surface onto the image plane. As a result, the same objects generally appear in different places on images acquired from different view angles. This precludes the straightforward approach of image differencing on which change detection algorithms rely. Detailed orthorectification can restore some geometric consistency (on the rare occasion when a high resolution elevation model is available) but it cannot account for the loss of information that results from the parallax viewing effect (foreshortening or layover discussed in section 2). Airborne platforms are not subject to the constraints of satellite orbits and can sometimes acquire multitemporal imagery from near identical viewing angles if sufficient navigation and attitude control can be achieved but, at present, this is rarely the case for satellites with pointable sensors. Because of the high relief in urban environments, and the high resolution of the sensor, sufficiently precise positional consistency is difficult to attain. Even if such positional consistency

could be attained, the images would have to be collected under nearly identical illumination conditions to prevent differences in shadow projection from overwhelming any actual change that may have occurred between image acquisition times. In summary, existing methods of multitemporal change detection require a degree of geometric consistency that is rarely attainable with VHR imagery. While it is attainable in principle, it is rarely attainable in practice because of the difficulty of obtaining multiple images from nearly identical view angles. The problem is further compounded by temporal variations in illumination geometry that are beyond the control of the analyst or imagery provider. At present, the most effective means of change detection with VHR imagery is visual comparison. However, the R-I-M strategy allows for quantitative change detection using moderate resolution imagery in the reconnaissance phase to isolate potential change areas for subsequent analysis with VHR imagery.

Synthesis

Strengths of VHR imagery – The strengths of VHR imagery are related to the vast information content and the comparative ease with which information can be extracted from it - relative to aerial photography. Pointable, calibrated, low noise, meter to submeter scale, multi-resolution, spatially coincident multispectral/panchromatic sensors provide a low cost, logistically expedient imaging resource that opens avenues of analysis and quantitative information that is only beginning to realize its immense potential. At this point in time, most of the strengths of VHR imagery cannot yet be exploited with available tools and knowledge. Aside from the obvious strengths discussed above and throughout the report, a less obvious strength is its potential for consistency. A calibrated radiometric sensor confers enormous benefits to applications that benefit from quantitative analysis and comparison of imagery collected at different times and places. Most of the analyses discussed above could be applied to digital scans of aerial photographs or uncalibrated digital photographs but it would be difficult to impossible to conduct accurate quantitative comparisons of re-

sults obtained in different times and places. An even less obvious strength of modern VHR imagery is the dynamic range. The most widely available VHR imagery (Quickbird & Ikonos) offer 11 bits of brightness range; $2^{11} = 2048$ brightness levels within a single scene but with adjustable gain the total number of brightness levels can be significantly higher among scenes acquired under different gain/bias settings. A typical digital photograph or scan provides only $2^8 = 256$ brightness levels but without calibration these brightnesses are only relative to the rest of the scene and cannot be compared to images acquired at different times or places.

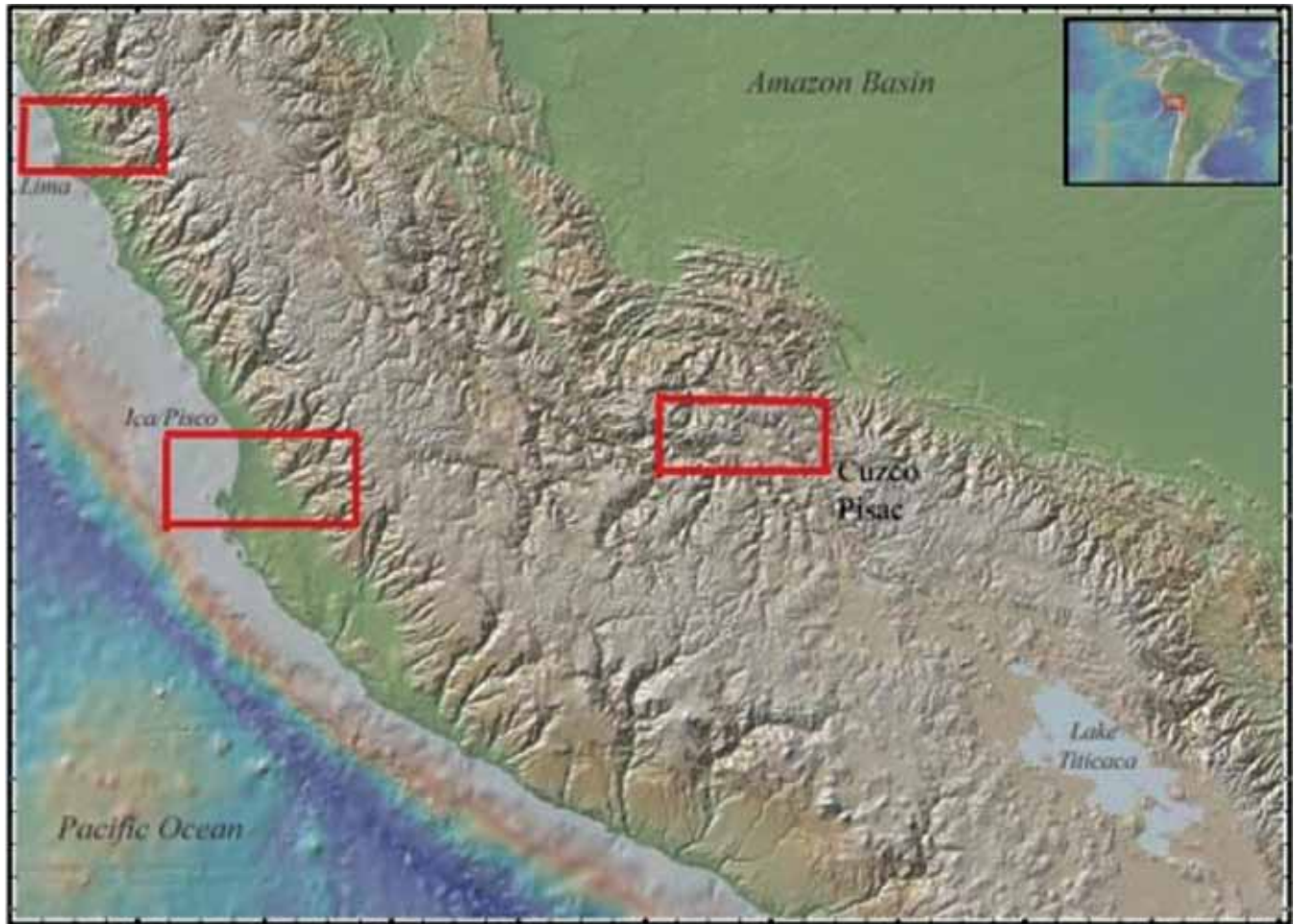
Weaknesses of HR RS imagery – The weaknesses of VHR imagery are related to its inherent limitations, as well as the disparity between the user’s expectations and the reality of the imagery and tools’ limitations. Many of the inherent limitations have been discussed throughout the report – along with the some common disparities between expectation and reality for specific combinations of tool and image. As with the strengths, many of the weaknesses are sufficiently obvious that they do not warrant discussion here. Some of the less obvious weaknesses have also been discussed throughout the report. Specifically, the inherent tradeoffs that limit when and where the imagery can be acquired and the tradeoffs that limit spatial, spectral and temporal resolution. The spatial and temporal limitations are more intuitive than the spectral limitations. The preceding discussion of spectral separability of different objects composed of similar materials (e.g. pervious & impervious) gives some indication of the potential ambiguities that may not be obvious. Ironically, one of the primary weaknesses of VHR imagery is related to its major strength: information content. Most VHR imagery contains far more information than can be easily quantified with currently available tools. However, this is more a weakness of our current state of knowledge than of the imagery itself. As analytical methods more closely approach and

approximate the analytical abilities of the human eye-brain the limitations on information capture will be reduced. At present, the disparity between the qualitative information visible to an analyst and the quantitative information that even an experienced analyst can extract from an VHR image is immense. If an analyst, or decision maker, does not understand the limitations of the available tools and recognize the disparity between what can be seen and what can be measured, the potential for wasted resources and erroneous conclusions is immense. This report is an attempt to give analysts and decision makers some indication of the strengths and limitations of the combination of tool and imagery.

Examples

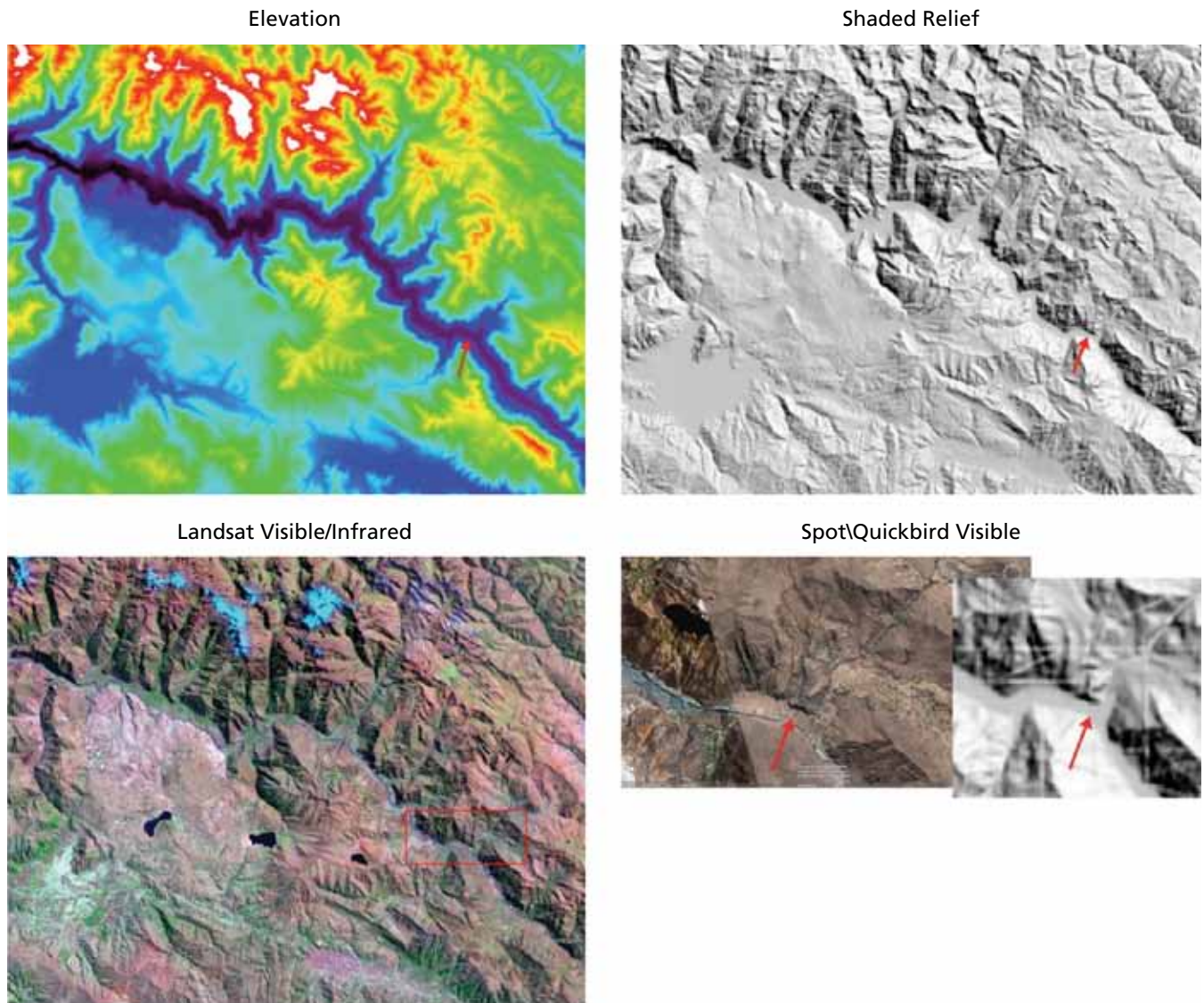
This section contains a set of examples illustrating how VHR imagery from Quickbird can be combined with moderate resolution optical imagery and digital elevation models to investigate potential hazards in highland Peru. The region is chosen for its multi-hazard exposure to climatic, seismic, volcanic and gravitational hazards. Many of the examples used already throughout the survey have come from this region. The rapid convergence of two tectonic plates produces an immense amount of gravitational and thermal energy concentration and release in the form of regional uplift, crustal stress accumulation and magma genesis. In addition, its location on the eastern edge of the Pacific Ocean places it squarely within the primary impact area of the coupled ocean/atmosphere phenomenon referred to as the El Nino. The result is high climatic variability with extreme rainfall events at the edge of the coastal desert and high sensitivity to longer term global warming in the highlands. This, coupled with extensive rural to urban migration, results in rapid urban growth into hazard prone environments within a developing economy.

Figure A 16: Topographic index map for example locations in Peru.



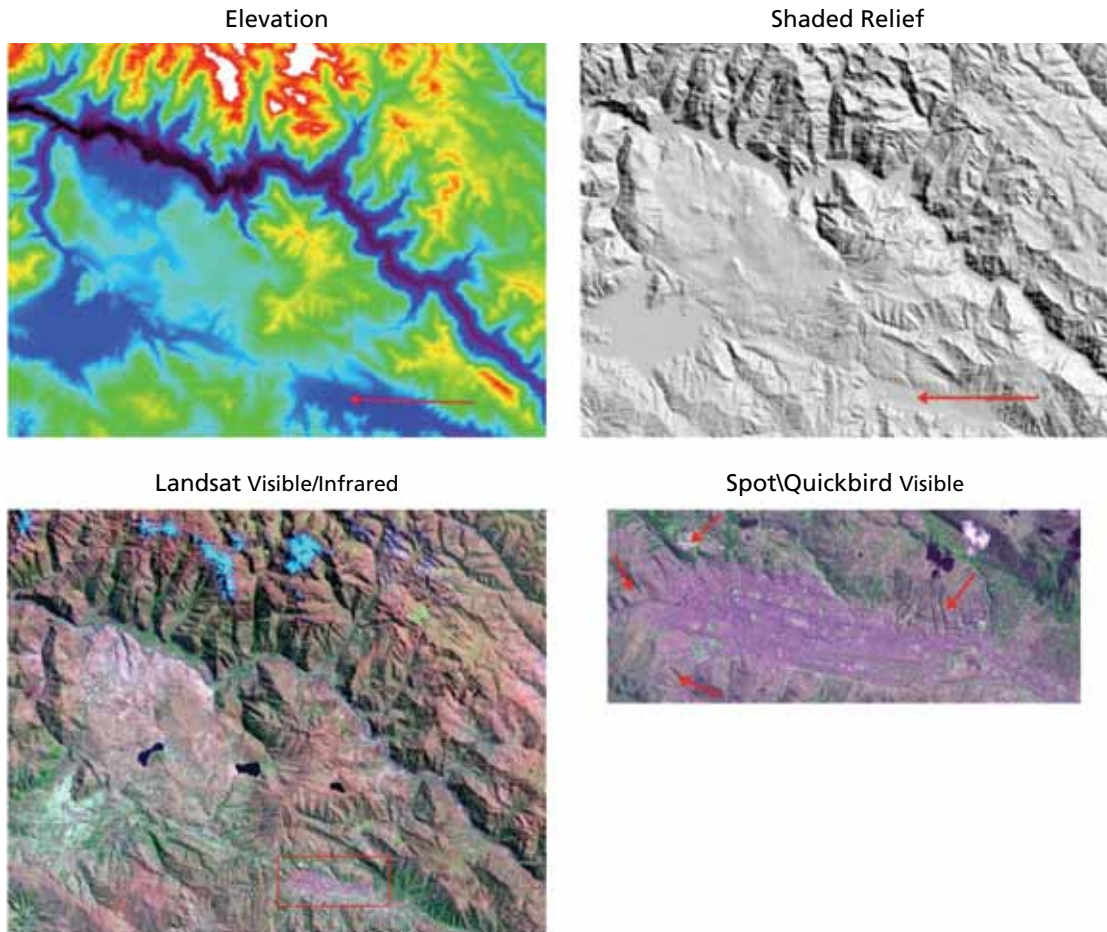
False illumination from northwest emphasizes rugged topography throughout the Andes as well as on the altiplano and flanking slopes. The bathymetric trench (dark blue) running parallel to the Pacific coastline is a result of eastward subduction of the Pacific plate beneath the overriding South American plate. Compressional uplift and melting of the downgoing plate are responsible for the mountain building, erosional incision and volcanism that create the Andes. Friction and stress release along the plate boundary result in some of the largest, and most frequent, earthquakes on Earth. In addition, the extreme topography in combination with infrequent but intense precipitation produces steep, unstable slopes, flash floods and large scale mass movements throughout the region. Despite the diversity of natural hazards this region has been continuously inhabited longer than any other region in the western hemisphere and was the center of the largest pre-columbian empire civilization in the western hemisphere. At present, the area is experiencing rapid population growth and rapid unplanned urbanization in marginal, hazard prone environments. Examples from Lima, Ica/Pisco, and the Cuzco-Valle Sagrado regions have been used as illustrations throughout the report. The slope and elevation information used in this map are derived from a global 3" (~90 meters at the equator) digital elevation model produced from Synthetic Aperature Radar (SAR) measurements collected by the Shuttle Radar Topographic Mapping Mission (SRTM). These elevation data are available, free of charge, for most land areas of latitudes less than ~57° N/S and can be used to produce crude slope maps highlighting a variety of hazard-prone environments.

Figure A 17: Topography and land cover of Pisac and the Sacred Valley.



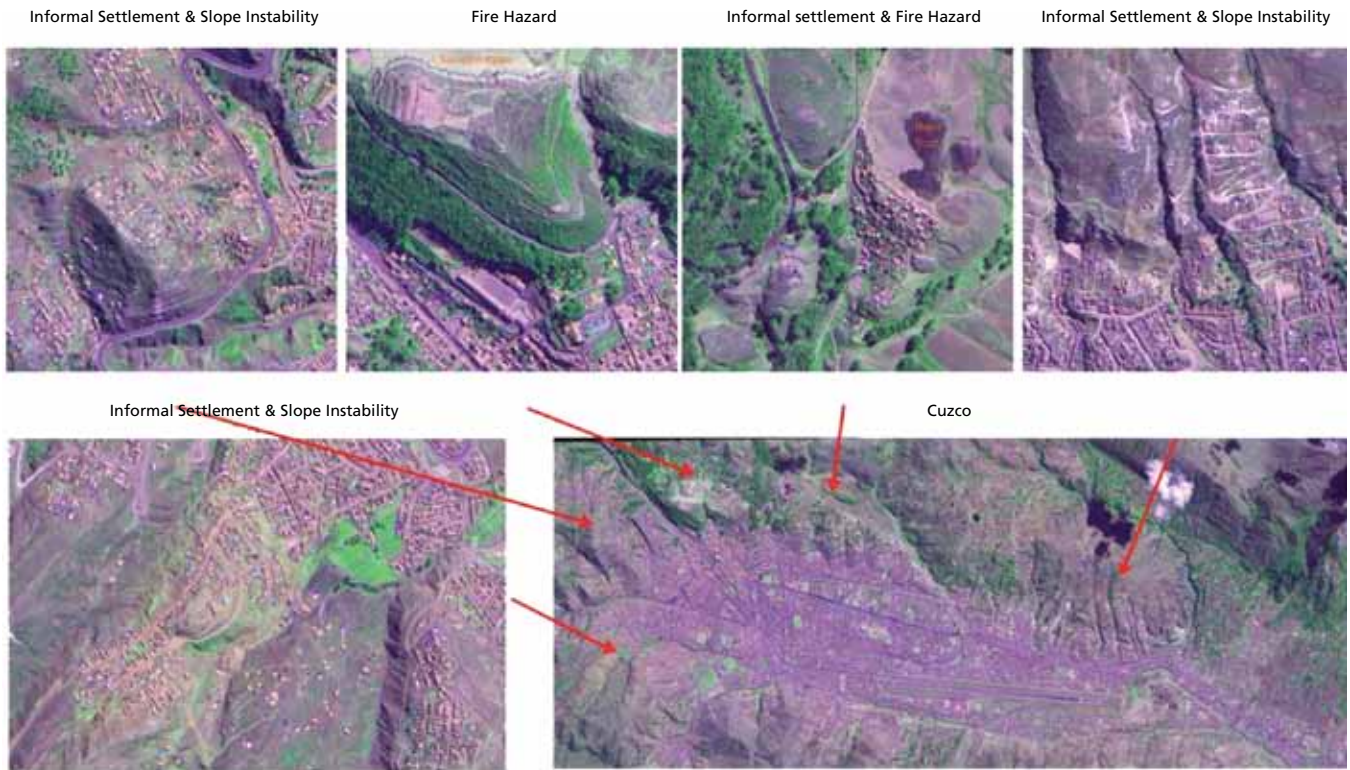
SRTM 90 m DEM (UL) illustrates the >2000 m relief of the Sacred Valley. The shaded relief map illustrates (UR) the extreme slopes but also reveals numerous errors (lineations in LR inset) in the 90 m elevation model. Landsat moderate resolution (30 m) visible/infrared imagery shows dry season land cover (post harvest) and location of Pisac (LL- right center red box). Overlaid Quickbird/Spot imagery shows steep, potentially unstable slopes above Pisac as well as finer scale steep topography not resolved by the 90 m DEM. Red arrows show location of Pisac in the increasing resolution zoom sequence in Figure A 7. The entire valley is a cultural asset at risk from rapid development.

Figure A 18: Topography and land cover of Cuzco and the Sacred Valley.



SRTM 3" topography illustrates the >2000 m relief of the Sacred Valley. The shaded relief map illustrates the extreme slopes but also reveals numerous bad data (linear features). Landsat 7 imagery shows dry season land cover - post harvest and location of Cuzco (LL bottom center right). Quickbird imagery shows extent of development in and around Cuzco as well as finer scale steep topography not resolved by the 90 m DEM. Red arrows show locations of full resolution examples in Figure A 19.

Figure A 19: Topography and land cover of Cuzco and the Sacred Valley.



SRTM 3" topography illustrates the >2000 m relief of the Sacred Valley. The shaded relief map illustrates the extreme slopes but also reveals numerous bad data (linear features). Landsat 7 imagery shows dry season land cover - post harvest and location of Cuzco (LL bottom center right). Quickbird imagery shows extent of development in and around Cuzco as well as finer scale steep topography not resolved by the 90 m DEM. Red arrows show locations of full resolution examples in Figure 8.4.

Glossary of Terminology

Accuracy & Precision For the purposes of this report, **Accuracy** is defined as the degree of conformity to truth or to a standard or model while **Precision** is defined as the degree of refinement with which an operation is performed or a measurement stated. For example, it is more accurate to represent pi ($\pi = 3.14159265\dots$) as 3 than 4 and 3.1 than 3.2 while it is more precise to represent pi as 3.1415 than 3.14.

Band – a spatial array of measurements of some physical quantity. In the case of VHR imagery the bands of an image are generally measurements of optical radiance (or proportional to it).

Channel – an independent component of brightness and/or color in a visual display. Generally represented by a gray shade or primary color (Red/Blue/Green or Cyan/Magenta/Yellow) in which brightness of each display pixel corresponds to the magnitude of the quantity in that image band and pixel.

Display – the visual depiction of an image. Generally a 2D array of pixels in which the brightness of each pixel represents the magnitude of the physical quantity in one or more bands at a specific spatial location.

IFOV – the angular Instantaneous Field Of View of a sensor determining the physical size (spatial dimensions) the pixel on the target.

Image – an N-dimensional array of measurements of some physical quantity where at least two of the dimensions are geographic or spatial. In spatially uniform grids the 2 spatial dimensions are generally implicit in the row and column index of each distinct pixel. The remaining N-2 dimensions comprise distinct bands of the image.

Pixel – a spatially explicit set of physical measurements generally corresponding to a projection of a sensor's Instantaneous Field of View (IFOV). Component of an image.

OR

Pixel – a spatially explicit location on a display of variable color and/or brightness. Component of a display.

Platform – the vehicle on which a sensor is carried. Generally either an aircraft or a satellite.

Satellite – a platform in orbit around Earth. Generally not powered. Motion dictated by Kepler's Laws of orbital motion.

Sensor – a device used to measure the energy radiated, emitted or reflected from a target. A webcam is an example of a passive sensor that relies on an external energy source (e.g. a lamp). A radar gun is an example of an active sensor that emits its own energy source (radar waves). A digital camera with a flash is can be used as either an active sensor (with the flash) or a passive sensor (without).

Spatial resolution – the spatial dimension(s) of the pixel resulting from the projection of the sensor's IFOV onto the target. Higher spatial resolution = smaller pixel area.

Spectral resolution – the range of spectral wavelengths to which a sensor is sensitive in a specific spectral band. Higher spectral resolution = finer color discrimination.

Swath – the area imaged by a scanner in a single pass. Determined by the width of the sensor's total field of view in the direction perpendicular to motion.

Target – the feature being imaged. Broadly, the Earth surface. Generally, the things on the Earth surface being imaged by the sensor. Specifically, a physical entity or collection of entities within the sensor's IFOV.

Endnotes

- 1 This report has been prepared in a collaboration of the Institute to the Protection and Security of the Citizen (IPSC), Joint Research Centre (JRC) of the European Commission in Ispra, Italy, and the World Bank's Development Research Group with funding from the Global Facility for Disaster Risk and Recovery (GFDRR) and JRC. The report authors are Daniele Ehrlich and Gunter Zeug (JRC), Christopher Small (Columbia University) and Uwe Deichmann (World Bank, DECRG). Piet Buys contributed to early field work in Legazpi and Sana'a. Sandra Eckert provided useful comments and help with graphics. We would like to express our appreciation to the government officials and researchers in the Philippines who supported the field visits and provided invaluable information, in particular Mayor Noel E. Rosal and his staff at the Departments of City Planning and Social Welfare, especially Maria Marlene Manaya and Joseph B. Esplana; Cedric Daep, Regional Disaster Coordinator of Albay Province; staff of the Philippine Volcano Observatory, the National Mapping & Resource Information Authority, the National Disaster Coordination Council, and the Department of the Interior and Local Government provided helpful guidance and information; and Mukami Kariuki, Zoe Trohanis and Cathy Vidar at the World Bank. Although not covered in detail in this report, this study also generated information from high resolution satellite data for inputs into a hazard management program in Sana'a, Yemen. In Sana'a, the authors would like to thank the Al-Saylah-Project Implementation Office, Capital Secretariat of Sana'a, in particular Aref Taher and Ahmed Omar, for supporting our field mission; H.E. Abdelrahman Al Akwa'a, Mayor of Sana'a, H. E. Dr. Yehia El Shoebi, former Mayor of Sana'a and H.E. Mr. Amin Jumaan, Vice-Mayor of Sana'a Municipality; Moeen Al Mohaqeri, deputy mayor for technical affairs; the Sana'a CDS team including Ahmed Abdelwahed and Namir Zainal; as well as Sameh Naguib Wahba and Madhu Raghunhat at the World Bank. Stuart Gill, Asmita Tiwari and Henrike Brecht provided helpful comments on an earlier draft of this report.
- 2 Estimates in constant 2000 US Dollars based on the EM-DAT hazard loss inventory (www.emdat.be). Definition of economic losses follows EM-DAT.
- 3 ISDR (2009) based on EMDAT data. Between 1975 and 2008, 78.2% of mortality in significant natural disasters occurred in only 0.3% of recorded events.
- 4 See, for instance, Pacific Disaster Center: www.pdc.org/emi.
- 5 New satellites are frequently launched into orbit. An up-to-date list of Earth Observation satellites is available from http://en.wikipedia.org/wiki/List_of_Earth_observation_satellites.
- 6 A more specialized application of web based data sharing platforms for risk analysis is GeoNode (www.geonode.org). It is a geo-spatial data sharing initiative of the Central America Probabilistic Risk Assessment (CAPRA).
- 7 This technical appendix was prepared by Dr. Christopher Small, Lamont-Doherty Earth Observatory, Columbia University.



Global Facility for Disaster Reduction and Recovery

1818 H Street, NW
Washington, DC 20433, USA
Telephone: 202-458-0268
E-mail: drm@worldbank.org
Facsimile: 202-522-3227



Special thanks and appreciation are extended to the partners who support GFDRR's work to protect livelihood and improve lives: ACP Secretariat, Arab Academy for Science, Technology and Maritime Transport, Australia, Bangladesh, Belgium, Brazil, Canada, China, Colombia, Denmark, Egypt, European Commission, Finland, France, Germany, Haiti, India, International Federation of Red Cross and Red Crescent Societies, Ireland, Italy, Japan, Luxembourg, Malawi, Mexico, The Netherlands, New Zealand, Norway, Portugal, Saudi Arabia, Senegal, South Africa, South Korea, Spain, Sweden, Switzerland, Turkey, United Kingdom, United Nations Development Programme, United States, UN International Strategy for Disaster Reduction, Vietnam, The World Bank, and Yemen.